

Advances in applications of the physics of fluids to severe weather systems

Howard B Bluestein

School of Meteorology, University of Oklahoma, 120 David L Boren Blvd,
Suite 5900 Norman, OK 73072, USA

E-mail: hblue@ou.edu

Received 2 February 2007, in final form 30 May 2007

Published 6 July 2007

Online at stacks.iop.org/RoPP/70/1259

Abstract

This article is a review of the basic dynamics of severe convective storms. The dynamics are in most instances described with the aid of the vorticity and divergence equations subject to the Boussinesq approximation. The behaviour of ordinary-cell convective storms in the presence of different amounts of vertical shear and its relation to the surface cold pool are explained. The role of vertical shear in the propagation of, and rotation in, supercells is described in detail. How cold pool production, buoyancy, and environmental vertical shear control the structure of mesoscale convective systems is discussed and the mechanism for the production of vortices in them is described. The wind field in tornadoes based on laboratory experiments, simulations, and observations is explained from the dynamics of vortices that interact with an underlying surface. Various theories for tornado formation are presented and evaluated. Avenues for future research using both numerical simulations and new and emerging observing systems are highlighted.

(Some figures in this article are in colour only in the electronic version)

This article was invited by Professor A Kostinski.

Contents

	Page
1. Introduction	1262
2. The basic equations	1262
2.1. The equations of motion	1262
2.2. Thermodynamics	1263
2.3. Conservation of mass and the Boussinseq approximation	1264
2.4. The vorticity equation	1265
2.5. The divergence equation	1266
2.6. Ertel's potential vorticity	1267
3. Ordinary-cell convective storms	1267
3.1. Observed structure and life cycle	1267
3.2. Gust fronts in the absence of significant vertical wind shear	1268
3.3. Gust fronts in the presence of vertical shear	1270
4. Supercells	1271
4.1. Observed supercell behaviour and early theories	1271
4.2. Observed supercell structure	1272
4.3. The production of mid-level rotation	1276
4.4. Interaction of vertical shear and buoyancy: linear and nonlinear pressure effects	1277
4.4.1. Convective-storm dynamics for straight hodographs.	1281
4.4.2. Convective-storm dynamics for curved hodographs.	1281
4.4.3. Straight versus curved hodograph dynamics: two paradigms.	1282
4.4.4. Sensitivity of simulated supercell structure to environmental thermodynamic and cloud microphysics parameters.	1283
4.5. The deep convergence zone (DCZ)	1284
4.6. The production of low-level rotation	1284
4.7. The life cycle of the mesocyclone and cyclic mesocyclogenesis	1285
4.8. Supercell structure and behaviour in relation to inhomogeneities in the environment, and interactions with neighbouring storms and surface boundaries	1285
4.8.1. Neighbouring cell interaction.	1286
4.8.2. Movement across outflow boundaries or fronts.	1286
5. Mesoscale convective systems	1288
5.1. Formation	1288
5.2. Morphology	1289
5.3. The dynamics and thermodynamics of mature MCS squall lines	1291
5.4. The production of vortices in MCSs	1294
6. Tornadoes	1296
6.1. Types of tornadoes	1297
6.2. Vortex dynamics	1298
6.2.1. Vortex structure.	1298
6.2.2. Vortex formation: tornadogenesis.	1308

7. Future research	1314
7.1. Numerical simulations	1314
7.2. Observations	1314
Acknowledgments	1315
References	1316

1. Introduction

Severe weather systems are responsible for property and crop damage, interruption of travel and outdoor activity, and, in the most extreme cases, injuries and death. While the adjective ‘severe’ generally refers to damaging phenomena, it is recognized that what is damaging to one type of structure may not be damaging to another, owing to differences in the integrity of construction and the nature of the land surface. In the US, ‘severe’ weather (associated with *local* storms) is defined more narrowly by the Storm Prediction Center of the National Weather Service as having one or more of the following: tornadoes, winds in excess of 25.8 m s^{-1} (58 mph), or hail greater than 1.9 cm (3/4 in) in diameter, regardless of whether or not there is actual damage (Doswell 2001).

In this paper, only severe weather systems that are convective (and necessarily, local) in nature are considered. Severe events in tropical cyclones and intense winter-season, extratropical cyclones, for example, which are not local but cover a much broader area, are not considered. In addition, flooding and lightning are not sufficient for an event to be characterized as ‘severe’, even though each may be responsible for damage, injuries, and death. To maintain a manageable focus, this paper details the physics of just the airflow and precipitation distribution in severe convective storms. The reader is directed elsewhere for detailed discussions of hail formation (Knight and Knight 2001) and cloud electrification (Williams 2001).

The purpose of this review is to summarize advances made in the last quarter century in our understanding of the physics of severe convective storms. Advances in observing systems, particularly in radar meteorology, and advances in computer technology and modelling techniques, have spurred on investigations of what causes severe convective storms and their characteristics. By applying physical reasoning to observations (from both quantitative measurements and from visual observations and photographs) and controlled numerical experiments, the fundamental processes responsible for storm type and the severe weather associated with each type of storm have been identified. The following two sections, respectively, describe the physics of the two types of convective building blocks, ‘ordinary cells’ and ‘supercells’. The next section details the dynamics of larger conglomerates of convective cells, ‘mesoscale convective systems (MCSs)’. Tornadoes, which can form in either type of convective cell and in some MCSs but are less well understood, are discussed in the penultimate section. Finally, the future directions for emerging research are described in the last section.

2. The basic equations

Three basic laws are used to diagnose the physical processes in severe convective storms; they are Newton’s equation of motion applied to a fluid (the ‘equations of motion’), the first law of thermodynamics applied to a fluid, and a statement of the continuity (conservation) of mass, including dry air, moist air and the various forms of water substance (e.g. Bluestein 1992, 1993).

2.1. The equations of motion

The equations of motion are separated into the horizontal and vertical components, each of which is different. The horizontal equation of motion in vector form is as follows:

$$D\mathbf{v}_h/Dt = \partial\mathbf{v}_h/\partial t + \mathbf{v} \cdot \nabla\mathbf{v}_h = -\alpha_0\nabla p' \quad (2.1)$$

where D/Dt indicates a derivative following air-parcel motion, \mathbf{v} is the wind velocity, \mathbf{v}_h is the horizontal component of the wind velocity, α_0 is the specific volume of air (reciprocal of

density) at the surface (including water vapour and other water substance such as liquid water and ice), and p' is the perturbation pressure, defined in terms of a reference pressure p that is a function of height only and t is time. (The acceleration induced by the Coriolis force $\sim fU$, where $f = 2\Omega \sin \phi$, U is the horizontal wind speed, Ω is the rotation rate of the Earth about its axis and ϕ is the latitude. It follows that accelerations induced by the Coriolis force are significant for time scales $\geq 1/f$. The Coriolis force is therefore not included unless the time scale of the phenomenon considered is at least 6 h. Molecular and turbulent friction are $\sim \mu \partial^2 U / \partial z^2$, where μ is the molecular/eddy coefficient of viscosity; μ or molecular viscosity is small and the turbulent term is significant typically only in the lowest kilometre or so, where $\partial^2 U / \partial z^2$ is relatively large. For the sake of simplicity, turbulent and molecular friction are not included here or in subsequent equations; it is thus assumed that all the variables are time and spaced averaged for the scales of motion we are considering and that sub-grid-scale turbulence is ignored.)

The vertical equation of motion is as follows:

$$Dw/Dt = -\alpha_0 \partial p' / \partial z + B, \quad (2.2)$$

where w is the vertical component of the wind, the vertical velocity and B is the buoyancy, and where

$$B = (\alpha' / \alpha_0)g = gT'(1 + 1.609r_v - r_l - r_i) / T_0 \quad (2.3)$$

and where g is the acceleration of gravity, α' is the deviation of specific volume α from α_0 , T' is the deviation of temperature T from its environmental value, T_0 is the environmental temperature, r_v is the water-vapour mixing ratio, r_l is the liquid-water mixing ratio and r_i is the ice mixing ratio. The vertical equation of motion is similar to the horizontal equation of motion, except that there is an additional term that represents the acceleration induced by the buoyancy force. The buoyancy force, which is created by thermodynamic processes and includes the effects of gravity, may be diminished or reversed by the loading of water substance. In both the horizontal and vertical equations of motion the molecular viscosity terms may be neglected when considering air motion not right next to the surface. (For large-scale motions, i.e. those for which the horizontal scale is much longer than the vertical scale, which is on the order of the depth of the troposphere (~ 10 km), there is no buoyancy force, vertical air-parcel accelerations are negligible, and the vertical pressure-gradient force is exactly counteracted by gravity (Ogura and Phillips 1962, Emanuel 1994, see equation (1.3.16)). This situation is called a state of *hydrostatic* balance, a consequence of which is that the mass of air in column alone determines the pressure at the bottom of the column.)

2.2. Thermodynamics

The first law of thermodynamics for the atmosphere is given as follows:

$$dQ = C_v dT + p d\alpha, \quad (2.4)$$

where Q is the heat energy, C_v is the specific heat at constant volume of a volume of air containing a mixture of dry air, water vapour and other water substance (liquid and frozen). 'Diabatic' heating (from changes in the phase of water substance, turbulent heat transfer from the surface and radiation) results in changes in temperature and pressure. The dynamics of convective storms is affected most by the latent heat released or absorbed when water droplets condense from water vapour, when water droplets evaporate, when ice crystals form directly from water vapour, when water droplets freeze into ice, when ice melts into water, and when ice particles sublimate. Details about these change-in-phase processes are known as 'cloud microphysics'. Since the cloud microphysical processes are not completely understood and

not easily observable, they are parametrized in terms of quantities that can be measured, such as temperature and pressure.

Turbulent heat transfer from a heated land surface during the day or when cold air flows over a much warmer ocean is frequently very important for cloud formation. Radiative cooling at cloud top or horizontal gradients in radiative heating, e.g. at cirrus-anvil edges, can also be significant (Markowski *et al* 1998, Markowski and Harrington 2005), but are not of primary dynamical importance for convective storms.

The adiabatic form of the thermodynamic equation, expressed in terms of the time rate of change of variables, is given by

$$C_p DT/Dt - \alpha Dp/Dt = 0, \quad (2.5)$$

where C_p is the specific heat at constant pressure. Changes in temperature are thus related only to changes in pressure. The adiabatic form of the thermodynamic equation is useful for describing the thermodynamic changes associated with horizontal and vertical air motions outside of convective storms: rising air generally is cooled and sinking air is warmed, the amount of cooling/warming varying as the lapse rate of temperature.

2.3. Conservation of mass and the Boussinesq approximation

The equation of continuity, which is a statement for conservation of mass, for a compressible atmosphere is as follows:

$$(1/\alpha_0) D\alpha_0/Dt = \nabla \cdot \mathbf{v}. \quad (2.6)$$

For convective storms, however, the atmosphere may be approximated as an incompressible fluid, so that

$$\nabla \cdot \mathbf{v} = 0 \quad (2.7)$$

even though the following ideal gas law

$$p\alpha = RT, \quad (2.8)$$

governs the behaviour of air in a compressible atmosphere, where R is the mass-based gas constant (including the effects of both dry air and water vapour). To a good approximation, the compressibility of the atmosphere may be ignored in the equation of continuity (*only* in the equation of continuity) if the air motions in the atmosphere are relatively shallow. The set of governing equations are called the *Boussinesq equations* (Ogura and Phillips 1962, Emanuel 1994); strictly speaking, they describe air motions for shallow cumulus clouds and the boundary layer, the region near the ground that is affected by it (typically up to ~ 1 km above ground level (AGL), but up to as much as 3 km AGL or more in heated, arid regions).

It is seen from the Boussinesq equation of continuity (2.7) that the adiabatic form of the thermodynamic equation (2.5) is

$$DT/Dt = 0. \quad (2.9)$$

Since severe convective systems are typically deep, extending up to the tropopause and slightly beyond (~ 10 – 15 km AGL), the following better approximation to the equation of continuity is often used:

$$w \partial \ln \alpha_0 / \partial z = \nabla \cdot \mathbf{v}. \quad (2.10)$$

In this form of the continuity equation, which is a simplification of (2.6) in which local time derivatives and horizontal gradients are neglected, only the vertical variations of specific volume (or density) are retained; it is known as the *anelastic* equation of continuity and is

used in some models and in Doppler radar analyses. To keep analyses of the dynamics of convection simple, however, the *Boussinesq* continuity equation is most frequently used; by ignoring the vertical effects of compressibility, the overall physics are changed only slightly and fundamental results are not altered qualitatively. The results of numerical simulations conducted with models that are fully compressible (using (2.6)) support the analysis of storm dynamics in a qualitative sense using the *Boussinesq approximation*.

One of the benefits of using the *Boussinesq* (or *anelastic*) approximation is that sound waves are not permitted (time derivatives in the continuity equation are absent). Thus, the complicating effects of sound waves, whose frequencies are much higher than those of gravity waves (~ 1 cycle/10 min), in which the mass and wind field mutually respond to each other, and whose time scale is characteristic of severe convective storms (significant changes $\sim O(10$ min)), are not included; it is not expected that sound waves affect storm behaviour. On the other hand, there is evidence that convective storms, and tornadoes in particular, can themselves generate detectable sound waves in the infrasound region (Bedard 2005). Three-dimensional cloud models have been developed, however, that permit sound waves and thus do not make use of the Boussinesq approximation. Numerical procedures such as ‘time-splitting’ have been developed that allow one to include the full effects of compressibility without actually representing all the terms in the model equations at the highest frequencies (Klemp and Wilhelmson 1978, Wilhelmson and Klemp 1978, Skamarock and Klemp 1992): relatively low-frequency processes such as advection and buoyancy are separated from relatively high-frequency, sound-wave propagation processes such as the pressure-gradient force and the divergence, and each are integrated using different time steps. For diagnostic purposes, it is sufficient, though, to use the Boussinesq approximation to examine the major dynamical effects.

Conservation of mass is extended to include water vapour and the various forms of water substance in the following equation:

$$Dq/Dt = -\nabla \cdot (qv) + q\nabla \cdot v + E + S - C - D, \quad (2.11)$$

where q is the specific humidity, E is the evaporation rate per unit mass of moist air, S is the sublimation rate, C is the condensation rate and D is the deposition rate, and the first two terms on the right-hand side come from the advective term. The various types of water substance can be broken down into many more categories (e.g. the deposition and sublimation rates can be specified separately for different types of ice crystals and other forms of frozen water) than those represented in (2.11), which is a highly simplified representation of what actually happens in the atmosphere. Additional equations can be specified for conversion rates from ice to liquid water (e.g. due to melting, etc). Our inability to make *in situ* measurements of cloud particles and hydrometeors everywhere, simultaneously, in a convective storm, for its entire duration, is a major obstacle in our quest to understand completely and to be able to predict, the evolution of convective storms.

2.4. The vorticity equation

It is useful when analysing the dynamics of severe convective storms (and of weather systems in general) to use modified forms of the equations of motion (2.1) and (2.2). A (time-dependent or *prognostic*) vorticity equation can be derived from (2.1) and (2.2) by applying the curl operator to them, so that

$$D/Dt(\nabla \times v) = [(\nabla \times v) \cdot \nabla]v - \nabla \times (\alpha \nabla p') + \nabla \times (Bk), \quad (2.12)$$

where k is a unit vector pointing upwards and $\nabla \times v$ is the three-dimensional vorticity. An advantage of expressing the equations of motion as a vorticity equation is that pressure does

not appear. Thus, it is possible to analyse the circulations in the horizontal plane and in vertical planes without explicitly considering pressure, which is simpler than using (2.1) and (2.2) and having to consider both pressure and wind.

The vertical component of (2.12)

$$D\zeta/Dt = \underset{1}{\partial\zeta/\partial t} + \underset{2}{\mathbf{v}_h \cdot \nabla\zeta} + w\underset{2}{\partial\zeta/\partial z} = -\underset{1}{\delta\zeta} + \underset{2}{\mathbf{k} \cdot (\partial\mathbf{v}/\partial z \times \nabla w)} + \underset{3}{\mathbf{k} \cdot (\nabla p' \times \nabla\alpha_0)} \quad (2.13)$$

where $\zeta = \mathbf{k} \cdot \nabla \times \mathbf{v}$, the vertical component of vorticity, $\delta = \partial u/\partial x + \partial v/\partial y$, the horizontal divergence, x and y are coordinate axes that point to the east and north, respectively, and u and v are the components of the horizontal wind in the x and y directions, respectively. Terms 1 and 2 on the left-hand side of (2.13) (when multiplied by -1) represent horizontal and vertical advection of vorticity, and terms 1, 2 and 3 represent stretching (the divergence term), tilting, and the solenoidal effect. The latter occurs when the atmosphere is baroclinic, i.e. when isobars are not parallel to lines of constant density, so that the pressure-gradient force has a horizontal gradient.

The component of (2.12) along the y axis is

$$D/Dt(\partial u/\partial z - \partial w/\partial x) = \underset{1}{(\partial u/\partial x + \partial w/\partial z)(\partial u/\partial z - \partial w/\partial x)} + \underset{2}{(\partial v/\partial z \partial u/\partial y - \partial v/\partial x \partial w/\partial y)} - \underset{3}{\partial B/\partial x} \quad (2.14)$$

where $\partial u/\partial z - \partial w/\partial x$ is the component of vorticity about the y axis. Term 1 represents the stretching of vorticity about the y axis, 2 represents tilting of vorticity about the z and/or x axes onto the y axis, and 3 represents baroclinic generation. Equations (2.13) and (2.14) are used frequently to analyse convective-storm dynamics.

2.5. The divergence equation

An equation for divergence may be derived from (2.1) and (2.2) by applying the divergence operator to them. Since the flow in a Boussinesq fluid is nondivergent, the divergence equation below is time independent (*diagnostic*, as opposed to *prognostic*):

$$\alpha_0 \nabla^2 p' = -[(\partial u/\partial x)^2 + (\partial v/\partial y)^2 + (\partial w/\partial z)^2 + 2(\partial u/\partial y \partial v/\partial x + \partial w/\partial x \partial u/\partial z + \partial w/\partial y \partial v/\partial z)] + \partial B/\partial z. \quad (2.15)$$

The diagnostic divergence equation is used to compute pressure from the three-dimensional distribution of wind. Thus, the circulations associated with convective storms are computed from the vorticity equation, while the three-dimensional pressure field that is consistent with the circulations is computed from the divergence equation. It is therefore not appropriate to infer that a pressure field *causes* an existing wind field, but rather that it is consistent with it. One can, however, use knowledge of the pressure field to compute pressure-gradient forces that will change the wind field in the future. Both (2.12) and (2.15) are used in tandem to analyse storm dynamics.

If the fully compressible, time-dependent version of the equation of continuity (2.6) were used, then the divergence equation would contain time derivatives (not shown). In nature, sound waves transmit information relating the pressure field to the wind field. By eliminating them, we in effect assume that their speed is infinite, so that information linking the pressure field to the wind field is instantaneous and they are linked by a Poisson equation.

2.6. Ertel's potential vorticity

Another method for analysing convective storm dynamics involves the use of Ertel's potential vorticity Z , which is given as follows:

$$Z = \alpha[(\nabla \times \mathbf{v}) \cdot \nabla s], \quad (2.16)$$

where s is the specific entropy, $s = C_p \ln \theta$, and θ is the potential temperature, which is conserved for adiabatic motions (i.e. $D\theta/Dt = 0$). (If the air is saturated and/or has water substance suspended in it, then θ must be modified.) Potential temperature is the temperature an air parcel would have if brought adiabatically to a reference level and is given as follows:

$$\theta = T(p/p_0)^{R/C_p}, \quad (2.17)$$

where p_0 is the pressure at the reference level, which is usually 1000 hPa. The statement of conservation of potential temperature is equivalent to the adiabatic form of the thermodynamic equation (2.5). In the absence of diabatic heating and molecular and turbulent viscosity, Ertel's potential vorticity is conserved, so that

$$DZ/Dt = 0 = D/Dt[(\nabla \times \mathbf{v}) \cdot \nabla \theta]. \quad (2.18)$$

Conservation of Ertel's potential vorticity is like conservation of angular momentum for rigid bodies: when the gradient of potential temperature decreases (θ surfaces spread farther apart), the fluid contracts and spins up about the axis of the gradient, and vice versa. Equation (2.18) is derived from (2.5), (2.6), (2.12) and (2.16). So, (2.18) can be used to estimate the future three-dimensional distribution of Z , from which, under certain conditions and using appropriate boundary conditions, it is possible to retrieve the temperature and winds fields. In severe convective storms, diabatic heating plays a prominent role, so that Z is not conserved. However, if it is assumed that latent heat of condensation from the formation of cloud material is absorbed by the air parcel (a moist-adiabatic process), then θ may be replaced by θ_e , the equivalent potential temperature, which is conserved for moist-adiabatic processes.

3. Ordinary-cell convective storms

Detailed radar studies of convective storms began during *The Thunderstorm Project* in Florida and Ohio in the late 1940s (Byers and Braham 1949). With the advent of three-dimensional nonhydrostatic cloud models and Doppler radar in the 1970s, significant advances have been made in our understanding of all types of convective storms, regardless of whether or not they produce severe weather.

3.1. Observed structure and life cycle

A convective updraft forms when air is heated and/or lifted so that its condensation level is reached; cloud base is at the condensation level (when the air is simply lifted to its condensation level, without regard to any heating, the condensation level is called the *lifting condensation level* (LCL)). Eventually the leading edge of the rising air in the cloud reaches its equilibrium level (EL), where its buoyancy decreases to zero. Typically, the equilibrium level for convective storms is at the tropopause. The vertical velocity of the rising air (w) may be estimated, using (2.2), as

$$w = (2 \text{CAPE})^{1/2}, \quad (3.1)$$

where CAPE, the convective available potential energy, is the vertically integrated energy acquired by the rising air as a result of the upward buoyancy force acting on it:

$$\text{CAPE} = g_{\text{LFC}} \int^{\text{EL}} B \, dz = g_{\text{LFC}} \int^{\text{EL}} [T_c(z) - T_0(z)]/T_0(z) \, dz \quad (3.2)$$

where the LFC (level of free convection) is the level at which an upward-moving parcel of air first acquires positive buoyancy, $T_0(z)$ is the vertical profile of temperature in the environment of the cloud, and $T_c(z)$ is the vertical profile of temperature inside the cloud. In many instances the LFC is also at cloud base, but not necessarily. The derivation of (3.1) makes use of the assumption that unsaturated air outside the cloud does not dilute the updraft via turbulent mixing at the cloud's edge and (3.1) does not account for precipitation loading or water vapour in the air. In addition, the vertical gradient of the perturbation-pressure field is neglected. Estimates of the vertical velocity in convective storms are typically $\sim O(10 \text{ m s}^{-1})$; in the strongest storms, vertical velocity may exceed 50 m s^{-1} (Musil *et al* 1986, Bluestein *et al* 1988). In nature, there is some *entrainment* of environmental air that decreases the CAPE; the widest updrafts endure the least entrainment. Eventually, precipitation particles in the updraft grow large enough that they acquire a terminal fall speed that allows them to fall back into the updraft, if the environment in which the convective cloud is produced has no or relatively weak vertical wind shear. At this stage, radars detect precipitation suspended aloft. At high levels ice crystals are produced and an anvil forms as the air spreads out laterally where the updraft weakens with height.

Eventually, precipitation loading completely destroys the updraft and a downdraft is produced. A gush of rain hits the ground and both the air and the rain spread out laterally. The life cycle of an 'ordinary-cell' convective storm is less than an hour, the time it takes buoyant air to reach the tropopause and then fall to the ground as precipitation.

The updraft region in a convective storm is called a 'cell'. The same terminology is used to describe the precipitation region detected by a meteorological radar. Since precipitation regions once were associated with an updraft region, a one-to-one correspondence can be made between the updraft cell and the radar-observed precipitation cell, even though in the latter there may not be any updraft remaining.

3.2. Gust fronts in the absence of significant vertical wind shear

When rain falls out into unsaturated air or when unsaturated air is entrained into a region of cloud droplets and/or raindrops, some of the water drops and droplets evaporate and the air is cooled and becomes negatively buoyant. The negative thermodynamic buoyancy, enhanced by the negative buoyancy from water loading, drives a downdraft that hits the ground, where it spreads out laterally. Gustly winds mark the leading edge of the cooler air, which is called a *gust front*.

The amount of cooling behind a gust front depends upon the dryness of the air, the depth over which evaporation takes place, and the sizes of the water drops and droplets. At present, numerical cloud models have difficulty reproducing temperature deficits behind gust fronts accurately, mainly owing to uncertainties in the amount of and droplet size distributions of the precipitation and cloud droplets (Gilmore *et al* 2004, Cohen and McCaul 2006). Droplet size distributions vary according to the origin of the air; for example, droplet size distributions in the tropics are different from those in continental regions of midlatitudes.

In midlatitudes over land, when clouds build upwards into relatively dry environmental air, the potential for evaporative cooling is great and very strong downdrafts and gust fronts are possible. When both the winds and the vertical shear is weak, the downdraft may be

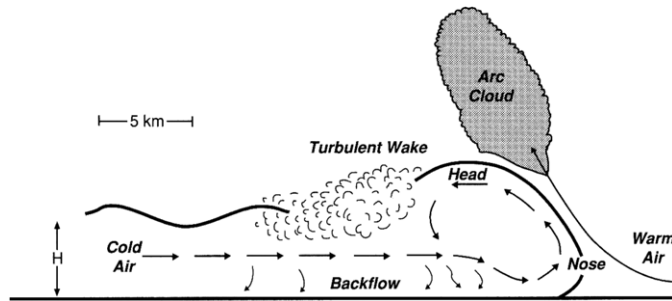


Figure 1. Idealized vertical cross section through a gust front. From Droegemeier and Wilhelmson (1987); adapted from a number of sources.

circularly symmetric and regions of very strong lateral gradients in wind can be produced near the ground, about the centre. Very strong downdrafts that reach the ground are called *microbursts*, which can be very hazardous to aircraft landing or taking off: aircraft that enter a microburst experience a brief period when the airflow is opposite that of the aircraft motion, followed by a brief period when the airflow is in the same direction as that of the aircraft motion. Thus, the aircraft experiences a brief period of enhanced lift, followed by a period of diminished lift. Too much overcompensation for the period of enhanced lift can result in stalling and crashes as the aircraft pulls away from the centre of the microburst. Microbursts may be strong enough to cause ‘straight-line’ wind damage at the surface, especially if the downdraft is intense and narrow and/or if there is a strong-enough component of the ambient wind near the ground.

Microbursts have been classified as being ‘dry’ or ‘wet’ (Wakimoto 2001). Dry microbursts occur over relatively arid terrain when cloud base is relatively high. Thus, the potential for evaporative cooling is great as water drops and droplets fall through unsaturated air for a relatively long time. On the other hand, wet microbursts occur when the atmosphere is relatively moist and cloud base is relatively low, so that the potential for evaporative cooling is relatively small. In this case, negative buoyancy is created mainly from water loading. Cooling from the melting of ice particles on the way down in a region of precipitation may enhance the negative buoyancy in both dry and wet microbursts.

The depth of the ‘pool’ of cold air near the ground is important dynamically, because it determines the motion of the leading edge of the ‘cold pool’. Generally the depth of the cold pool behind a gust front ranges from several hundred metres to several kilometres. The deeper and colder a cold pool is, the greater the hydrostatic pressure excess behind the cold pool. At the leading edge of the cold pool, a hydrostatic pressure-gradient force is directed from the cold side to the warm side. The leading edge of the cold pool then is forced towards the warm air (figure 1). Much of the cold pool moves as a material surface like a ‘density current’.

In the simplest model of a density current, the air behind the gust front is assumed to be at rest and the cold air mass within the cold pool does not mix with the ambient air outside the cold pool. The speed c of the cold pool, in the absence of surface drag is

$$c = K[g(\rho_D - \rho_L)/\rho_L H]^{1/2}, \quad (3.3)$$

where K is an empirical constant $\sim 1-1.5$, H is the depth of the cold pool, ρ_D is the density of the air in the cold pool and ρ_L is the density of the ambient air outside the cold pool. This formula is similar to that for of the phase speed of a shallow-water gravity wave, even though in the case of the latter net mass is not transported forward, while in the case of the former mass is transported forward. Surface drag retards the motion of a density current. In nature, the

top of the cold pool is not necessarily level, the air behind the gust front is not resting, and some dilution of the cold pool occurs when the warmer drier air above it mixed into it as Kelvin-Helmholtz, shear-induced eddies are produced along the interface (Droegemeier and Wilhelmson 1987). The leading edge of a gust front often has a deeper 'head' (figure 1).

In the reference frame of the moving density current, ambient air slows down as it approaches the leading edge and rises up and over the leading edge (figure 1). This upward motion at the leading edge of the density current may be inferred also using the component of the vorticity equation (2.14) that is oriented parallel to the leading edge:

$$D/Dt(\partial u/\partial z - \partial w/\partial x) = -\partial B/\partial x. \quad (3.4)$$

Thus, horizontal vorticity (about the y axis) is generated baroclinically as air encounters the leading edge, so that there is a rising branch just ahead of the leading edge and a sinking branch just behind it.

3.3. Gust fronts in the presence of vertical shear

Typically, in the absence of vertical wind shear, a cold pool will spread out at the surface and no convective cells will be triggered along the periphery of the cold pool in response to the lifting of ambient air. However, if the vertical wind shear vector over the depth of the cold pool is oriented so that the horizontal vorticity vector associated with it has a substantial component in the direction opposite to that of the baroclinically generated horizontal vorticity at its leading edge, then there is a likelihood that air will be lifted enough to reach its condensation level and trigger a new convective cell. This behaviour can be understood in terms of the horizontal vorticity equation (3.4) expressed as

$$\partial/\partial t(\partial u/\partial z - \partial w/\partial x) \approx 0 \approx -u\partial/\partial x(\partial u/\partial z) - \partial B/\partial x. \quad (3.5)$$

When the rate of generation of horizontal vorticity baroclinically is nearly counterbalanced by the advection of horizontal vorticity from vertical shear in the environment, there is a maximum in upward motion along the leading edge of the density current and the probability of the triggering a discrete new cell is increased (figure 2). This theory is known as RKW theory, after Rotunno, Klemp and Weisman, who proposed it in the late 1980s (Rotunno *et al* 1988). The reader is referred, for further details, to Xue *et al* (1997), who numerically investigated the effects of varying the depth of a low-level layer of constant shear (with respect to the depth of the cold pool) and of varying the magnitude of the shear.

A series of ordinary-cell convective storms that form as new updrafts are triggered along the leading edge of the cold pool comprise what is referred to as a *multicell* convective storm/complex. Fovell and Dailey (1995) and Fovell and Tan (1998) have numerically investigated multicell behaviour and have found that new cells grow approximately once every 15 min. The periodic nature of new cell growth is linked to the temporary suppression of new cell growth by sinking motion on the flanks of the existing updraft; these sinking regions are associated with the horizontal circulations induced by the gradient of buoyancy at the edges of the buoyant updraft (see equation 3.4)). When the new updraft has propagated back towards the rear side of the convective complex, if it ever does, then a new updraft may be triggered as the suppression of new cell growth ceases. Also, in some simulations the moist boundary layer is deepened upstream from the region where new convective growth is suppressed and new cell growth is accelerated.

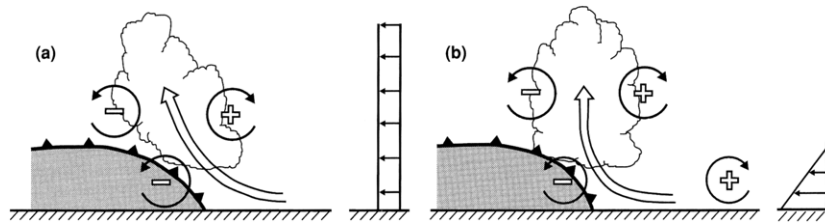


Figure 2. Idealized vertical cross section through a gust front. The cold pool is shaded and its edge is marked by a cold-front symbol. Thick arrows denote gust-front relative air motion. Thin, circular arrows denote sense of horizontal vorticity generated at the edge of the cold pool, generated at the edge of the cloud, and present in the environment. The vertical variation of the environmental wind is shown at the right in each panel. In (a) there is no vertical shear in the environment and the updraft leans towards the cold pool, owing to the generation of horizontal vorticity at the edge of the cold pool; in (b) there is vertical shear in the environment at low levels and the updraft is erect, owing to the counteraction of the environmental vertical shear. From Rotunno *et al* (1988).

4. Supercells

Much has been learned about convective storms from conventional radar observations and more recently from Doppler radar observations, storm chasers, and three-dimensional nonhydrostatic cloud models (Bluestein and Wakimoto 2003, Jorgensen and Weckwerth 2003, Wilhelmson and Wicker 2001, Davies-Jones *et al* 2001, Wakimoto 2001).

4.1. Observed supercell behaviour and early theories

In ordinary-cell convective storms and multicellular complexes, individual cells last only for approximately the duration of time it takes air at low levels to enter into the cloud base, rise through the updraft, and then exit the storm near the tropopause or in precipitation-loaded and/or evaporatively induced downdrafts (the 'advective time scale'). For a storm extending up to the tropopause and for updrafts $\sim 10 \text{ m s}^{-1}$, the advective time scale $\sim 10 \text{ km}/10 \text{ m s}^{-1} \sim 10^3 \text{ s}$, which is roughly consistent with the observed life cycle of $\sim 30\text{--}50 \text{ min}$ of ordinary-cell convective storms, first noted during the Thunderstorm Project in Florida and Ohio in the 1940s (the total time observed includes the 'dissipating stage', when only downdrafts are noted and precipitation material falls to the ground). In the late 1950s and early 1960s, however, a few storms were observed on radar that persisted for much longer periods of time. Furthermore, ordinary cells move along approximately with the pressure-weighted (i.e. mass-weighted) mean wind in the layer in which they are embedded, while the long-lived cells instead propagate to the *right* of the mean wind. Keith Browning named these convective storms *supercells* mainly owing to their longevity (Browning and Donaldson 1963).

Without Doppler radar it was difficult to determine precisely how the wind field in supercells differed from that in ordinary cells. However, it was inferred from analyses of time series of radar reflectivity and analyses of wind data collected from aircraft outside of storms that the main updraft in a supercell rotated (Fujita and Grandoso 1968) and it was suggested that this characteristic was responsible for their 'deviant' motion and at least in part indirectly for their longevity. Some supercells produced tornadoes and it was therefore thought that there is a connection between storm-scale rotation and the much smaller-scale tornado. Early analyses of supercell dynamics drew upon an analogy between the interaction between spinning solid bodies and the airflow around them (Fujita 1965). However, supercells are not solid bodies embedded with the airflow: they are part of the

airflow itself and air circulates up, through them, and then out from them. Furthermore, these early theories did not consider thermodynamics or precipitation microphysics. However, it was recognized that the vertical shear of the wind in the environment of the storm plays an important role.

During a hail project in Alberta conducted in the late 1960s (Chisholm and Renick 1972, Marwitz 1972a, 1972b, 1972c) it was found that supercell storms formed in an environment of much stronger vertical shear than that of ordinary cells and in an environment of stronger shear than that of multicell storms. Early theories correctly pointed out that in supercells, owing to vertical shear, precipitation falls out away from the main updraft, allowing the updraft not to weaken as precipitation falls back into it. It was also suggested that the source of storm-scale rotation in them was due to the tilting of horizontal vorticity in the environment (Barnes 1968, 1970). The horizontal vorticity is associated with the vertical shear of the environmental wind (figure 2).

According to the *thermal-wind relation*, which is a consequence of the observed approximate (*geostrophic*) balance between the large-scale pressure-gradient force and the Coriolis force and of hydrostatic balance, the magnitude of the vertical shear of the geostrophic wind (which is approximately the same as the vertical shear of the total wind, i.e. of the geostrophic + the ageostrophic wind) is proportional to the horizontal gradient of temperature normal to the vertical-shear vector (Bluestein 1992):

$$\partial v_g / \partial z \approx g / f T \mathbf{k} \times \nabla T \quad (4.1)$$

where v_g is the geostrophic wind and f is the Coriolis parameter ($2\Omega \sin \phi$, where Ω is the rotation rate of the Earth about its axis and ϕ is the latitude). Thus, supercells should be found preferentially when there are strong horizontal temperature gradients (e.g. near fronts and baroclinic waves in the upper troposphere) and when there is the potential for strong, buoyant updrafts.

In addition, supercells were found to be prolific producers of large hail (Nelson and Young 1979); the hail was hypothesized to be related to the very strong updraft located in the supercells and to recycling of water substance in and out of the updraft. This strong updraft was inferred from the *weak-echo region* (WER) and *bounded weak-echo region* (BWER) seen in their radar reflectivity pattern, from which it was inferred that large-enough (i.e. radar-detectable) particles did not form until relatively high up in the cloud because it takes a minimum amount of time for cloud droplets to grow into precipitation-size particles and in a very strong updraft, it does not take long for air coming from low altitudes to reach very high altitudes: surrounding the core of the updraft, where the updraft strength was weaker, radar-detectable particles formed at much lower altitude. The high intensity ($\sim 50 \text{ m s}^{-1}$) of updrafts in supercells was confirmed from measurements made by a storm-penetrating, armoured aircraft (Musil *et al* 1986).

4.2. Observed supercell structure

A leap in our understanding of supercells occurred during the 1970s as a result of storm chasers, who documented the visual cloud structure of supercells (figure 3), the advent of the use of Doppler radar which led to detailed depictions of the wind field in supercells (e.g. Heymsfield 1978, Brandes 1978, 1981, 1984, Ray *et al* 1981) and the nearly simultaneous advent of three-dimensional, nonhydrostatic cloud models, that could be used to do controlled experiments (Schlesinger 1975, Klemp and Wilhelmson 1978).

Idealized models (figure 4) and real radar imagery depict the relationship between the main updraft and the two main downdrafts, storm-relative wind flow and radar reflectivity structure

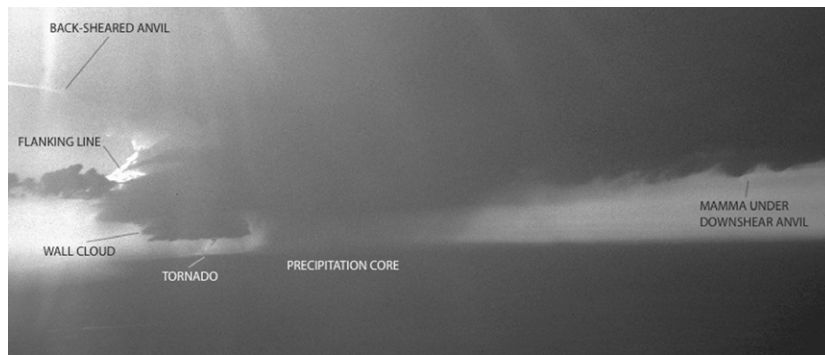


Figure 3. A tornadic supercell, viewed to the west, from a National Ocean and Atmospheric Administration (NOAA) aircraft, in southwest Kansas, on 26 April 1991. Photograph copyright H Bluestein.

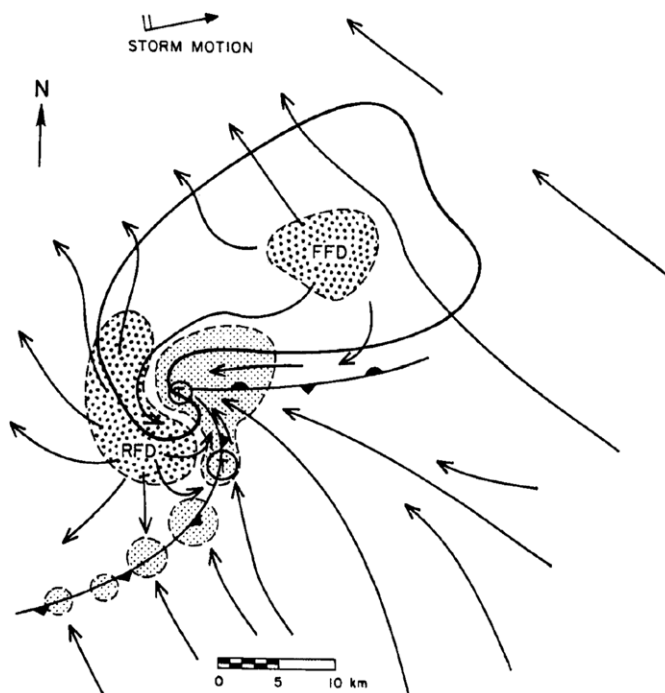


Figure 4. Idealized plan view of a supercell near the ground. The thick line denotes the outer edge of the radar echo. The cold-front symbol denotes the edge of the cold pool. The RFD and FFD are coarsely stippled; updrafts are finely stippled. Tornadoes tend to occur at the locations of the encircled 'Ts'. From Lemon and Doswell (1979).

(figure 5). The main updraft is located within the deepest convective cloud, above a cloud base lowered as a *wall cloud* (figure 3). The wall cloud forms when cooler, but more humid air from the adjacent forward-flank downdraft (FFD) enters the updraft and lowers the condensation level; the lowering of cloud base is *not* caused, to any significant extent, by the lowering of the pressure under cloud base. If the cloud base were lowered as a result of a pressure

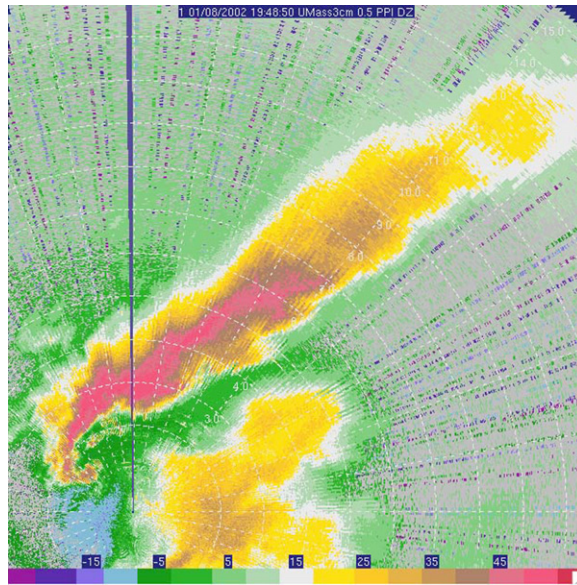


Figure 5. Radar depiction of a tornadic supercell in northeast Kansas on 8 May 2003. Color-coded radar reflectivity is given in dBZ at the bottom of the panel. From the U. Mass, mobile X-band Doppler radar. The hook echo is seen at the lower-left hand side of the panel; the tornado was located at the tip of the hook. Range markers are plotted (in white) every km.

drop, then the wind speeds would be much stronger than what is observed (the necessary drop in pressure to lower the condensation the amount observed would be associated with a very strong horizontal pressure gradient; assuming *cyclostrophic balance*, in which there is a balance between a radially inward-directed pressure-gradient force and an outward-directed centrifugal force, it can be shown that the wind speeds would be unrealistically strong). Tornadoes are frequently observed in the vicinity of the wall cloud. The rear-flank downdraft (RFD) forms and pushes against the gust front that is located adjacent to the *hook echo*, to the rear of the main body of the storm. The *flanking line*, a band of convective clouds adjacent to the tallest cloud towers, which are associated with the main updraft, is often present along the RFD gust front. Since the cloud surface on the downshear side (i.e. in the direction of a vector that represents the difference between the wind vector at an altitude above and the wind vector at an altitude below) of the storm often appears smooth, it is inferred that the air is stable with respect to lifting by a finite upward displacement (the cloud surface would otherwise appear bubbly).

The most intense precipitation is found just downshear from the main updraft (to the right of the wall cloud, when viewed from a location to the right of the direction in which the storm is moving). The most intense precipitation and highest radar reflectivity are frequently co-located with an optically translucent region, while less intense precipitation is located in an optically opaque region, nearby. This observation may be interpreted as meaning that the region of heaviest precipitation is composed of widely scattered, large raindrops and hailstones, and the region of the less intense precipitation is composed of more densely packed smaller raindrops and hailstones.

Storm chasers have noticed that the region behind the RFD is sometimes optically translucent and contains little if any precipitation and the region where there is typically the most intense precipitation is also optically translucent and contains almost no rain, but some

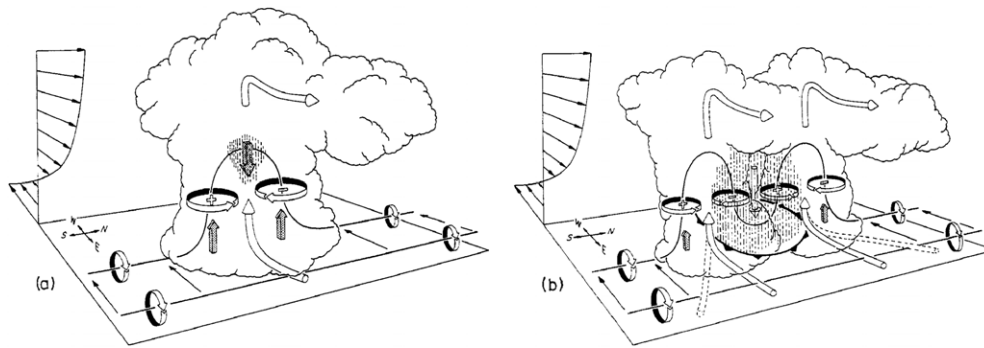


Figure 6. Schematic illustrating how horizontal vorticity pointing to the north (associated with westerly vertical wind shear) is deformed by a convective-storm updraft so that counter-rotating vortices are produced at midlevels (a). Precipitation falls out in between the vortices and new sets of counter-rotating vortices are produced both to the north and south; the convective storm splits into two mirror-image members (b). Shaded arrows denote updrafts and downdrafts. Cold-front symbol in (b) marks the edge of the cold pool. Environmental variation of wind with height is depicted at the southwestern edge of each panel. From Klemp (1987); reprinted with permission from the *Annual Review of Fluid Mechanics*, volume 19 ©1987 by Annual Reviews www.annualreviews.org.

hail. The only rain observed falls out from the anvil, relatively far from the storm's main updraft. Such storms are called low-precipitation (LP) supercells (Bluestein and Parks 1983). On the other hand, the region behind the RFD is sometimes optically opaque and contains an abundance of precipitation and the region where there is typically the most intense precipitation is also optically opaque and contains rain and/or hail. Such storms are called high-precipitation (HP) supercells (Moller *et al* 1990, Doswell *et al* 1990). The LP and HP supercells are the extreme ends of a spectrum of a variation of supercell types in which precipitation efficiency is the variable. The idealized visual model depicts the *classic* supercell, i.e. a supercell in which the precipitation efficiency is greater than that of an LP supercell, but less than that of an HP supercell.

Interesting questions concerning differences in the thermodynamics of LP and HP storms arise in the context of tornado formation and are addressed in a later section. When there is little if any rain, the potential for the production of an evaporatively cooled pool of air near the ground is very low; when there is a lot of rain and it falls out into relatively dry air, the potential for the production of an evaporatively cooled pool of air is very high.

The reason(s) why precipitation efficiency varies so widely in supercells is (are) not known very well because the details of the precipitation processes are not very well understood. However, it has been found from numerical-simulation experiments that when the vertical shear is relatively weak or nonexistent at high levels, ice particles from the anvil can seed growing convective towers in the storm's main updraft, so that precipitation processes are enhanced; when the shear is relatively strong at high levels, ice particles from the anvil are blown far downstream and do not seed the same storm from which the ice particles were formed. Thus, the character of the high-level vertical shear may determine the precipitation efficiency (Rasmussen and Straka 1998). It is possible, however, for ice particles produced in an anvil in environment of strong upper shear to fall out into the updraft of a nearby supercell and seed it, thereby enhancing the precipitation in the adjacent storm. Such a hypothesis may explain why sometimes LP and HP supercells are observed in close proximity (when the environments are similar) or why LP storms sometimes become transformed into HP supercells (Bluestein and MacGorman 1998).

4.3. The production of mid-level rotation

When a buoyant updraft rises in an environment of vertical shear, which represents horizontal vorticity (figure 6), some of the latter is converted into cyclonic (*vertical*) vorticity and some is converted into anticyclonic (*vertical*) vorticity as a result of tilting (cf equation (2.12)) along the edges of the updraft that are situated in a direction normal to the shear vector. We first consider, for simplicity, an atmosphere in which the shear profile (i.e. the vertical variation of the shear) is unidirectional (shear does not change direction with height) and is constant (shear does not vary with height). For westerly wind shear, which according to the thermal-wind relationship (4.1) is associated with a north-to-south directed temperature gradient (cold to the north, warm to the south), a cyclonic vortex will form on the equatorward side of the updraft and an anticyclonic vortex will form on the poleward side. Another way of saying this is that an initially horizontally oriented vortex line (which represents the direction of the three-dimensional vorticity vector) that points to the pole is distorted by the updraft so that it is deformed into an upside-U shape; the vortex line has a component that points upwards on the equatorward side and downwards on the poleward side. Thus, the vertical component of vorticity on the equatorward (poleward) side has a component in the direction of (in the direction opposite to that of) the rotation vector of the Earth.

Another way to analyse the production of vertical vorticity in a vertically sheared environment by an updraft is to make use of the conservation of potential vorticity (2.18) (Davies-Jones 1984). If diabatic heating and friction are ignored, then potential vorticity is conserved. When air approaches and enters the updraft at low levels from the equatorward side, it begins with its vorticity vector pointing towards the pole. It is assumed that in the environment the potential temperature increases with height (this configuration represents a gravitationally stable atmosphere). Then, the potential-vorticity vector is zero because the potential-temperature gradient vector is normal to the vorticity vector, and according to (2.16) must always remain zero. However, since potential temperature is conserved for adiabatic and frictionless processes (2.18), the updraft distorts the potential-temperature field so that it bulges upwards (figure 7). Thus, there is now a component of potential-temperature gradient that is directed radially outward from the updraft. It is therefore seen that the three-dimensional vorticity vector must change from being directed from the equator to the pole to having a component directed vertically: in particular, on the equatorward (poleward) side of the updraft the potential-temperature gradient vector becomes oriented upwards and towards the equator (pole). Thus, in order that the potential-vorticity vector remain zero, the vorticity vector must become directed upwards and poleward on the equatorward side and downwards and poleward on the poleward side. In nature, the atmosphere becomes saturated before it becomes buoyant, so that equivalent potential temperature rather than potential temperature is a relevant component of potential vorticity. When air enters the updraft at low levels from the western side, i.e. when the storm-relative wind vector is oriented in the direction normal to the vorticity vector, there is 'crosswise' vorticity (figure 7(b)). When air enters the updraft at low levels from the southern side, i.e. when the storm-relative wind vector has a component in the direction of the vorticity vector, there is 'streamwise' vorticity (figure 7(c)). The problem of determining what controls updraft-relative motion will be considered subsequently. When there is streamwise vorticity, the storm updraft and vertical vorticity are correlated, so that low-level convergence tends to enhance the vorticity.

In nature, cyclonic-anticyclonic couplets are observed in Doppler radar observations of the midlevels of supercells (figure 8). When a Doppler radar scans a supercell at midlevels, the signature of a cyclonic-anticyclonic couplet is noted. These cyclonic-anticyclonic couplets are

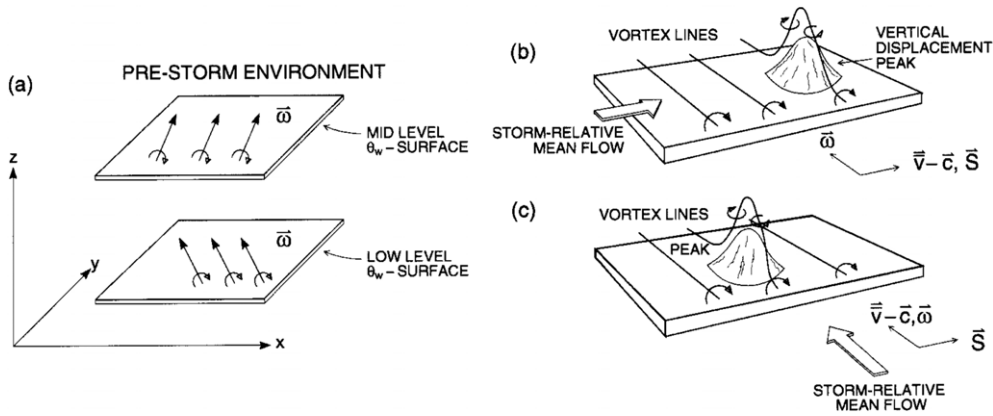


Figure 7. Idealized depiction of how conservation of potential vorticity can show how streamwise and crosswise vorticity can be produced by the deformation of isentropic surfaces by an updraft in an environment of vertical wind shear. In (a) the isentropic surfaces are undisturbed (and horizontal). In (b), counter-rotating vortices are produced when the updraft deforms an isentropic surface into a mountain shape, but the storm-relative wind is normal to the vorticity vector everywhere; in (c), the storm-relative wind has a component in the direction of vorticity vector everywhere. From Davies-Jones *et al* (2001), which was adapted from Davies-Jones (1984).

usually most pronounced at midlevels because (1) updrafts in supercells are strongest at upper levels in the troposphere, so that the horizontal vertical-velocity gradients are also strongest there and (2) vertical shear is usually strongest in the lower half of the troposphere. The net result is that the tilting of horizontal vorticity is strongest at midlevels. When these vortices are intense and long lived they are called *mesocyclones* and *mesoanticyclones*; the mesocyclones are usually the focus of attention rather than the mesoanticyclones because they are associated more frequently with severe weather (Donaldson 1970, Stumpf *et al* 1998).

4.4. Interaction of vertical shear and buoyancy: linear and nonlinear pressure effects

In the previous section the vorticity equation was used to explain the formation of a counter-rotating vortex pair when a strong updraft interacts with horizontal environmental vorticity. The divergence equation (2.15) is now used to examine the effects of the interaction of the buoyant updraft with environmental vertical shear on the pressure field. It turns out these counter-rotating vortices play an important role in updraft propagation. An analysis of (2.15) can be used to explain how and why supercell updrafts propagate because regions of upward-directed perturbation-pressure gradients promote upward accelerating air that can lead to updraft production, while downward-directed regions of perturbation-pressure gradients promote downward decelerating air that suppress updraft production and promote downdraft production. The propagation velocity of updrafts can be determined by using Petterssen's formula for the motion of the extrema of scalar fields (Petterssen 1956, Bluestein 1992, Davies-Jones 2002), which depends on the horizontal gradient of the field of the vertical-perturbation-pressure gradient. It was noted earlier in a discussion of potential-vorticity conservation that updraft propagation is very important because it is an important contributor to streamwise vorticity and vertical vorticity production. Updraft propagation can also be used to explain the longevity of supercells and the production of strong, low-level vortices, as will be shown subsequently.

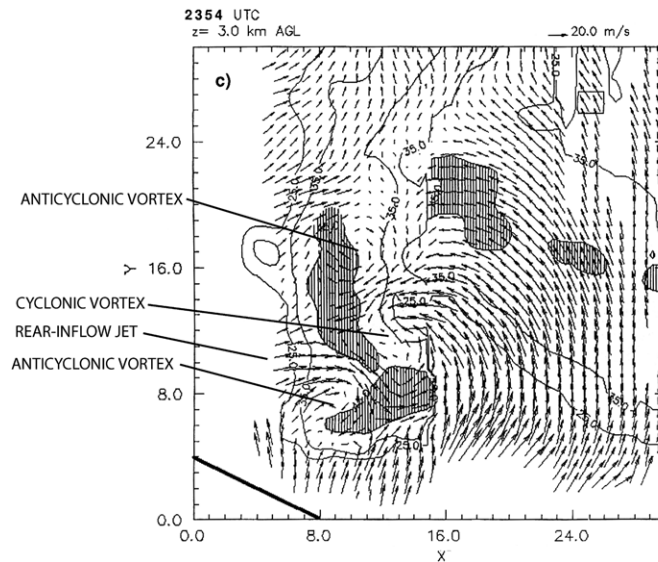


Figure 8. Analysis of the wind field (vectors) and radar reflectivity (solid lines, in dBZ) in a non-tornadic supercell on 22 May 1995 in the eastern Texas Panhandle, at 3 km above the ground. Areas of reflectivity in excess of 45 dBZ are shaded. Tick marks denote 1 km spacing. Synthesized from data from an airborne Doppler radar during VORTEX (Verifications of the Origin of Rotation in Tornadoes Experiment); adapted from Bluestein and Gaddy (2001).

The right-hand side of the divergence equation (2.15) may be expressed as

$$-[(\partial u/\partial x)^2 + (\partial v/\partial y)^2 + (\partial w/\partial z)^2] - 1/2[|D_s|^2 - |\omega|^2] + \partial B/\partial z,$$

where $|D_s|$ is magnitude of the resultant three-dimensional deformation and $|\omega|$ is the magnitude of the three-dimensional vorticity (ω). Thus, the shape of the three-dimensional pressure field is determined to some extent by terms involving vertical and horizontal shears of each component of the wind, including deformation and vorticity. With proper boundary conditions, the pressure field can be determined. Since the operator on the left-hand side of (2.15) is a (3D) Laplacian, the sign of each forcing function on the right-hand side of (2.15) is of the opposite sign of the contribution to pressure from each one.

To isolate the effects of the updraft on its environment, each variable is expressed in terms of the environmental (mean) value and the perturbation (primed) storm value. Thus,

$$u = U(z) + u'(x, y, z, t), \quad (4.2)$$

$$v = V(z) + v'(x, y, z, t), \quad (4.3)$$

$$w = w'(x, y, z, t). \quad (4.4)$$

In (4.2)–(4.4) it is seen that the environmental horizontal wind field \mathbf{V} is chosen, for simplicity, to be horizontally homogeneous, varying only as a function of height, and the vertical environmental wind field is zero (i.e. ‘resting’). The storm-related wind field, however, varies as a function of three-dimensional space and time. In nature, there are inhomogeneities in the environmental wind field, but they are neglected and usually are considered to be second-order effects. Also, there is often a band of mesoscale ascent where convective storms are triggered, but the speed of the ascending air (e.g. along fronts, outflow boundaries, etc) ($\sim 1 \text{ m s}^{-1}$) is an order of magnitude less than that of buoyant updrafts ($\sim 10 \text{ m s}^{-1}$).

Thus, using (4.2)–(4.4), it is seen that (2.15) may be expressed as

$$\begin{aligned} \alpha_0 \nabla^2 p' = & -[(\partial u'/\partial x)^2 + (\partial v'/\partial y)^2 + (\partial w'/\partial z)^2] \\ & -2(\partial u'/\partial y \partial v'/\partial x + \partial w'/\partial x \partial u'/\partial z + \partial w'/\partial y \partial v'/\partial z)] \\ & -2[\partial w'/\partial x \partial U/\partial z + \partial w'/\partial y \partial V/\partial z] + \partial B/\partial z \end{aligned} \quad (4.5)$$

The terms on the right-hand side not involving buoyancy are separated into the following linear terms

$$2[\partial w'/\partial x \partial U/\partial z + \partial w'/\partial y \partial V/\partial z] = -2\partial \mathbf{V}/\partial z \cdot \nabla w' \quad (4.6)$$

and nonlinear terms

$$\begin{aligned} & -[(\partial u'/\partial x)^2 + (\partial v'/\partial y)^2 + (\partial w'/\partial z)^2] \\ & +2(\partial u'/\partial y \partial v'/\partial x + \partial w'/\partial x \partial u'/\partial z + \partial w'/\partial y \partial v'/\partial z)] \end{aligned}$$

(Rotunno and Klemp 1985). The nonlinear terms proportional to $[(\partial u'/\partial x)^2 + (\partial v'/\partial y)^2 + (\partial w'/\partial z)^2]$ are called the *fluid extension terms* and the nonlinear terms proportional to $[(\partial u'/\partial y \partial v'/\partial x + \partial w'/\partial x \partial u'/\partial z + \partial w'/\partial y \partial v'/\partial z)]$ are called the *shear terms*.

To interpret physically the terms on the right-hand side of (4.5) more easily, the perturbation pressure p' is decomposed as follows:

$$p' = p'_{\text{dyn}} + p'_b \quad (4.7)$$

where p'_{dyn} and p'_b represent the perturbation pressure associated with dynamic effects (the wind field) and with buoyancy, respectively. In turn, the dynamic perturbation pressure is decomposed as follows into linear and nonlinear parts,

$$p'_{\text{dyn}} = p'_L + p'_{\text{NL}} \quad (4.8)$$

The nonlinear shear terms in (4.5) can be expressed as the following:

$$- [(\partial u'/\partial x)^2 + (\partial v'/\partial y)^2 + (\partial w'/\partial z)^2] - 1/2[|D'_{3d}|^2 - |\omega'|^2], \quad (4.9)$$

which represents deformation and vorticity (Bluestein 1993). In particular,

$$D'^2_{3d} = (\partial w'/\partial y + \partial v'/\partial z)^2 + (\partial u'/\partial z + \partial w'/\partial x)^2 + (\partial v'/\partial x + \partial u'/\partial y)^2 \quad (4.10)$$

where D'^2_{3d} is the square of the resultant deformation of the perturbation three-dimensional wind when the axis-of-dilatation/axis-of-contraction is aligned at a 45° angle from the x in the x - y , x - z and y - z planes and

$$|\omega'|^2 = (\partial w'/\partial y - \partial v'/\partial z)^2 + (\partial u'/\partial z - \partial w'/\partial x)^2 + (\partial v'/\partial x - \partial u'/\partial y)^2, \quad (4.11)$$

where ω' is the vorticity vector of the perturbation three-dimensional wind field. The forcing function involving vorticity alone is called *spin* (Davies-Jones 2000).

Davies-Jones (2002) has proposed that the nonlinear terms be decomposed slightly differently; the sum of the fluid extension and shear terms (Rotunno and Klemp 1985) involving deformation are called *splat*; the remaining terms are the *spin*. Davies-Jones (2002) argued that this decomposition is more physical because the terms are invariant with respect to rotations of the coordinate axes. For the purposes of understanding supercell dynamics, the Rotunno and Klemp (1985) decomposition is considered here, owing to its simplicity.

The fluid extension part of the nonlinear term contributes to positive perturbation pressure and the deformation part contributes to positive perturbation pressure, while the spin part contributes to negative perturbation pressure, because the forcing functions associated with the fluid extension and deformation are each positive definite, while that associated with spin is negative definite. The main nonlinear effects are therefore as follows: regions of sharp

gradients in the wind field or strong deformation are associated with positive perturbation pressure. Regions of strong vorticity (cyclonic or anticyclonic), are associated with negative perturbation pressure; cyclones and anticyclones are therefore associated with centres of negative perturbation pressure.

Ordinary-cell convective storms are dominated by the behaviour of the buoyancy term in the vertical equation of motion. It can be seen from the vertical equation of motion (2.2), the equation of continuity (2.7), and (3.1) that the effects of the vertical-perturbation-pressure term become comparable to and exceed the effects of buoyancy when

$$R = \text{CAPE}/[1/2U^2] < 1, \quad (4.12)$$

where R is the *Bulk Richardson number* (Weisman and Klemp 1982) and U is the scale of the horizontal wind associated with the storm (i.e. the perturbation component, not that of the environment). From (4.12) it is seen that the dynamics of the convective storm include the dynamical effects of the storm-related (perturbation) wind field when the kinetic energy associated with the storm-related horizontal wind is greater than the buoyant energy in the updraft. If the horizontal momentum of air flowing into the storm's updraft is approximately conserved as it rises up into the storm without mixing with environmental air, then the perturbation horizontal wind velocity at any level is just given by the vector difference between the environmental wind at that level and the wind in the sub-cloud boundary layer. So, the scale of the horizontal component of the perturbation wind (U) is a measure of the vertical shear of the environmental wind (multiplied by the difference between the altitude of the level and the mean altitude of the sub-cloud boundary layer). In other words, R is small and the vertical-perturbation-pressure-gradient force is comparable to or greater than the buoyancy force when the vertical shear is large compared with the CAPE. Severe-storm forecasters use this criterion to determine whether or not supercell convection is possible.

It is seen in numerical-simulation experiments that the upward forcing due to the vertical-perturbation-pressure-gradient force is sometimes even greater than that due to buoyancy, especially at low levels where the buoyancy is relatively high and when the vertical shear is very strong, as it sometimes, for example, in the environment of landfalling hurricanes (McCaul and Weisman 1996). Storms in landfalling hurricanes can have dynamically driven updrafts that are as strong as those in the Great Plains.

It is possible that R can be small when the CAPE is very low and the vertical shear is not very strong, but when the CAPE is low the buoyancy is also low and consequently so is the vertical-perturbation-pressure gradient force itself. When the shear is extremely strong, even though the CAPE is relatively high, but R is small, it is difficult for a convective storm to develop because initially the shear makes the updraft lean over so much that the top of the storm may become detached from the updraft. It is easily seen that the nonlinear effects dominate over the linear effects when $R < 1$. When $R \sim 1$, both the nonlinear and linear effects are of the same magnitude (Davies-Jones 2002).

To analyse the dynamics of convective storms when an updraft interacts with vertical shear, it is easiest first to consider an environment characterized by a hodograph (plot of wind versus height that is represented by the locus of points marked by the tip of the wind vectors at each height, with each wind vector plotted at a common origin). When the hodograph is straight, the vertical shear vector always points in the same direction; when the hodograph is curved, the vertical shear vector changes direction with height. A straight hodograph may be associated with a wind profile in which the wind direction changes with height, even though the vertical-shear direction does not vary with height. It is assumed in the following analyses that $R < 1$, so that the effects of the vertical-perturbation-pressure-gradient force are comparable to that of buoyancy and that the buoyancy is substantial.

4.4.1. Convective-storm dynamics for straight hodographs. At the onset of convection, a buoyant updraft in an environment of strong vertical shear, most of which is concentrated in the lower half of the troposphere and that does not change direction (or magnitude) with height produces a couplet of counter-rotating vortices that are strongest at midlevels (figure 8); in the Northern Hemisphere, the cyclonic (anticyclonic) member is found to the right (left) of the updraft with respect to the vertical shear vector. Perturbation low-pressure areas are associated at midlevels with each of the vortices (the nonlinear spin). Since the vortices are strongest at midlevels and the perturbation-pressure deficit is proportional to the square of the perturbation (storm-related) vorticity (4.9), upward-directed perturbation-pressure forces are found in lower levels, below the altitude of the strongest vorticity. Thus, new updrafts may be triggered off-shear from the original updraft.

In the absence of any precipitation, the updraft splits into two parts; each new updraft then acts on the environmental shear to produce two new updrafts on each flank of the split updrafts; the process continues so that the two outer updrafts propagate to the right and left of the shear vector, respectively. The inner updrafts are likely to be situated in a region where precipitation falls, where there is evaporative cooling, and consequently the original updraft decays; in the absence of precipitation, these inner updrafts will propagate towards each other. The net result is that the updrafts following the original updraft split and propagate apart. Such behaviour is observed in radar imagery and in numerical simulations.

In nature, straight (or nearly straight) hodographs are frequently found above the boundary layer, but not in the boundary layer itself, owing to turbulent friction. The vertical variation of vertical shear in the well-known Ekman profile has a marked change in direction with height (e.g. Bluestein 1992).

When $R \ll 1$, the linear effects are not as great as the nonlinear effects, so that the former are regarded as modifying the behaviour as prescribed by nonlinear dynamics. From (4.6) it is seen that upshear (downshear) from an updraft the perturbation pressure is relatively high (low). When the hodograph is straight and most of the shear is below midlevels, and when the updraft increases with height, then there is an upward- (downward-) directed perturbation-pressure-gradient force on the downshear (upshear) side. Thus, the linear effects of shear interacting with an updraft are to trigger convection on the downshear side and suppress it on the upshear side (figure 9(a)).

4.4.2. Convective-storm dynamics for curved hodographs. When the hodograph is curved and R is not too small, the dynamics of the convective storm are dominated by the linear term. Suppose a hodograph turns 180° in the clockwise direction, with height (figure 9(b)). It is seen from this figure that there is an upward- (downward-) directed perturbation-pressure-gradient force on the right (left) side ('right' and 'left' refer to the concave and convex sides of the hodograph, respectively). Thus, the linear term favours enhancement of updraft propagation to the right of the hodograph and suppresses updrafts on the left side. When the hodograph turns 180° in the counterclockwise direction with height (not shown), the linear term favours enhancement of propagation to the left of the hodograph. In nature, hodographs tend more often to curve in the clockwise direction with height in regions where there is potential buoyancy (Bluestein and Banacos 2002).

In the limit of a completely (clockwise-turning) circular hodograph (Beltrami flow), the cyclonic vortex becomes nearly coincident with the updraft, so that nonlinear propagation becomes negligible, while the linear effects cause propagation towards the concave side of the hodograph. In nature, hodographs frequently have both curved and straight sections.

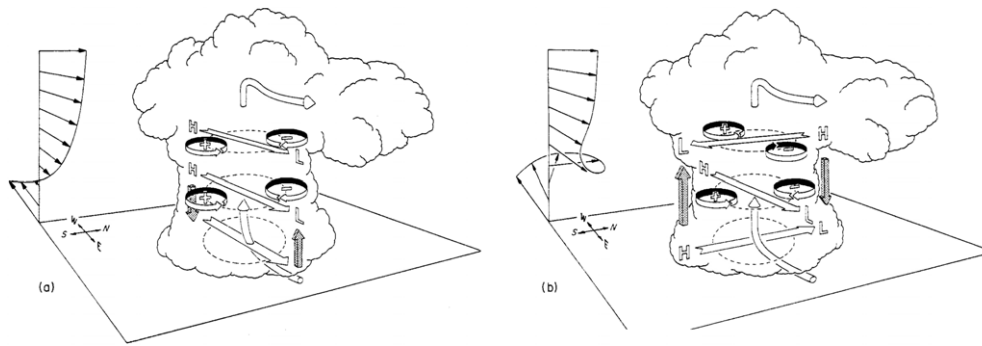


Figure 9. As in figure 6, but the unshaded, flat arrows indicate the horizontal pressure-gradient force, which is directed from relatively high (H) pressure to relatively low (L) pressure. The storm-relative airflow is indicated by the round, unshaded arrows. In (a) the vertical shear vector points to the east (i.e. is westerly) at all levels; in (b) the vertical shear vector turns from southerly at low levels, to westerly at midlevels, to northerly at higher levels. The horizontal pressure-gradient force in (a) is directed towards the east (i.e. is westerly) at all levels; in (b) it turns from southerly at low levels, to westerly at midlevels, to northerly at higher levels. In (a) there is an upward-directed (downward-directed) pressure-gradient force on the downshear (upshear) side of the storm; in (b) there is an upward (downward) directed pressure-gradient force on the right (left) side of the storm, with respect to the vertically averaged vertical-shear vector. From Klemp (1987); reprinted with permission from the *Annual Review of Fluid Mechanics*, volume 19 ©1987 by Annual Reviews www.annualreviews.org.

4.4.3. Straight versus curved hodograph dynamics: two paradigms. In the past two decades, the dynamics of supercells have been explained using two main approaches (Weisman and Rotunno 2000): (a) the ‘vertical shear perspective’ and (b) the ‘helicity approach’. In the former, the main idea is that the storm propagates because the storm is rotating; in the latter, the main idea is that storm generates rotation because it is propagating. According to the vertical shear perspective, the basic physical processes responsible for supercell behaviour are the tilting of environmental horizontal vorticity and the subsequent propagation owing to the rotation-produced (nonlinear effect) and turning of the hodograph with height (linear effect).

According to the helicity approach, which was sparked by the hypothesis that helicity, which is given by

$$H = \mathbf{v} \cdot \boldsymbol{\omega} \quad (4.13)$$

suppresses turbulent dissipation (Lilly 1986) (so that storms having relatively high helicity, i.e. rotating updrafts, are more long lived), is that an updraft that propagates normal to the mean shear vector will preferentially develop cyclonic (anticyclonic) rotation if it moves to the right (left) of the shear vector (Davies-Jones 1984). This analysis is based on a study of the frictionless vertical vorticity equation for a Boussinesq atmosphere, linearized about a basic state in which there is vertical shear of the horizontal wind. A measure of the correlation between the updraft and the vertical vorticity is given by the storm-relative environmental helicity (SREH), which is similar to (4.13), except that \mathbf{v} replaced by the storm-relative value of \mathbf{v} . In practice, the SREH is usually integrated over h , the depth of the ‘inflow layer’ of the storm, which is often assumed to be 3 km:

$$\text{SREH} = \int_0^{3 \text{ km}} \mathbf{v}_{\text{rel}} \cdot (\nabla \times \mathbf{v}) \, dz. \quad (4.14)$$

When the SREH is relatively high, then the environment is deemed to satisfy a necessary condition for storm rotation (Davies-Jones *et al* 1990). From (4.14) it can be shown that the

magnitude of SREH is given by twice the area swept out by the storm-relative wind vector between the ground and height h (3 km). Thus, even if the hodograph is straight, the SREH is high if the updraft movement is far off the hodograph.

If a convective-storm updraft moves along with the mean wind and the hodograph is straight, there is no SREH. If the updraft propagates off the shear vector, then SREH develops. If the vertical shear vector at all altitudes is normal to the storm-relative wind as it is when there is a perfectly circular hodograph, then SREH is the highest. The problem with the helicity approach is that storm motion is not yet predictable from theory. In addition, storm motion is often influenced by the movement of its own gust front, which depends to some extent on cloud microphysics parameters and by factors external to the storm such as the motion of outflow boundaries, fronts, the dryline, and orography. An empirical technique for predicting storm motion that blends theory with observations is given by Bunkers *et al* (2000).

4.4.4. Sensitivity of simulated supercell structure to environmental thermodynamic and cloud microphysics parameters. While the overall behaviour of supercells can be explained qualitatively based on idealized soundings (i.e. on idealized vertical profiles of vertical wind shear and CAPE), significant differences in storm morphology (e.g. in the degree of surface cold outflow) and intensity (updraft speed, peak midlevel and surface vorticity) are found, especially when the CAPE is relatively low. McCaul and Weisman (2001) described variations in numerically simulated storm behaviour that correspond with variations in the altitude of maximum potential buoyancy. In most supercells in the Plains of the US, the CAPE is relatively high ($>1500 \text{ J kg}^{-1}$) and the level at which potential buoyancy is highest is around 6–10 km AGL. When CAPE is relatively low ($<1000 \text{ J kg}^{-1}$) and is concentrated at low levels, then the potential buoyancy at low levels can match the shear better (in the sense that $R \sim 1$ for buoyancy and shear at low levels); when the shear is relatively weak and is concentrated at low levels, the shear at low levels can match the CAPE better at low levels. Thus, supercells can occur that are relatively shallow, as in landfalling hurricanes (McCaul 1991, 1993) and in some midlatitude storms (Kennedy *et al* 1993, Monteverti and Quadros 1994, Knupp *et al* 1998). In these storms, the potential buoyancy is highest around 3 km AGL.

Gilmore and Wicker (1998) found that numerically simulated supercells have stronger surface outflow when the midtroposphere is relatively dry; when the shear is strong or when the dryness is concentrated at higher altitudes, however, this effect is less. The potential for evaporatively cooled downdrafts increases with increasing dryness, especially when the vertical shear is not too strong. Strong downdrafts are detrimental to storm longevity: when the surface outflow moves at the same speed as the updraft and midlevel mesocyclone, then storms can persist and intensify; when surface outflow moves faster than the updraft and midlevel mesocyclone, then storms weaken.

McCaul and Cohen (2002) found that the depth of the environmental, moist, boundary layer also significantly affects numerically simulated supercell morphology and behaviour. Such numerical experiments have relevance to explaining contrasting supercell behaviour in the relatively moist environments of the Central Plains of the US from that in the relatively dry environments of the High Plains. For example, in the former, the LCL and LFC are relatively low, while in the latter the LCL and LFC are relatively high. Therefore, the potential for evaporative cooling near the surface is higher in the latter case, since precipitation has farther to fall through a layer of unsaturated air; so, the dynamics of the cold pool play a more important role in storm behaviour. An interesting finding is that under some circumstances, storms in a low-CAPE environment may be more intense than storms in a high-CAPE environment, owing to vertical-perturbation-pressure gradients that act to enhance updraft intensity.

Gilmore *et al* (2004) and Cohen and McCaul (2006) have explored the effects of microphysical parametrizations on numerically simulated supercell behaviour. When the amount of rainfall is high relative to the amount of ice material, the evaporation is higher and colder surface cold pools may be generated, thus decreasing the likelihood of storm longevity.

From the studies of the effect of dryness and microphysics, it is concluded that knowing the behaviour of supercells is influenced not only by the vertical shear and CAPE, but also on the intensity of the surface cold pool and its effect on decoupling surface features from those aloft that are not affected by the cold pool.

4.5. The deep convergence zone (DCZ)

Supercells sometimes contain counter-rotating vortices at midlevels that are not necessarily created by the tilting of environmental horizontal vorticity (vertical shear) by the main updraft in the storm. They may be created by a downdraft acting on the environmental shear, or more likely by the updraft along the flanking line band, acting on baroclinically generated horizontal vorticity at the leading edge of the rear-flank gust front. In either case, an anticyclonic member of a couplet is found at midlevels along the right flank of the flanking line/rear-flank gust front, while a cyclonic member is found in the usual location (the southernmost and middle vortices, respectively, in figure 8) (Bluestein and Gaddy 2001). In this case, a strong *rear-inflow jet* may be nestled in between the anticyclonic and cyclonic members of the couplet. The structure and dynamics of this rear-inflow jet and vortex couplet may be similar to that of those found in mesoscale convective systems, to be discussed in more detail in section 5. To the best of the author's knowledge, there have not yet been any detailed numerical-simulation studies of the DCZ.

At the leading edge of the jet, there is a curved band of strong convergence. Typically there is a curved band of convergence at low levels along the flanking line, rear-flank gust front. When the band extends up to the midtroposphere (and perhaps higher), it is referred to as a deep convergence zone (DCZ) (Lemon and Parker 1996). There may be a vertical wall within which there is substantial mixing.

Another anticyclonic vortex may be found, paired with the cyclonic vortex, but on the left side of the mean vertical shear vector (the northernmost anticyclonic vortex in figure 8). This vortex is formed through tilting by the updraft of environmental shear (as described earlier). The net effect of all the tilting is that there can be a triad of vortices at midlevels of anticyclonic–cyclonic–anticyclonic vortices, with increased distance to the right of the vertical shear vector.

4.6. The production of low-level rotation

The production of mesocyclones in supercells at *midlevels* in the troposphere has been explained as a consequence of the tilting of environmental vertical vorticity along the edges of the main updraft. This explanation cannot explain how mesocyclones form at *low levels* because on a level surface vertical velocity must vanish, as a consequence of the kinematic lower-boundary condition. It has therefore been proposed that vertical vorticity at the surface could be that produced aloft and advected downwards by a downdraft (Davies-Jones and Brooks 1993, Walko 1993, Wicker and Wilhelmson 1995, Markowski *et al* 2003).

Low-level mesocyclones have also been explained as forming from baroclinically generated horizontal vorticity that has been tilted as air approaches the updraft (Rotunno 1981, Klemp and Rotunno 1983, Rotunno and Klemp 1985). Wicker (1996), however, demonstrated numerically how low-level, *environmental*, horizontal vorticity in the form of low-level shear

also affects low-level mesocyclogenesis. In short, the mechanisms for low-level and mid-level mesocyclogenesis are different. However, the two may interact, and this interaction will be discussed in a subsequent section on tornadogenesis.

Low-precipitation supercells do not have strong surface cold pools, owing to the lack of evaporation of raindrops. It would not be expected, then, that they have strong low-level mesocyclones unless there is strong, pre-existing horizontal vorticity in the boundary layer.

4.7. *The life cycle of the mesocyclone and cyclic mesocyclogenesis*

The degree of steadiness of the main updraft in supercells is an aspect of their behaviour that has been analyzed and discussed for many years (e.g. Browning 1965). It has been found, from both numerical-simulation studies and observational studies, that supercell updrafts are not as steady as had once been postulated. While multicell convective storms exhibit pulses in updrafts, sometimes at quasi-regular intervals (e.g. Fovell and Dailey 1995), supercells do also. At one end of the spectrum are supercells in which the updraft remains intense, but undergoes some slight variations in intensity, along with relatively long-lived mesocyclones.

At the other end of the spectrum are supercells in which discrete mesocyclones, particularly at low levels, periodically form and undergo well-defined life cycles (Burgess *et al* 1982, Adlerman *et al* 1999, Adlerman and Droegemeier 2002, 2005, Beck *et al* 2006). Such behaviour is called *cyclic mesocyclogenesis*. During surface mesocyclogenesis, the mesocyclone at low levels may become stronger than or not exactly coincident with the centre of the mesocyclone aloft, so that a downward-directed, dynamically driven, perturbation-pressure gradient forms and forces a downdraft, the rear-flank downdraft (RFD). Evidence for the rear-flank downdraft is also found in photographs, movies, and videos of the cloud base associated with a low-level mesocyclone, in which the disappearance of cloud material and a 'clear slot' are seen (Lemon and Doswell 1979). It is also likely that evaporative cooling and/or precipitation loading may also play a role in the RFD. Eventually, air from the rear-flank downdraft reaches the ground and curves around the mesocyclone, effectively cutting off the supply of ambient, moist, relatively warm, potentially buoyant air into the main updraft of the supercell. Such a process has been referred to as an *occlusion*, analogous to the occlusion process in synoptic-scale, extratropical cyclones (Bluestein 1993). The RFD downdraft is therefore also sometimes referred to as the *occlusion* downdraft. The curved, bulging nature of the leading edge of the RFD produces a curved band of convergence and rising motion along it, which is shaped like a horseshoe, or letter 'U'. The separation of the mesocyclone at low levels into a region of rising motion from one of sinking motion has been termed its 'divided structure'.

Following the occlusion, a new mesocyclone may form along the rear-flank gust front, and the periodic behaviour may continue. Adlerman and Droegemeier (2002, 2005) have studied cyclic mesocyclogenesis numerically and have shown how sensitive it is to the environmental conditions. It is easily seen how the intensity of the cold pool produced by the storm, if any, plays a role in whether or not there is cyclic mesocyclogenesis.

4.8. *Supercell structure and behaviour in relation to inhomogeneities in the environment, and interactions with neighbouring storms and surface boundaries*

In most numerical studies of supercell behaviour, the simulated supercell is isolated and embedded in a homogeneous environment. Richardson *et al* (2000), in considering the influence of horizontal variations in vertical shear and low-level moisture on convective-storm

behaviour, found that they can have significant effects. Variations in low-level moisture can affect the location, timing and intensity of new cell development. When vertical shear is strong, a convective storm may survive if even if it moves into a region too dry to support convective initiation.

There are also some distinctively different behavioural aspects of supercell behaviour that are related to the supercell's interaction with neighbouring storms and boundaries, and its movement across surface boundaries.

4.8.1. Neighbouring cell interaction. Even when the environment is favourable for the formation of a supercell, i.e. when the vertical shear and CAPE are matched so that the bulk Richardson number is within the range such that vertical-perturbation gradients are significant and vortices form, a supercell may not necessarily evolve from convective storms that are initiated. In some instances, when convective storms are initiated along a surface boundary, neighbouring cells may interact with each other so that supercells cannot evolve (Bluestein and Weisman 2000) (figure 10).

When relatively widely spaced convective storms are initiated along a boundary, the orientation of the boundary with respect to the mean vertical shear in the lower half of the troposphere matters. If the boundary is oriented normal to the mean shear vector, then convective storms split into right- and left-moving members and adjacent left- and right-moving cells collide with each other. Only the right moving, cyclonically rotating member at the right end of the line (facing the direction of the shear vector) and the left moving, anticyclonically rotating member at the left end of the line do not interact with their neighbours and can behave like isolated supercells. If the boundary is oriented along the mean shear vector, then left moving, anticyclonically rotating supercells move across the boundary into cooler and/or drier air and decay. With the exception of the cell on the downshear side of the boundary, right moving, cyclonically rotating cells interact with surface cold pools from adjacent cells. When the boundary is skewed at a 45° angle from the mean vertical shear, it is possible that all neighbouring right moving, cyclonically rotating cells and the left moving, anticyclonically rotating cell on the downshear end of the line do not interact with their neighbours and thus behave like isolated supercells. So, outbreaks of right moving, cyclonically rotating supercells are most likely to occur when the mean vertical shear is oriented at a 45° angle from the line along which they have been initiated.

4.8.2. Movement across outflow boundaries or fronts. As noted by Bluestein and Weisman (2000), cells initiated along a surface boundary sometimes cross the boundary. Atkins *et al* (1999) considered what happens when a numerically simulated supercell interacts with a pre-existing surface boundary. They found that low-level mesocyclones form earlier, are stronger, and are more long lived when a boundary is present. When a supercell crosses the boundary from the warmer side to the colder side, the low-level mesocyclone weakens; when the supercell propagates along the boundary or has a component of motion that is towards the warm side, the low-level mesocyclone is stronger.

In a homogeneous environment, the source of vorticity in low-level mesocyclones in supercells is largely from baroclinally generated horizontal vorticity associated the forward-flank boundary generated by the convective storm itself. When a supercell interacts with a baroclinic boundary such as an outflow boundary or a front, the forward-flank area of the storm is less likely to affect the formation of the low-level mesocyclone, while baroclinically generated horizontal vorticity associated with the pre-existing boundary makes a significant contribution to the formation of the mesocyclone at low levels.

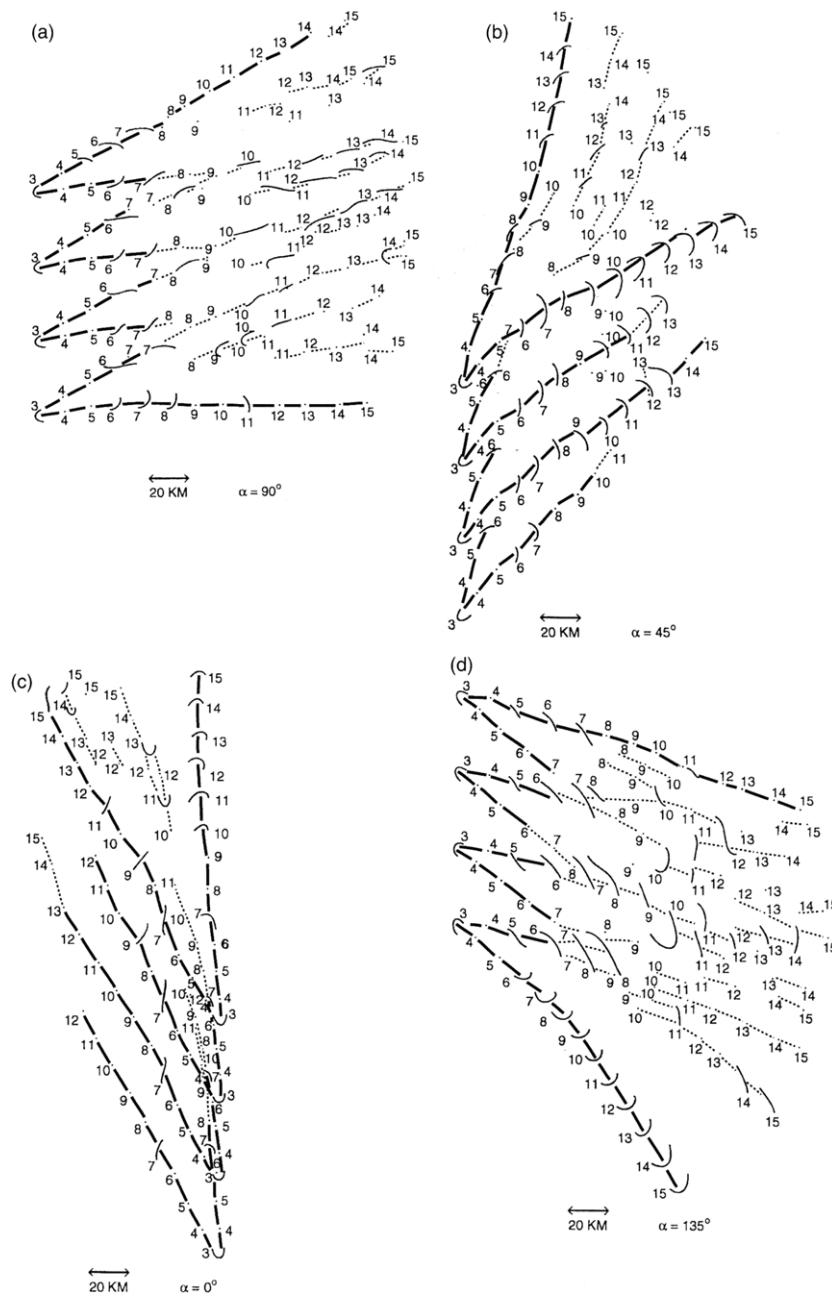


Figure 10. Tracks of updrafts, at 4 km above the ground, of simulated convective storms; updraft locations are marked every 10 min (numbers plotted are in $s \times 600$ from storm initiation). The vertical shear vector above 1.7 km is oriented (a) 90° , (b) 45° , (c) 0° and (d) 135° from the line along which buoyant bubbles, spaced apart by 30 km, were located. Bold, solid (dotted) cell tracks are shown for storms having supercell (ordinary cell) characteristics. From Bluestein and Weisman (2000).

It is thus concluded that just as the orientation of a boundary along which a broken line of storms is initiated is important in determining whether or not the cells can evolve into long-lived supercells, the orientation of a boundary is also important in determining whether or not a low-level mesocyclone in an isolated supercell will intensify or decay. When a supercell crosses a baroclinic boundary and the surface air becomes less potentially buoyant, the supercell and the midlevel mesocyclone may persist, but the low-level mesocyclone weakens. Thus, supercells that cross boundaries may maintain their intensity and rotational characteristics aloft, but it is unlikely that sustained rotation will be produced at low levels. It is therefore thought that it is unlikely that supercells that cross surface boundaries and do not remain along or just behind them will produce tornadoes.

5. Mesoscale convective systems

When convective storms are organized on a scale larger than the convective scale, their conglomeration is called a mesoscale convective system (MCS) (Maddox 1980, Zipser 1982). An MCS is composed of a contiguous area of precipitation that is ~ 100 km or greater across in at least one dimension. MCSs include both isolated complexes of convective storms and squall lines (lines of deep convective cells), some of which are relatively long, but narrow (Houze 1993). MCSs undergo evolution in which their organization and scale change with time. The individual convective storms that make up at least part of an MCS are considered building blocks. The building blocks may be ordinary cells or supercells. Portions of some MCSs during parts of their life may be composed of both a line of convective cells (or a solid convective line) and (a broader region of) stratiform precipitation. In parts of the US, much of the annual precipitation falls in MCSs (Fritsch *et al* 1986). While MCSs occur in both midlatitudes and the tropics, the focus of this discussion will be on MCSs in midlatitudes.

Since Doppler radar observations and three-dimensional nonhydrostatic numerical cloud models have become available, the major aspects of MCSs have been explained at least qualitatively. The following is a discussion of how MCSs form and a discussion of their two-dimensional and three-dimensional wind and thermodynamic structure.

5.1. Formation

MCSs frequently begin as squall lines, which form in a number of ways (Bluestein and Jain 1985) (figure 11). When convective cells break out along a line, but the cells are initially discrete and then eventually the spaces between adjacent cells fill in with heavy precipitation, the process is referred to as *broken-line* formation. Such a process often occurs along surface boundaries such as fronts and outflow boundaries and sometimes along the dryline (a surface boundary separating relatively cool, moist, marine air from relatively, warm, dry, continental air; in the US, the marine air is from the Gulf of Mexico and the dry air is from the elevated terrain of southwest US and Mexico (Bluestein 1993)). When one convective cell forms, and subsequent cells form just upstream with respect to storm motion, the process is called *backbuilding*; eventually, a line forms as newer and newer cells extend the length of the line. When a region of convective cells conglomerates into a convective line the process is called *broken areal* formation. When a convective line appears within an area of stratiform precipitation, the process is called *embedded areal* formation.

The most common types of MCS formation are probably the broken-line and backbuilding processes. In these situations, narrow lines of deep convection are produced during the early stages of squall-line formation. These narrow lines usually form in air masses that are

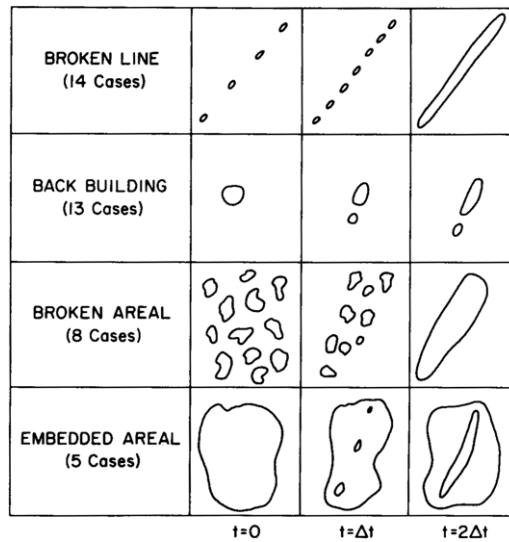


Figure 11. Idealized horizontal radar-echo distribution as a function of time for the four major ways in which MCSs form. From a climatological study by Bluestein and Jain (1985).

potentially unstable with respect to air based in the boundary layer. Since the broken areal and embedded areal mechanisms involve pre-existing convective cells or pre-existing stratiform precipitation, they probably involve convection that is not based at or near the surface, but rather that is elevated.

Upward forcing of potentially unstable moist air along a line or through the backbuilding process is not the only way to form an MCS that has a line configuration. Numerically simulated lines can also evolve from initially isolated cells that trigger secondary cells along the gust front of the original cell. As the gust front spreads out, new convective cells can break out along the arc of the outward expanding cold pool (e.g. Weisman and Klemp 1984). Such a process is a good example of the upscale growth of convective systems, from an isolated cell to a mesoscale convective system, without the need for any forcing along a line.

5.2. Morphology

While many MCSs begin as narrow, squall lines, they broaden with time. A narrow, leading convective line eventually may develop a trailing region of stratiform precipitation that is much broader than the narrow width of the leading convective line (figure 12). While the rainfall rate in the stratiform precipitation region is less than that in the more intense leading convective line, an observer in the former would experience precipitation for a much longer period of time than an observer in the latter, and so the total rainfall experienced may be largely due to that from the stratiform region. In between the intense leading convective line and the stratiform precipitation region there is a region of weaker precipitation rate (a narrow zone of weaker radar reflectivity at low levels) called the *transition zone* (Smull and Houze 1985, Smull and Houze 1987a). The leading convective line is preceded by a gust front, above which there is a shelf cloud (figure 13), which is formed as environmental air ahead of the MCS is lifted over the cold pool behind the gust front.

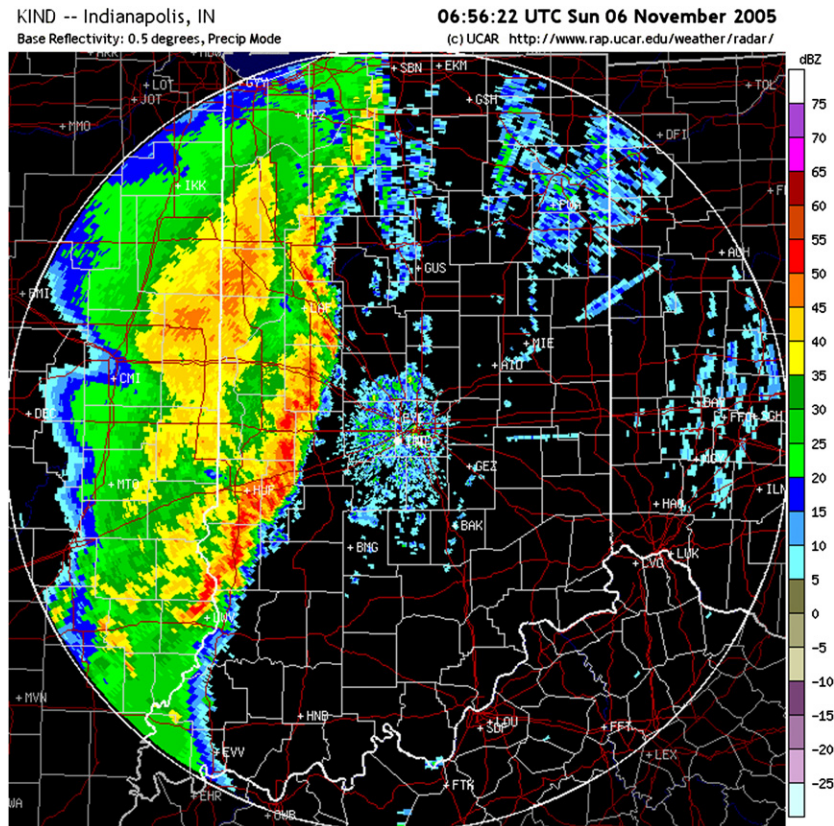


Figure 12. Radar reflectivity (colour coded in dBZ, to the right) depiction of a squall line, having a leading convective line (red band on the eastern side of the echo mass), a transition zone (coded green) to the rear (west) of the leading convective line and a mesoscale region of trailing stratiform precipitation (coded yellow and orange) to the rear of the transition zone. From the National Weather Service WSR-88D Doppler radar at Indianapolis, Indiana, on 6 November 2005.

When the leading convective line is followed by a stratiform precipitation region that is centred approximately to the rear (with respect to MCS motion) of the MCS, the MCS is said to be *symmetric* (Houze *et al* 1990) (figure 14). When the leading convective line, however, is centred or is more intense off to the south, southwestern or western side (in the plains of the US), the MCS is said to be *asymmetric*.

It was found in the 1980s from Doppler radar studies that a jet of unsaturated, environmental air enters the stratiform precipitation from the rear side of the MCS. This jet is called the *rear-inflow jet* (Smull and Houze 1987b), and aids in the production of a cold pool at the surface as the stratiform precipitation falls into the unsaturated air and cools evaporatively. Ascending front-to-rear air motion is found above the rear-inflow jet, in the anvil cloud region (figure 13), which is composed of water substance formed in the leading convective line. New convective cells form ahead of the leading convective line and eventually become the leading convective line, while the dissipating rear edge of the leading convective line is absorbed into the trailing stratiform precipitation area. An area of enhanced radar reflectivity is observed in the stratiform precipitation area at the freezing level; this *bright band* is a result of ice particles coated with water, which have a higher radar reflectivity than the snow above and the rain below.

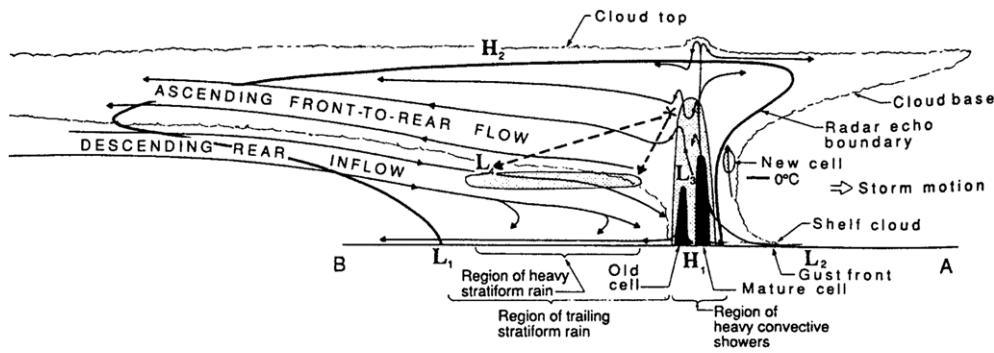


Figure 13. Vertical cross section through an idealized squall line, from the front edge (to the right) to the rear (to the left). From Houze *et al* (1989).

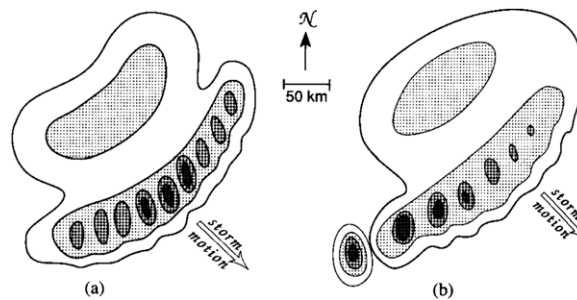


Figure 14. Idealized models of the radar reflectivity distribution in (a) a symmetric and (b) an asymmetric MCS. Shaded regions denote more and most intense radar echoes, according to the darkness of the shading. From Houze *et al* (1990).

5.3. The dynamics and thermodynamics of mature MCS squall lines

The behaviour of mature MCS squall lines can be understood as an extension of RKW theory, discussed earlier (section 3.3) in connection with the behaviour of gust fronts in the presence of vertical shear (Rotunno *et al* 1988). As a brief review, the two-dimensional aspects of the evolution of a convective summarized by Weisman (1992) (figure 15) are considered. First, before precipitation falls, when deep convection is initiated, the convective cloud leans in the downshear direction, since baroclinically generated horizontal vorticity is produced along the edges of the cloud in response to the latent-heat release from condensation; this vorticity is augmented by the import of low-level environmental horizontal vorticity on the downshear side (figure 15(a)). Later, after precipitation falls and an evaporatively produced cold pool is produced, the circulation induced at the leading edge of the cold pool is balanced by the circulation induced by the import of environmental horizontal vorticity associated with the environmental vertical shear at low levels (figure 15(b)).

As the convection system evolves, the cold pool may build up in intensity and deepen if more and more precipitation evaporates, so that the rate of generation of horizontal vorticity baroclinically at the leading edge of the cold pool is no longer balanced by the advection of environmental vorticity, but instead overwhelms it. The resulting circulation produced at the leading edge of the convection system is now in the upshear direction and air flowing into the convective system moves rearwards with respect to the convective system, carrying cloud

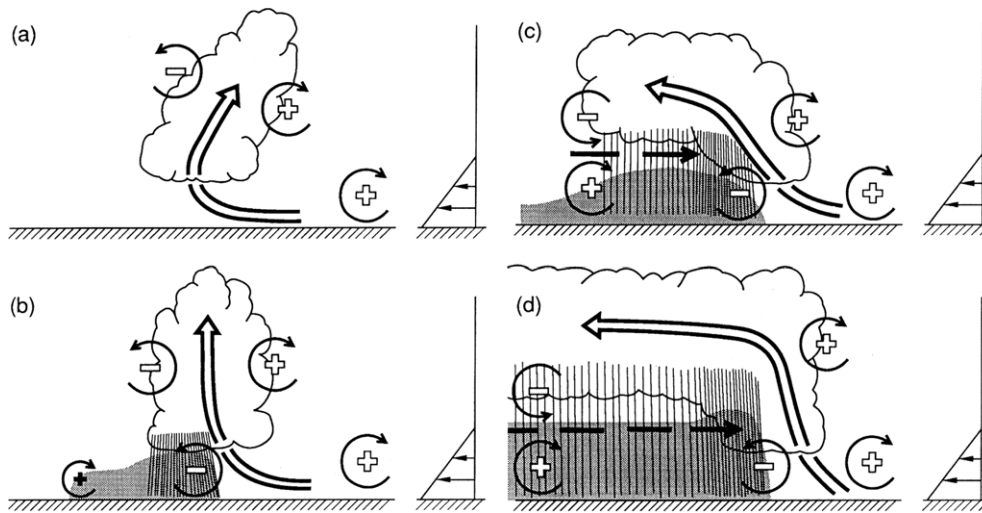


Figure 15. Idealized depiction of the evolution of an MCS. Vertical cross sections showing the storm-relative airflow (thick arrows), sense of horizontal vorticity (circular arrows), rear-inflow jet (dashed lines with leading arrow) cold pools (shaded areas) and the vertical variation of the environmental wind (lower right of each panel). In (a) the cloud leans in the downshear direction, owing to the predominance of the environmental horizontal vorticity; in (b) the cloud is erect as the cold pool has formed and there is a balance between the baroclinically generated horizontal vorticity at the leading edge of the cold pool and the import of environmental horizontal vorticity; in (c) the cold pool has become more extensive and the system leans in the upshear direction, owing to the overwhelming baroclinic generation of horizontal vorticity at the leading edge of the cold pool; in (d) the system again becomes more erect, as the import of horizontal vorticity generated baroclinically at the rear edge of the cold pool has been advected to the leading edge by the rear-inflow jet. From Weisman (1993),

particles and precipitation with it. Thus, the stratiform precipitation region forms to the rear of the leading convective line (figure 15(c)).

The development of the transition zone just to the rear of the leading convective line is likely microphysical (Rutledge and Houze 1987, Biggerstaff and Houze 1993, Braun and Houze 1994): it has been suggested that there is less aggregation above the melting layer than farther to the rear of the convective system at the same altitude, because midlevel subsidence just to the rear of the leading convective line reduces the availability of small ice crystals, while a mesoscale updraft farther to the rear (Houze 1989) enhances the growth of particles there (a mesoscale downdraft is found at lower levels). In addition, precipitation particles falling out just to the rear of the leading convective line originate at low levels and thus have less time to grow than particles originating at higher levels, which travel farther back and have a much longer period of time with which to grow. The largest particles fall out quickly near the leading convective line, while the smaller particles with smaller fall speeds are advected farther rearwards before they fall out and are available for precipitation formation.

At the rear edge of the convective system, baroclinically generated horizontal vorticity is generated aloft as a result of latent-heat release in the cloud and below as a result of the cold pool. The horizontal vorticity produced aloft is opposite in direction to that produced below, so that a rear-inflow jet develops (figure 15(c)). The strength of the rear-inflow jet is proportional to the CAPE, since the higher the CAPE, the greater the temperature excess in the cloud above and the lower the hydrostatic pressure deficit underneath the cloud; the stronger the low-pressure deficit under the cloud, the greater the rear-to-front pressure-gradient force.

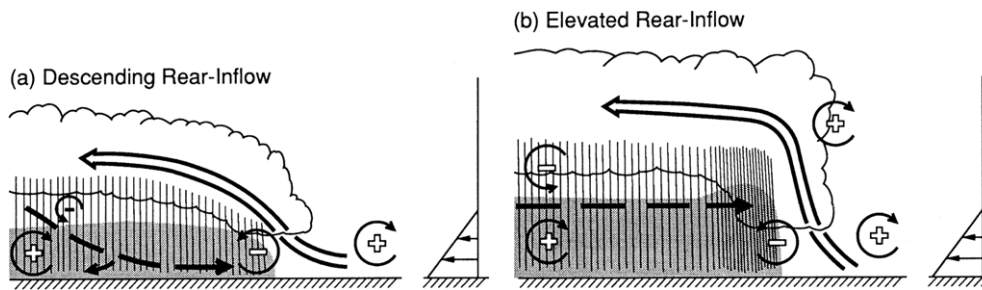


Figure 16. As in figure 15, but idealized vertical cross sections in an MCS of (a) descending rear-inflow and (b) elevated rear-inflow. From Weisman (1992).

The rear-inflow jet advects unsaturated air into the system, thus enhancing the cold pool even more through continuing evaporative cooling. The most important consequence of the rear-inflow jet, however, is that there is horizontal vorticity associated with it of opposite sign just above and below it. Eventually, the horizontal vorticity associated with the vertical shear just underneath the rear-inflow jet, which is the same sign as that of the low-level environmental shear ahead of the system, is advected forward through the convective system until it reaches the leading edge, where it now can re-establish a balance between the baroclinically generated horizontal vorticity at the leading edge of the cold pool, and the horizontal vorticity advected into it, so that the rising branch of the circulation at the leading edge is stronger and deeper (figure 15(d)). Thus, the dynamics of the convective system itself result in a re-invigoration of the system and promote longevity. Above the rear-inflow jet, the horizontal vorticity is the same sign as that induced by the leading edge of the cold pool, so that the updraft is turned again toward the rear of the system. The rear-inflow jet of the type seen in figures 15(d) and 16(b) is called, more specifically, an *elevated rear-inflow jet*.

When the rate of generation of horizontal vorticity at the rear of the convective system is greater below at the rear edge of the cold pool than it is above at the rear edge of the cloud, the rear-inflow jet descends as it passes through the convective system (figure 16(a)), owing to the overwhelming effect of the horizontal vorticity associated with the rear, cold pool edge. In this case, this feature is called a *descending rear-inflow jet*, and the horizontal vorticity just below it, which is opposite in sign to that of the baroclinically generated horizontal vorticity at the leading edge of the cold pool, is not advected all the way to the leading edge as it is by the elevated rear-inflow jet. A consequence of the descent of the rear-inflow jet is that rate at which horizontal vorticity is generated baroclinically at the leading edge of the cold pool is *not* balanced by the advection of horizontal vorticity (into it), so that the MCS is not as long lived as it would have been if the rear-inflow jet were elevated.

In summary, the main factor determining whether or not a rear-inflow jet is elevated or descending, i.e. whether or not the convective system can be long lived or not, depends on the relative horizontal buoyancy gradients at the rear edge associated with warm, cloud above and the cold pool below. Weisman (1992) found in numerical simulations that in general, when the CAPE is low to medium and the vertical shear is weak to moderate the rear-inflow descends to the surface behind the leading edge of the gust front. When the CAPE is high and the vertical shear strong, the rear-inflow jet is elevated. Further refinement of the estimates of how rapidly horizontal vorticity is generated at the leading edge of the cold pool and especially at the rear edge of the cold pool depends on cloud microphysics and the consequent melting and release of latent heat of condensation and fusion and on water loading, which reduces the buoyancy inside clouds.

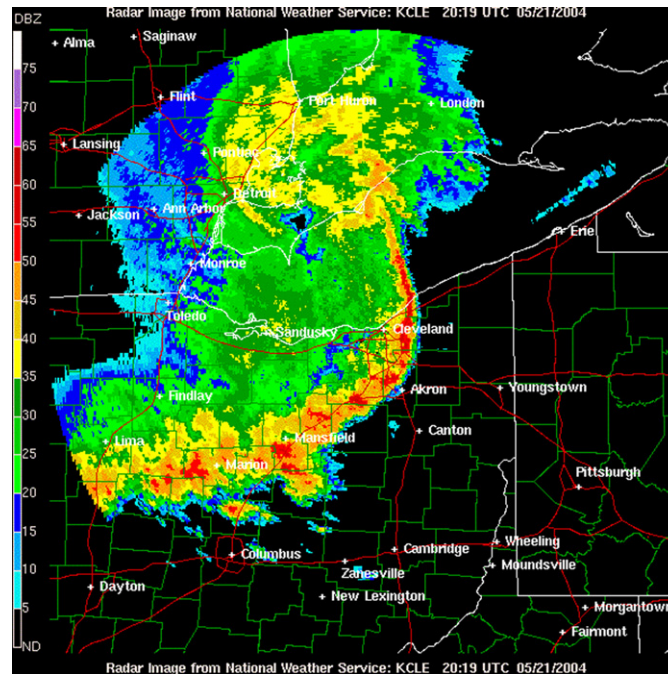


Figure 17. Radar reflectivity (colour coded in dBZ, to the left) depiction of a bow echo. From the National Weather Service WSR-88D Doppler radar at Cleveland, Ohio, on 21 May 2004.

5.4. The production of vortices in MCSs

In the preceding discussions of the dynamics of MCSs, only the two-dimensional aspects of squall line MCSs were considered. It has been found observationally that many MCSs are three-dimensional and several types of vortices can occur at low and/or midlevels. For example, Fujita (1978) identified and named the *bow echo* (figure 17), in which a 40–100 km long convective line segment bulges outwards and is associated with damaging straight-line winds at the surface (Przybylinski 1995).

In addition, bow echoes sometimes produce counter-rotating vortices at either end of the line at $\sim 2\text{--}3$ km AGL: in the Northern Hemisphere, an anticyclonic (cyclonic) vortex is produced on the right (left) side of the end of the line with respect to the mean vertical-shear vector. Weisman (1993) named these features *bookend vortices* (figure 18). Bow echoes early in their life tend to be symmetrical, but later in their life the cyclonic bookend vortex becomes stronger than the anticyclonic bookend vortex. The bow echoes develop into a comma shape (figure 17) as an asymmetric MCS. The cyclonic vortex is favoured over the anticyclonic vortex because in a stratiform precipitation region, convergence at midlevels, above a low-level downdraft and below an upper-level updraft, acts on the Earth's vorticity to produce cyclonic vorticity. The cyclonic bookend vortex is known as a *mesoscale convective vortex (MCV)* (Weisman and Davis 1998, Maddox 1980, Menard and Fritsch 1989, Stirling and Wakimoto 1989, Brandes 1990, Bartels and Maddox 1991, Smull and Augustine 1993, Fritsch *et al.* 1994). It is thought that over the warm ocean surface, under the proper environmental conditions, a tropical cyclone can develop from an MCV. MCVs, unlike mesocyclones (and mesoanticyclones) in supercells, are larger in scale (as large as 100s of km) and can last much longer (up to days). Weisman (1993) found in numerical-simulation experiments that

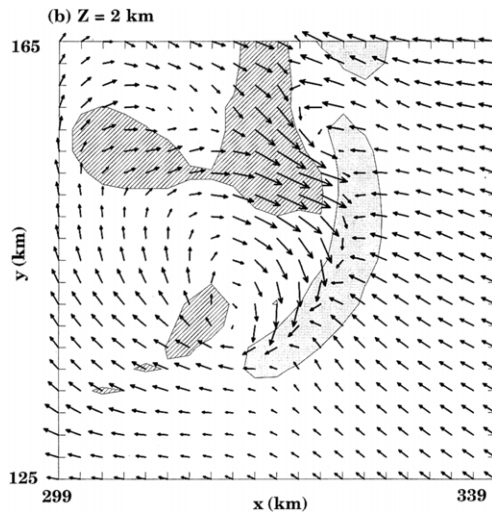


Figure 18. Numerically simulated bookend vortices (anticyclonic and cyclonic, to the south and north, respectively) at 2 km above the ground. Vectors represent storm-relative airflow. Shaded (cross hatched) regions denote updrafts (downdrafts) of at least 5 (2) m s^{-1} ; air rises along an arc at the leading edge, while the rear-inflow jet is mostly descending. From Weisman and Davis (1998).

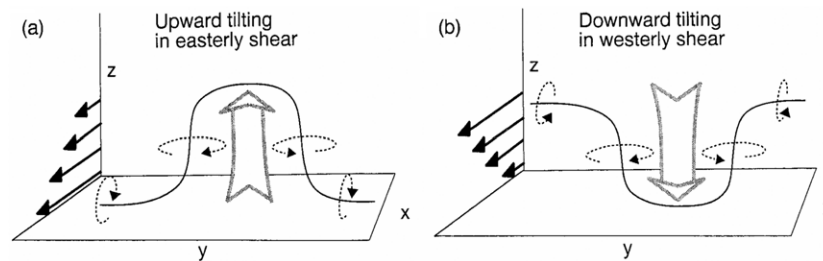


Figure 19. Idealized depiction of the production of counter-rotating vortices through the tilting of (a) easterly shear in by an updraft and (b) westerly shear by a downdraft. The former occurs as air rises over the leading edge of gust front along which low-level easterly shear has been generated baroclinically; the latter occurs when a precipitation-induced downdraft acts on environmental horizontal vorticity associated with westerly vertical wind shear. From Weisman and Davis (1998).

the production of bow echoes with bookend vortices and strong surface winds is most likely in environments of high CAPE and strong low-level vertical wind shear. When a rear-inflow jet forms as described in section 5.3, it is enhanced by the development of bookend vortices, which can focus the rear-inflow jet into the centre of the convective system.

Some bookend vortices originate as the cyclonic and anticyclonic vortices along the right and left flanks of a pair cells that originated from the splitting of a parent supercell; the radar echo expands as cold outflow in between the two members of the splitting cell forces new convective cells to grow in between them. The vortices in effect are produced when a downdraft acts on strong or deep westerly vertical shear (figure 19(b)) and occur early in the life of an MCS. However, since most bookend vortices form along the ends of a pre-existing line segment, Davis and Weisman (1994) suggested that bookend vortices can be produced when an updraft tilts horizontal vorticity that is baroclinically generated at the leading edge of the

gust front (figure 19(a)). In this scenario, which occurs later on in the lifetime of an MCS, after a substantial cold pool at the surface has been built up, and in an environment of only weak-to-moderate vertical wind shear, the low-level horizontal vorticity that is generated baroclinically along the edge of cold pool is tilted at the leading edge of the MCS by the leading-edge updraft; tilting results in an anticyclone to the right of the environmental, low-level westerly vertical shear and a cyclone to the left of the environmental, low-level westerly vertical shear. These vortices are advected rearwards by the front-to-rear relative flow (Weisman and Davis 1998). It is not known what controls the horizontal scale of the bookend vortices, but it is conjectured that they must be spaced so that they act to strengthen the rear-inflow jet enough to affect the dynamics of the leading edge of MCS so that it is long lived enough to be able to generate the bookend vortices.

6. Tornadoes

Tornadoes are rapidly rotating columns of air that make contact with the ground. They are either connected to a or situated underneath a cumuliform, buoyant cloud above. They are sometimes, but not always, visible as a funnel cloud when the pressure deficit in them is low enough such that water vapour condenses and cloud particles form. When the air is too dry or the pressure not low enough for a condensation funnel to form, the tornado may be visualized as a column of rotating dust or debris.

Lasting anywhere from just a few seconds to an hour or more, most tornadoes last only ~ 10 min. The diameter of a tornado is usually ~ 200 m, but can vary from as narrow as ~ 10 m to as wide as ~ 1.5 – 2 km. Most tornadoes are distinctly narrower than mesocyclones, which are ~ 2 – 5 km in diameter. Tornadoes are perhaps the most violent and destructive of all the severe weather phenomena that localized convective storms produce.

Wind speeds in tornadoes range from ~ 20 to ~ 140 m s⁻¹. Efforts have been made to estimate wind speeds in tornadoes based on the nature and extent of the damage they inflict (Fujita 1981). The *Fujita 'F-scale'*, which ranges from F0 (18–32 m s⁻¹; 40–72 mph) to F5 (117–142 m s⁻¹; 261–318 mph), is not calibrated; i.e. the relationship between wind speed and damage has not actually been measured under controlled conditions (Wurman and Alexander 2005). The Fujita scale was replaced by the *Enhanced Fujita (EF) scale* (McDonald and Mehta 2004, McCarthy *et al* 2006) in 2007; unlike the F-scale, it is calibrated to some extent.

Most tornadoes rotate cyclonically, though anticyclonic tornadoes are also observed, sometimes alone, but also in tandem with nearby cyclonic tornadoes (e.g. Fujita 1981). Some tornadoes contain even smaller-scale vortices within them that rotate about the main axis of the tornado (figure 20). These sub-tornado-scale vortices have been called *suction vortices* or *satellite vortices* or 'secondary vortices'.

When a rotating column of air is visualized as a condensation funnel that does not appear to be making contact with the ground (i.e. it visibly terminates well above the ground and no surface debris cloud is apparent), then the feature is referred to as a *funnel cloud*. It is not always clear whether or not a funnel cloud is associated with a strong circulation at the ground, especially if the ground surface does not contain material that is easily swept airborne or if the atmosphere is very dry. Tornadoes that appear over the water are called *waterspouts*. Tornadoes have been observed over all types of terrain, including mountainous areas (Fujita 1989, Bluestein 2000, Moneteverdi *et al* 2006).

The two main scientific problems related to tornadoes are explaining their structure, particularly their three-dimensional wind distribution and why they form. To date, it cannot be predicted very well whether or not a parent convective storm will go on to produce a tornado.



Figure 20. A multiple-vortex tornado on 3 May 1999 near Verden, Oklahoma, as viewed from its north. The parent supercell of this tornado tracked to the northeast and produced an F5 tornado in Oklahoma City and Moore about an hour later. Five or six condensation funnels are visible, leaning in towards the centre of the main circulation at the ground. Photograph copyright H Bluestein.

Owing to the difficulties in collecting detailed observations in the right place for a sufficiently long period of time, and the difficulty in numerically simulating both a convective storm and a tornado together, tornadoes are the least well understood of all phenomena associated with convective storms.

Early research on tornadoes consisted mostly of serendipitous *in situ* measurements, studies with conventional radar and photogrammetric analyses of debris movies. Fixed-site Doppler radar networks in the 1970s and early 1980s afforded a look at the wind field in storms with spatial resolution on the scale of ~ 500 m–1 km and temporal resolution ~ 2 –5 min. Storm chasers began to document storm features in a systematic way beginning in the 1970s and with *in situ* instrumentation in the 1980s (Bluestein 1999). Laboratory experiments in vortex chambers were carried out in the 1970s and 1980s (Church and Snow 1993). Numerical simulations of convective storms on the storm scale, with nested grids used to simulate sub-storm vortices, were also first carried out then. Airborne Doppler radars were first used to probe severe convective storms in the early 1990s and especially during VORTEX in 1994 and 1995 (Bluestein and Wakimoto 2003). Radars mounted on aircraft allowed storms to be followed and documented, with 300 m spatial resolution, for longer time durations, but the time between aircraft passes was ~ 5 min and features near the ground could not be detected very well, owing to ground-clutter contamination. Mobile, ground-based radars mounted in vans or trucks were first used in the late 1980s; while it was difficult to follow storms as well as in an aircraft, data in tornadoes near the ground could be obtained with even higher spatial resolution and at much shorter time intervals. Large-eddy simulations (LES) of tornadoes (vortices interacting with the ground and isolated from their parent storms) were first carried out in the late 1990s using grid spacing as short as ~ 1 –3 m in some places, so that the turbulent aspects of tornadoes could be better represented (Lewellen *et al* 1997).

6.1. Types of tornadoes

Tornadoes may be classified according to whether or not they are associated with a pre-existing, larger-scale circulation. The largest and most intense, and consequently the most damaging, are associated with a mesocyclone in a parent supercell. This type of tornado is called a *supercell tornado* or a *Type I tornado* (Davies-Jones *et al* 2001).

Other tornadoes are not associated with a mesocyclone and are sometimes referred to as *non-supercell tornadoes* or *Type II tornadoes* (Davies-Jones 2001). These tornadoes appear in a number of different situations.

- (a) Some are found under growing cumuliform towers, often even before precipitation has hit the ground. Since these frequently look like waterspouts that are pendant from lines of cumulus congestus, they are colloquially known as *landspouts* (Bluestein 1985). When the air is very dry, landspouts appear as rotating whirls of dust near the ground, without any condensation funnel overhead. They begin near the ground and sometimes expand upwards towards cloud base. (Although this type of tornado is found in ordinary-cell convective storms, it is also found in supercells, but not in association with the mesocyclone.)
- (b) Some, which appear along the edge of gust fronts as rotating dust whirls, are colloquially known as *gustnadoes*. Since gust fronts are found in all types of convective storms, gustnadoes are found in both supercells and ordinary-cell convective storms.
- (c) Some are not readily visible, forming within regions of precipitation along lines of convection, particularly along cold fronts (Carbone 1982, 1983) and in bow echoes (Forbes and Wakimoto 1983, Przybylinski 1995, Trapp *et al* 2005).
- (d) Funnel clouds pendant from relatively high-based cumuliform clouds have been observed (Bluestein 1994), while others appear from very ragged-looking convective clouds over mountainous terrain (Bluestein 2005). These funnel clouds do not appear to have circulations that make contact with the ground and become tornadoes.

6.2. Vortex dynamics

The problems of what determines the character of the wind field in a tornado and what determines whether or not a tornado will form have been addressed using laboratory models of vortices and numerical models of vortices under idealized, laboratory-model-like conditions. While these idealized models do not include the effects of external convective-storm features producing and interacting with the vortex and translating along and do not include the asymmetric effects present in nature, such as the advection of cooler/warmer and moister/drier air from specific quadrants, they have been very useful in elucidating many of the observed characteristics of tornadoes in nature.

Axisymmetric, tornado-like vortices in laboratory models (or ‘simulators’) are driven from above by an exhaust fan; air is drawn into a rotating lower section, where it acquires vertical vorticity. While there are a number of parameters that are not allowed to vary, such as the size of the opening into which the horizontally converging air at the bottom turns into the updraft aloft, measurements have been made that bear good resemblance to observations and that have been analysed dynamically. To simulate idealized laboratory vortices, the difficult problems of what boundary conditions to use and how to account for sub-grid scale motions must be addressed. The reader is referred to Davies-Jones *et al* (2001) for a summary these more technical issues.

6.2.1. Vortex structure. The idealized vortex that is produced may be thought of as an intense (‘primary’) vortex driven by convergence acting on pre-existing vorticity; the vortex rubs against the ground, where friction slows it down. The radial and azimuthal components of the equations of motion for axisymmetric motions in a nonrotating atmosphere, including

turbulent friction, are given in cylindrical coordinates as follows:

$$\begin{aligned} Du/Dt &= \partial u/\partial t + u\partial u/\partial r + w\partial u/\partial z - v^2/r \\ &= -\alpha_0\partial p/\partial r + v(\partial^2 u/\partial r^2 + 1/r\partial u/\partial r - u/r^2 + \partial^2 u/\partial z^2), \end{aligned} \quad (6.1)$$

$$Dv/Dt = \partial v/\partial t + u\partial v/\partial r + w\partial v/\partial z + uv/r = v(\partial^2 v/\partial r^2 + 1/r\partial v/\partial r - v/r^2 + \partial^2 v/\partial z^2), \quad (6.2)$$

where u is the radial-wind component, v is the azimuthal wind component, r is the radial coordinate, z is the vertical coordinate and ν is the eddy coefficient of viscosity (e.g. Davies-Jones 1986, Rotunno 1977, 1979). The vertical equation of motion is

$$\begin{aligned} Dw/Dt &= \partial w/\partial t + u\partial w/\partial r + w\partial w/\partial z \\ &= -\alpha_0\partial p/\partial z + B + v(\partial^2 w/\partial r^2 + 1/r\partial w/\partial r + \partial^2 w/\partial z^2), \end{aligned} \quad (6.3)$$

where $B = gT'/T_0$. The equation of continuity in a Boussinesq atmosphere for axisymmetric motions is

$$1/r\partial/\partial r(ru) + \partial w/\partial z = 0. \quad (6.4)$$

The adiabatic form of the thermodynamic equation is

$$DT'/Dt = (\partial/\partial t + u\partial/\partial r + w\partial/\partial z)T' + w\partial T_0/\partial z = \kappa(\partial^2/\partial r^2 + 1/r\partial/\partial r + \partial^2/\partial z^2)T', \quad (6.5)$$

where κ is the eddy coefficient of turbulent diffusivity.

The effects of surface friction are felt in the *boundary layer* (Lewellen 1976), where a radially inward directed pressure-gradient force (acceleration is $-\alpha_0\partial p/\partial r$) is countered mainly by a frictionally reduced radially outward directed centrifugal force (acceleration is v^2/r). (It is assumed that the azimuthal wind speed is less than it is above the boundary layer and that the radial pressure-gradient force in the boundary layer is the same as it is at the top of the boundary layer, where there is approximate *cyclostrophic balance*, i.e. balance between the radially outward directed centrifugal force and the radially inward directed radial pressure-gradient force.) The imbalance of forces near the ground drives radial inflow. The resulting radial-wind flow pattern in the vertical plane is called the 'secondary' circulation. The boundary layer flow may be laminar or turbulent, depending on the Reynolds number, so that the degree of smoothness of the surface underneath the vortex can play a role in the nature of the flow. It is thought that in nature, tornado boundary layers are turbulent because the surface of the Earth is relatively rough. The tornado boundary layer is around 100 m deep. The *surface layer* of the tornado is made up of approximately the lowest 10 m above the ground, where the stress is height independent owing to turbulent eddies.

Ekman-like instability is possible in the boundary layer, owing to friction and rotation. As a consequence of Ekman instability, horizontal roll vortices may form at an angle of $\sim 15^\circ$ to the left of the flow above the boundary layer, as realized in spiral bands in hurricanes (Faller 1963).

The region of the tornado above the boundary layer is divided up into an inner *core* region and an *outer flow* region (Lewellen 1976) (figure 21). In the latter, which extends beyond the core 1 km or more, air flows radially inwards, rises as it approaches the core, and angular momentum is conserved (there is no turbulent friction). So,

$$v(r)r = A, \quad (6.6)$$

where A is a constant equal to the angular momentum, and air parcels therefore spin up as they approach the centre of the vortex. It follows that the radial profile of azimuthal wind outside the core is

$$v(r) = A/r. \quad (6.7)$$

In the outer flow region, then, there is potential flow (no vorticity).

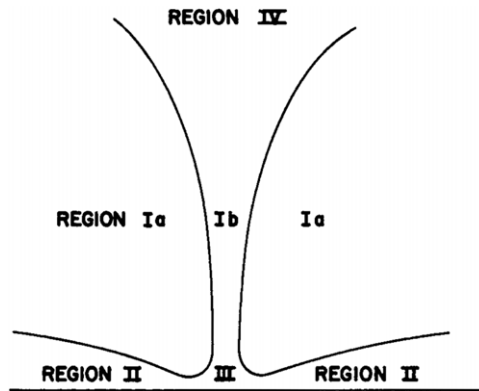


Figure 21. Conceptual model of the different flow regions of an idealized axisymmetric tornado. The vertical cross section depicts (a) regions Ia, above the boundary layer, outside the core, or the ‘outer region’, (b) Ib, the core, (c) II, the boundary layer or the ‘inflow layer’, (d) III, the corner region, and (e) IV, the termination region within the parent storm at middle or upper levels. From Davies-Jones *et al* (2001), as adapted from Lewellen (1976).

In the former, which spans the region from the centre of the vortex out to the radius of maximum azimuthal wind (or RMW, radius of maximum wind, also known as the ‘core radius’), there is solid-body rotation, as a result of turbulent diffusion: at the centre of the tornado, there must be zero azimuthal velocity and angular momentum; at the interface between the core and the outer flow region, the angular momentum is a constant fixed set by the environmental flow (cf (6.7)). If air parcels were brought towards the centre of the vortex, without radial mixing, then the azimuthal velocity would approach infinity and so would its radial gradient. So, an air parcel transported radially inwards towards the centre would therefore have to lose all its angular momentum as a consequence of radial mixing. If the vortex is stable with respect to lateral displacements, then it takes work to bring the air parcel in closer to the axis of the vortex. It follows from mixing theory that the radial gradient of azimuthal velocity must be a constant, or else there would be turbulent mixing that would smooth away irregularities, as in the surface boundary layer in the atmosphere (Bluestein 1992). Then it follows that in the core,

$$v(r) = \Omega r, \quad (6.8)$$

where Ω is a constant, which turns out to be the rotation rate of a solid body. It is worth noting that radial turbulent diffusion is responsible for bringing about a linear azimuthal wind profile close to the axis of the tornado, which itself is associated *without* any turbulent diffusion: i.e. diffusion produces a profile that reduces diffusion to zero.

The simplest model of a tornado is that of the *Rankine combined vortex*, which is a core of solid-body rotation surrounded by a region of potential flow, with no vertical motion. Recent mobile Doppler radar measurements of the wind field in tornadoes exhibit radial profiles of azimuthal wind that are similar to that of the Rankine combined vortex, except that there is a smooth transition from solid-body rotation to potential-like flow near the RMW (e.g. Tanamachi *et al* 2007) (figure 22). Unless the smooth transition in the data is an artefact, it is thought that radial diffusion at the interface between the core and the outer flow region is responsible for the smooth transition. The radial profile of azimuthal velocity in the presence of radial diffusion at the interface is called a *Burgers–Rott vortex*. The core radius is typically ~ 100 m, though it can be as narrow as only tens of metres across. The core radius is controlled by the amount of work needed to bring a ring of air in towards the centre of the

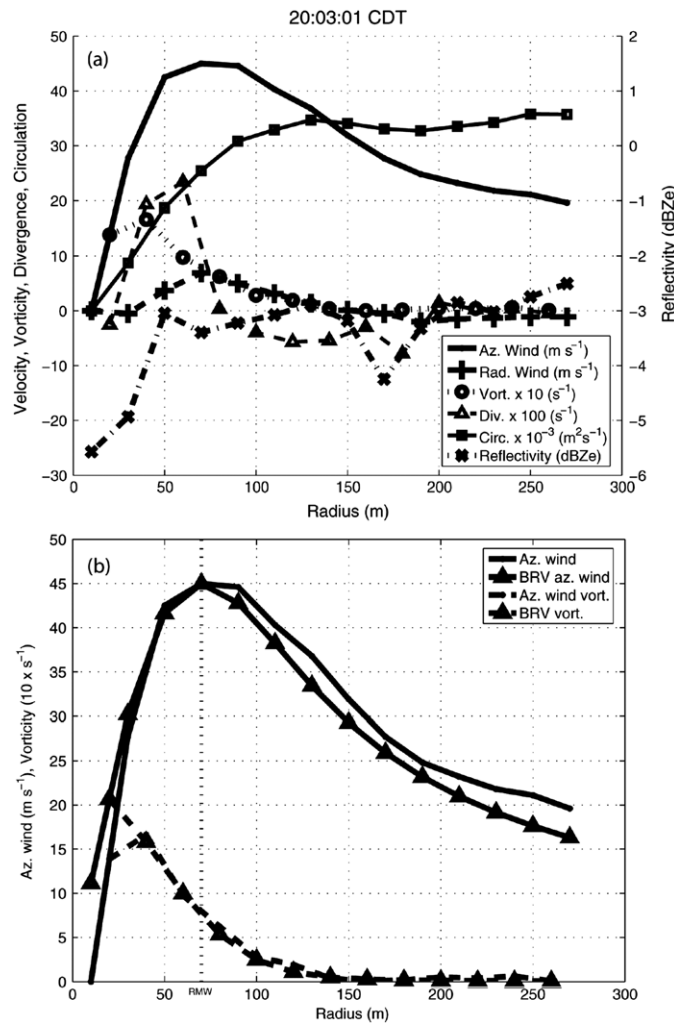


Figure 22. Radial profile of azimuthal wind ((a), (b); solid line) in a tornado on 15 May 1999 in north-central Kansas, based on data collected by a W-band (3 mm wavelength), mobile, Doppler radar. The fit of the profile to a Burgers–Rott vortex is seen in (b). Also plotted (a) are the radial profiles of azimuthally averaged radial wind, vorticity, divergence, circulation, reflectivity and (b) the vorticity in the Burgers–Rott vortex. See Tanamachi *et al* (2007) for details on how the data were collected and processed. From Tanamachi *et al* (2007).

tornado; the amount of work available is due mainly to the buoyancy above in the updraft, though nonhydrostatic upward pressure-gradient forces could also be significant (Wicker and Wilhelmson 1995) below the level of free convection if vorticity increases with height below cloud base. A climatology of the core radius in tornadoes based on mobile Doppler radar data has been compiled by Alexander (Alexander and Wurman 2006), though it is not yet published. Other measurements of core radius from mobile Doppler radars include Wurman and Gill (2000), Alexander and Wurman (2005), Bluestein *et al* (2003a), Tanamachi *et al* (2007) and Bluestein *et al* (2007a).

The pressure drop (Δp) in the core of a tornado (with respect to the pressure in the environment) may be estimated by integrating the equation of cyclostrophic balance for an

assumed radial profile of azimuthal wind

$$\alpha_0 \partial p / \partial r = v(r)^2 / r \quad (6.9)$$

radially inwards in an hydrostatic atmosphere, so that, for example, in a combined Rankine vortex,

$$\Delta p = v_{\max}^2 / 2\alpha_0, \quad (6.10)$$

where the pressure drop is given here with respect to the pressure at the radius of maximum wind, the core radius. For $v_{\max} \sim 140 \text{ m s}^{-1}$ and $\alpha_0 \sim 1 \text{ m}^3 \text{ kg}^{-1}$, $\Delta p \sim 100 \text{ hPa}$. Actual measurements of pressure drops in tornadoes at the ground (where turbulent friction is significant) of as much as 100 hPa (Lee *et al* 2004) have been made. Much of the pressure deficit in a tornado is a hydrostatic consequence of the warm, buoyant air column above it. The maximum wind speed in a tornado subject to (6.8) and (6.9) is referred to as the thermodynamic speed limit (Fiedler and Rotunno 1986):

$$v_{\max} \sim (\text{CAPE})^{1/2}. \quad (6.11)$$

This relation is similar to that for w_{\max} because the vertically integrated buoyancy, CAPE (cf equation (3.1)), is also the pressure deficit in a hydrostatic atmosphere across the core of a vortex in solid-body rotation (cf equation (6.10)), i.e. $v_{\max}^2 \sim \alpha_0 \Delta p \sim \text{CAPE} \sim w_{\max}^2$.

Perhaps the most complex portion of a tornado vortex is the *corner region* (figure 23), where the boundary layer bends upwards. Air parcel accelerations may be extremely large here as horizontally flowing air is diverted upwards and the azimuthal wind component increases rapidly because air parcels get closer to the central axis of the tornado than they do above the boundary layer in the outer flow region. In the outer flow region, the tornado vortex profile of azimuthal wind is very stable with respect to radial motions; in the corner region, the flow is less resistant to radial motions, owing to large radial shear in vertical velocity (Howard and Gupta 1962, Davies-Jones *et al* 2001). It is thought that light debris are lofted high in the parent storm in the corner region and then deposited downstream from the storm, sometimes at great distances from their source (Snow *et al* 1995, Magsig and Snow 1998).

In the corner region, when the vortex is strongest near the ground, a dynamic, downward-directed pressure-gradient force develops (see equation (4.9)), which acts to limit surface convergence and further vortex intensification. Such a process is responsible for rapid changes in vertical velocity with height. A large decrease in updraft speed with height can counteract the downward-directed pressure gradient (Lewellen and Lewellen 2006).

In addition, a large decrease in vertical velocity with height can lead to *vortex breakdown*, a phenomenon which is analogous to the *hydraulic jump* observed in nonrotating, stratified flows (Benjamin 1962) when there is a transition between upstream supercritical flow (the flow speed is faster than that of gravity waves) and downstream subcritical flow (the flow speed is slower than that of gravity waves). *Centrifugal waves* can be produced in tornadoes, owing to an imbalance between the radially inward-directed pressure-gradient force and the radially outward directed centrifugal force and resultant restoring forces (see (6.1)). These centrifugal waves can propagate vertically. Near the ground, where there is a strong updraft, the flow may be faster than that of vertically propagating centrifugal waves; above the ground, where the updraft decreases in magnitude, there may be a transition to a state in which the flow is no longer faster than that of vertically propagating centrifugal waves. The rotating updraft near the ground in the corner region is called an *end-wall vortex*. Above the level of transition from supercritical flow (with respect to centrifugal waves) to subcritical flow (with respect to centrifugal waves), there is a transition from laminar to turbulent flow known as *vortex breakdown*. This phenomenon has not yet been documented by Doppler radar, but has been seen in nature, especially from airborne platforms (Pauley and Snow 1988) that permit a

look down at the corner region in a tornado, which may otherwise be hidden from view at the surface by a debris cloud or a condensation funnel. It perhaps could be verified by observing the spectrum width (Doviak and Zrnic 1993) in radar volumes and determining if the spectrum width increases with height at the level at which vortex breakdown is expected. It may be, however, that the region of vortex breakdown may not have a high enough density of scatterers or that they are too small to detect well.

The *upper flow* region of a tornado is not well observed and not well understood. There have been some airborne radar measurements in tornadic supercells that show that some tornadoes can extend throughout much of the depth of the parent storm (Wakimoto *et al* 1996). If much of a tornado is embedded within an updraft, then the updraft advects vorticity upwards and it is not surprising that some of them can extend rather high up in the troposphere, especially when the updraft extends up to the tropopause. When a nonrotating updraft penetrates above the tropopause, a hydrostatic ‘cold dome’ is produced because air parcels become colder than their environment, just above the tropopause. Owing to the cold air aloft, there cannot be a hydrostatic pressure deficit underneath the updraft at the ground. Therefore, a rotating updraft, which must be accompanied by a pressure deficit at the centre, cannot produce a penetrating top in the lower stratosphere. So, the updraft must terminate at the tropopause, where there must be divergence. This divergence is forced because the radially outward centrifugal force overwhelms the radially inward-directed pressure-gradient force (Lilly 1969). Above the divergence there should be a downdraft, which may appear as a ‘crater’ in the cloud top (Davies-Jones 1986). So, we are led to the ironic conclusion that the anvil region above the updraft in a buoyant cloud that drives a ‘deep’ tornado may belie the hidden updraft below. There have been some observations of collapsing tops in thunderstorm anvils near the time of tornadoes (Fujita *et al* 1976).

The most important parameter defining idealized vortex behaviour in a simulated laboratory vortex is the *swirl ratio* (S), where

$$S = r_0 M / Q, \quad (6.12)$$

in which r_0 is the radius of updraft hole, M is the circulation at the edge of the updraft (vr) divided by 2π (i.e. the angular momentum) and Q is the volume flow rate of the updraft divided by π (Davies-Jones *et al* 2001). The swirl ratio is also given by the following:

$$S = v_0 / w, \quad (6.13)$$

where v_0 is the azimuthal wind component at the outer edge of the updraft hole (the edge of the updraft) and w is the mean vertical velocity in the updraft hole. The swirl ratio can be thought of as a measure of the relative amount of azimuthal flow compared with the amount of radial flow into the bottom of the vortex or, equivalently, the relative amount of vertical vorticity to (horizontal) convergence. The swirl ratio is physically significant because it determines whether or not a central downdraft develops in response to the pressure drop at the centre of the vortex: if the pressure drop is large enough, then the downward-directed pressure-gradient force can reverse the frictionally induced central updraft.

In nature, the swirl ratio is probably controlled by the magnitude of the updraft in the convective cloud above, which is related to both the buoyancy in the cloud and dynamic vertical pressure gradients and to the vorticity underneath the updraft. A change in updraft intensity while a convective cloud grows or decays or a change in the nature of the surface or a change in how much vorticity is produced may change the swirl ratio. It is difficult to relate the swirl ratio defined for a vortex simulator to the swirl ratio in nature because critical swirl transitions depend on the Reynolds number, which is different in the real atmosphere, and because there is uncertainty in how to interpret the parameters defined in the simulator, in the real atmosphere; nevertheless, it has been attempted in mesocyclones

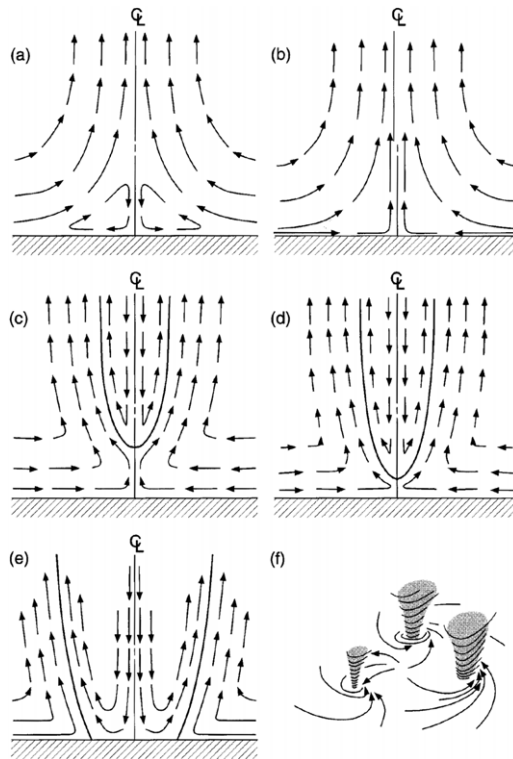


Figure 23. Idealized vertical cross sections of flow in a tornado/vortex near the ground as a function of the swirl ratio. (a) very low swirl ratio: flow does not enter the corner region and there is no tornado; (b) low swirl ratio: a weak, laminar, one-cell tornado; (c) moderate swirl ratio: laminar, upward jet in corner region breaks down into turbulent, two-cell vortex aloft, above the level of the bottom of the central downdraft; (d) slightly higher swirl ratio: similar to (c), but the level of vortex breakdown is near ground level; (e) higher swirl ratio: turbulent two-cell tornado, the central downdraft hits the ground, and radial inflow turns upwards at higher radius in an annular corner region; (f) high swirl ratio: the annulus of shear vorticity in the corner region becomes unstable and the tornado splits into smaller, multiple vortices. From Davies-Jones *et al* (2001), as adapted from Davies-Jones (1986).

and tornadoes (Wakimoto and Liu 1998, Lee and Wurman 2005). Typical swirl ratios in laboratory vortices range from ~ 0.1 – 1.5 ; in a multiple-vortex tornado, swirl ratios of ~ 2 – 6 were estimated from ground-based, mobile, Doppler radar data (Lee and Wurman 2005); in the parent mesocyclone of a tornado, swirl ratios of ~ 0.7 – 8 were estimated from airborne-Doppler radar analyses and increased with time rapidly when a tornado formed (Wakimoto and Liu 1998).

The behaviour of an idealized tornado-like vortex in a vortex simulator is summarized in Davies-Jones (1986) and Davies-Jones *et al* (2001) (figure 23). At low swirl ratio, a ‘one-cell’ vortex forms, in which there is rising motion along the central axis of the tornado (and sinking motion far from the central axis). For moderate swirl ratio, a downward-directed pressure gradient develops in response to a decrease in the intensity of the vortex with height, which forces a downdraft aloft along the central axis. In the corner region, rapidly rising air along the central axis encounters the central downdraft and vortex breakdown occurs. Above the level of vortex breakdown, there is a ‘two-cell’ vortex, in which there is sinking motion along the central axis, rising motion outside of the central axis and sinking motion far from the central

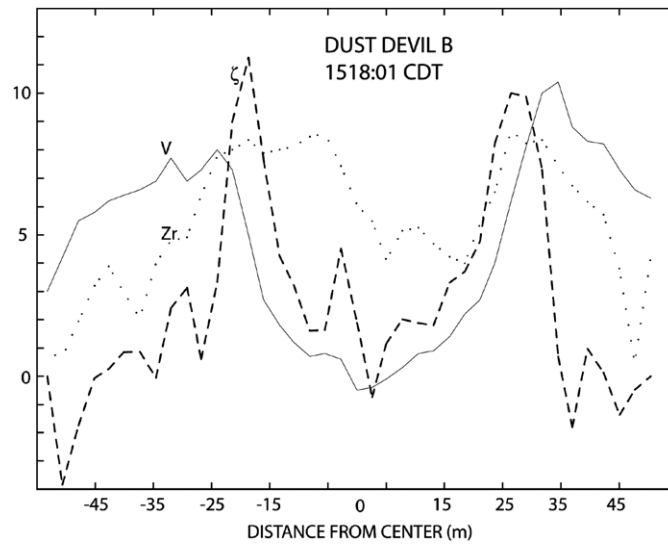


Figure 24. Radial profiles of azimuthally averaged azimuthal wind (solid line; m s^{-1}), vertical vorticity (dashed line; $\times 10 \text{ s}^{-1}$), and relative radar reflectivity (dotted line; dBZ) in a large dust devil in north-central Texas on 25 May 1999, based on data collected by a W-band, mobile Doppler radar. See Bluestein *et al* (2004a) for more details on how the data were collected and processed. From Bluestein *et al* (2004a).

axis. At some higher swirl ratio, the level of vortex breakdown lowers to the surface boundary layer and is then referred to as a *drowned vortex jump* (Maxworthy 1973, Snow 1982).

As the swirl ratio is increased some more, the width of the core of the vortex increases (because air turns upwards at a greater distance from the central axis) and the central axis sinking branch of the vertical circulation reaches the bottom. The vortex is now a relatively wide, two-cell vortex, and the radial profile of azimuthal wind is such that there is an annulus of strong shear vorticity flanked by downdraft at smaller radius and updraft at higher radius. This annulus of shear vorticity (created by the annulus of convergence that accompanies the rising branch of the vertical circulation), which has been also observed in dust devils (figure 24; Bluestein *et al* (2004a)), is barotropically unstable and breaks down into multiple, sub-tornado scale vortices (suction vortices) (Rotunno 1978) (figure 20). First, two small-scale, ‘secondary’ vortices form; with increasing swirl ratio, three to six vortices occur (e.g. Wurman 2002). These secondary vortices are responsible for producing cycloidal damage swaths (Fujita 1974). The damage inflicted by secondary vortices can be very intense, but highly localized. Each secondary vortex rotates around the central axis at \sim half the highest azimuthal wind speed of the primary vortex and the most unstable secondary vortices lean with height in the direction opposite that of the wind in the primary vortex. If the swirl ratio is then decreased, there is hysteresis, such that the transition in the number of secondary vortices decreases, but at higher critical swirl ratios. The transition from a one-cell to a two-cell vortex occurs \sim 0.5–0.7 in a laboratory simulator, depending upon the Reynolds number (Davies-Jones 1986).

Lewellen *et al* (2000) have defined a swirl ratio for the corner flow region only as

$$S_c = r_c M_\infty / Y, \quad (6.14)$$

where r_c is the core radius, M_∞ is the angular momentum outside the core and above the boundary layer and Y is the mass flux flowing out of the corner region. In this formulation, the vorticity is that of the core above the surface layer, while the convergence is that in the corner

region only. S_c is useful because for a given S , different corner-flow characteristics may be found with varying S_c .

Doppler radar estimates of the wind speeds in tornadoes frequently exceed the thermodynamic speed limit (6.11) by a substantial margin (Bluestein *et al* 1993), though there are some significant uncertainties regarding the representativeness of the radar and thermodynamic data (Davies-Jones *et al* 2001). It has been suggested that some of the discrepancy between the thermodynamic speed limit and observations might be a result of subsidence warming in the centre of a tornado, rather than buoyancy from latent-heat release (e.g. Walko 1988). In this case, air is warmed in the centre of the vortex much more rapidly than it can be via latent-heat release; a descending, dry air parcel warms at $\sim 10^\circ\text{C km}^{-1}$ and can become $\sim 10^\circ\text{C}$ warmer than the environment after only a few km if there is no radial mixing with its environment, while a saturated air parcel can become 10°C warmer than the environment only after ascending at least $\sim 5\text{--}6$ km, and then only under extreme circumstances. If air could descend from the tropopause to the boundary layer, extreme warming and hydrostatic pressure deficits would be possible. However, we argued earlier that in the core of a tornado vortex, there must be radial mixing before solid-body rotation sets in within the core radius; so extreme warming from subsidence is not likely, at least initially when there is radial mixing and nonbuoyant, environmental air gets mixed in. The time it takes the tornado vortex to develop solid-body rotation may be short compared with the time it takes environmental air to descend substantially. Furthermore, the air temperature near the ground would be much hotter than that anyone has ever observed, though it is not easy to confirm this by making temperature measurements in tornadoes; there are very few temperature measurements and those that exist are at the ground (Samaras 2004). Another possibility is that the descending air is saturated, so that it would not warm as rapidly as it would if it were unsaturated. It has been shown from infrared imagery that the lapse rate of temperature on the surface of a tornado condensation funnel is moist-adiabatic (Tanamachi *et al* 2006); measurements are not available inside the vortex aloft, though (unsuccessful) attempts have been made to obtain measurements using rockets with sensors launched from an aircraft (Colgate 1982).

Another mechanism for exceeding the thermodynamic speed limit is based on the failure of the hydrostatic assumption in the corner region, where parcel accelerations can be very large (Fiedler and Rotunno 1986) compared with the acceleration of gravity. In effect, it is the frictional interaction of the vortex with the ground that sets up a supercritical, end-wall vortex and allows for higher wind speeds. The frictionally induced vertical motions must match the vertical motions associated with the buoyancy aloft at the level of vortex breakdown. Wind speeds of $\sim 70\%$ greater than that consistent with the thermodynamic speed limit can occur at the level of vortex breakdown. The trick to reaching maximum possible intensity is to make sure that the level of vortex breakdown does not descend all the way to the ground, bringing with it a weaker, subcritical, broader vortex from above (but still more intense than the narrower vortex that would otherwise be present), or keeping the level of vortex breakdown too high above the ground: if the swirl ratio is too high, then vortex breakdown will reach the ground and 'maximum' intensity cannot be attained; if the swirl ratio is too low, then the end-wall vortex will be weaker. In nature, it is possible that the strongest winds are therefore not right at the ground, but elevated, at the level of vortex breakdown. Estimating tornado intensity from surface damage then may not be an accurate way of assessing the true intensity of a tornado. In addition, Fiedler (1994) has argued similarly that extremely high vertical wind speeds (supersonic) are possible in transient secondary vortices, though measurements inside secondary vortices in nature are especially difficult because they are so transient and small.

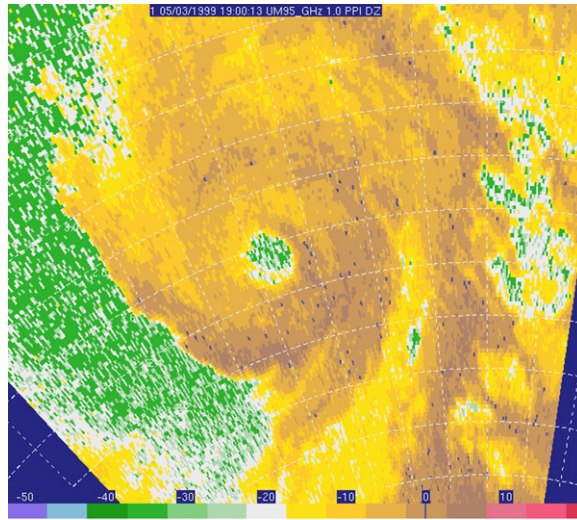


Figure 25. Horizontal cross section of radar reflectivity (colour coded in dBZ at the bottom) at a low level in a tornado near Verden, Oklahoma, on 3 May 1999, shortly after the photograph in figure 20 was taken, when the multiple-vortex tornado had turned into a single-vortex tornado; based on data collected by a mobile, W-band, Doppler radar. White range markings are shown every 200 m. View is to the southeast. See Bluestein and Pazmany (2000) for details on how the data were collected.

Radar-observed tornadoes (and vortices too weak to be classified as tornadoes and dust devils) frequently have a central weak-echo ‘eye’ (e.g. Fujita 1981, Wakimoto and Martner 1992, Wakimoto *et al* 1996, Wurman and Gill 2000, Bluestein *et al* 2004b, Bluestein *et al* 2003a, 2003b, Alexander and Wurman 2005, Tanamachi *et al* 2007, Bluestein *et al* 2007a) (figure 25). It is thought that the centrifuging radially outwards of precipitation particles and other debris into sheaths or rings leaves the centre of a tornado/small-scale vortex devoid of large scatterers (Snow 1984, Dowell *et al* 2005), leaving only scatterers too small to be detected by radar, or few at all. Ryzhkov *et al* (2005) and Bluestein *et al* (2007b) demonstrated, using polarimetric Doppler radar, that the rings of enhanced radar echoes in tornadoes are indeed most likely composed of debris (figure 26). However, it is still possible that sinking motions along the central axis of a tornado could also be responsible for some of the weakness in the radar echoes at the centre of a tornado (Wurman *et al* 1996).

The vertical structure of tornadoes observed by radar sometimes exhibits a bowl-shaped or otherwise closed-off bottom in radar reflectivity and an open, weak-echo or echo-free eye above (figure 27) (Wurman *et al* 1996, Bluestein *et al* 2004b, Alexander and Wurman 2005, Bluestein *et al* 2007a). The closing off of radar reflectivity near the ground is evidence of frictionally induced radial inflow of scatterers (Dowell *et al* 2005). Above the surface friction layer, centrifuging removes the largest pieces of debris and scatterers, while in the surface friction layer radial inflow may more than compensate for the outward centrifuging.

Doppler radar measurements in the surface friction layer are difficult to obtain, owing to ground-clutter contamination from trees, utility poles, houses, etc. and because the surface layer is so shallow that vertical resolution needed to discern vertical variations in wind speed is difficult to achieve in practice. Nevertheless, Bluestein *et al* (2007a) have provided some relatively high-resolution measurements that may indicate that the wind speed can increase by more than 25% in the surface friction layer.

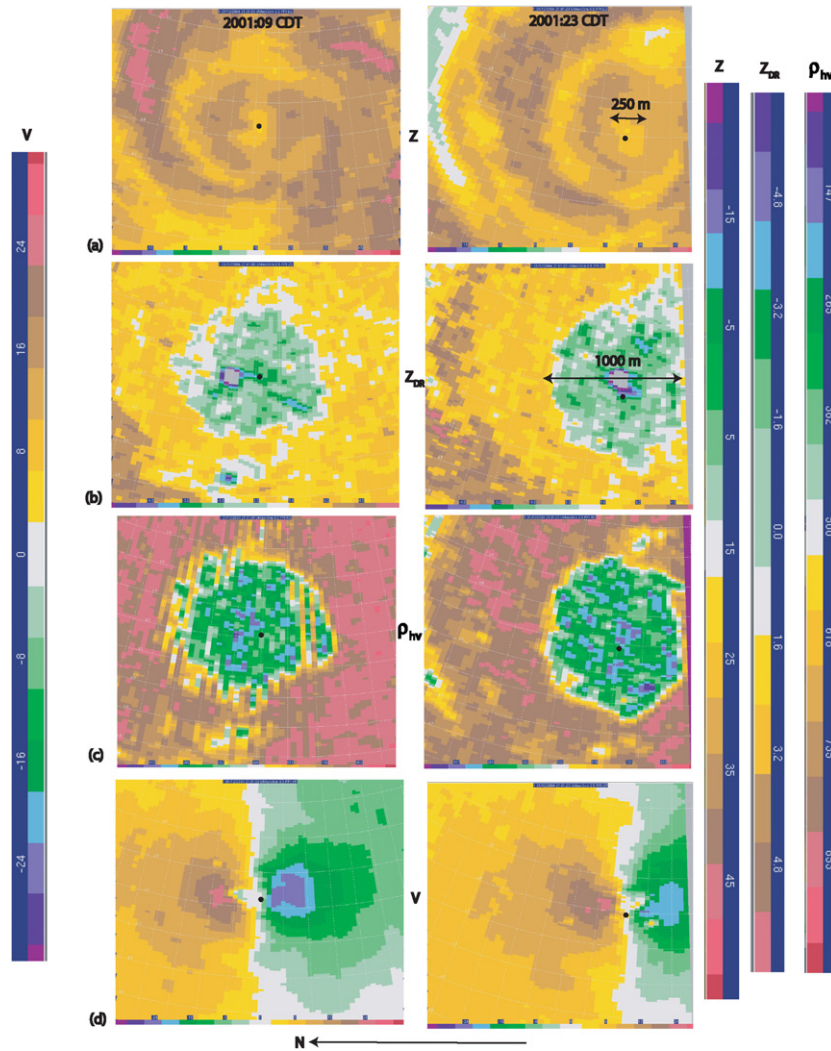


Figure 26. Horizontal cross section of (a) radar reflectivity (dBZ), (b) differential reflectivity (Z_{DR} in dB), (c) cross-correlation coefficient (ρ_{HV} , $\times 100$) and (d) Doppler velocity (m s^{-1}). Regions of $Z_{DR} \ll 1$ and $\rho_{HV} < 0.5$ are indicative of debris, rather than raindrops. The brown central ring in (a) is composed of debris, while the spiral bands of brown/red are composed of raindrops. The signature of a cyclonic vortex is evident in the red–purple/blue couplet in (d). From data collected by an X-band (3 cm wavelength), mobile Doppler radar. See Bluestein *et al* (2007b) for details on how the data were collected and processed. From Bluestein *et al* (2007b).

Spiral bands of enhanced radar echo seen around the tornado (e.g. Tanamachi *et al* 2007) are composed of raindrops and could be a result of Ekman instability, though to the best of the author’s knowledge this hypothesis has not been successfully tested.

6.2.2. Vortex formation: tornadogenesis. Rotunno (1986) has noted ‘the tornado does not fit a simple model like the spin-up that skaters experience when they pull in their arms.’ It may be inferred from observations that the proximity of tornado formation to surface boundaries

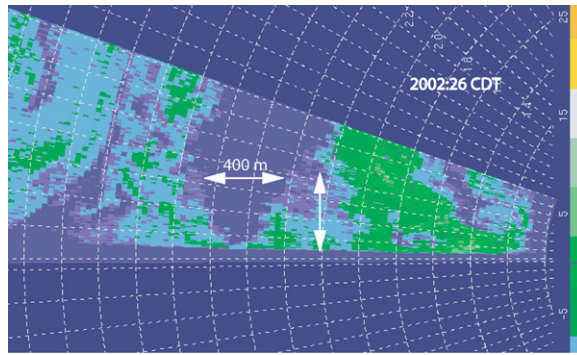


Figure 27. Vertical cross section of radar reflectivity (dBZ; colour code on the right) through the centre of a tornado on 12 May 2004 in south-central Kansas, based on data collected by a W-band, mobile Doppler radar. White range rings are shown every 200 m. See Bluestein *et al* (2007a) for details on how the data were collected and processed. From Bluestein *et al* (2007a).

separating warm, ambient air from evaporatively cooled outflow, and of very strong updrafts near the ground, ‘that complex boundary layer interactions are (also) important.’ To understand how tornadoes form, the source of their vorticity must be identified and the mechanisms for its rapid increase must be accounted for.

First, we consider how pre-existing vorticity can be increased to tornado intensity. Vorticity in a tornado is $\sim O(1\text{s}^{-1})$, since radial shear of the azimuthal wind $\sim 50\text{--}100\text{ m s}^{-1}/100\text{ m}$. Background vorticity associated with a mesocyclone is $\sim O(5 \times 10^{-3}\text{ s}^{-1})$, since radial shear of the azimuthal wind $\sim 20\text{ m s}^{-1}/5\text{ km}$. Considering only the divergence term in vorticity equation (2.13), it is seen that under the effect of a field of constant convergence at the base of a convective storm of $\sim 10\text{ m s}^{-1}/1\text{ km} = 10^{-2}\text{ s}^{-1}$, which is consistent with a buoyant updraft in a convective cloud above ($\partial w/\partial z \sim \partial u/\partial x$ and $\partial v/\partial y \sim 10\text{ m s}^{-1}/1\text{ km}$), the e-folding time for vorticity is $1/\text{convergence} \sim 100\text{ s}$, or on the order of a minute. In $\sim 9\text{ min}$, vorticity of tornado intensity can be ‘grown’ from mesocyclone vorticity. In $\sim 9\text{ min}$, air flowing at $\sim 10\text{ m s}^{-1}$ from the outer edge of a mesocyclone at the ground at 5 km radius would just make it to the centre of the tornado and then be transported upwards.

However, vorticity is scale dependent and it is possible, for example, to identify vortices such as dust devils, whose wind speeds can vary $\sim 10\text{ m s}^{-1}$ over only 10 m , having vorticity as high as that of tornadoes. Circulation, the area integral of vorticity, is therefore a better indicator of tornadic vortices. The circulation enclosing the core of an F1–F2 tornado $\sim \pi(100\text{ m})^2(1.0\text{ s}^{-1}) \sim 30\,000\text{ m}^2\text{ s}^{-1}$ (see actual measurements in Tanamachi *et al* (2007) and figure 22). (In contrast, the circulation of a dust devil is $\sim 600\text{ m}^2\text{ s}^{-1}$.) A circulation in a 5 km wide mesocyclone of $30\,000\text{ m}^2\text{ s}^{-1}$, with vorticity averaging $1.5 \times 10^{-3}\text{ s}^{-1}$, could be brought to 100 m radius in $\sim 9\text{ min}$.

Possible sources of vertical vorticity for tornadoes include horizontal vorticity generated baroclinically along the edge of an outflow boundary (Klemp and Rotunno 1983, Rotunno and Klemp 1985, Trapp and Fiedler 1995) or along the edge of water-loaded air and/or pre-existing horizontal vorticity (Wicker 1996) associated with boundary layer vertical shear, which is subsequently tilted onto the vertical as air parcels encounter the gradient in vertical velocity as they enter an updraft or pass in between an updraft and a downdraft. Unless air parcels turn very sharply upwards, tilting along the gradient of an updraft alone is insufficient to create a tornado because vertical vorticity is rapidly advected upwards, away from the ground (Davies-Jones 1982). It has been suggested that when a downdraft forms

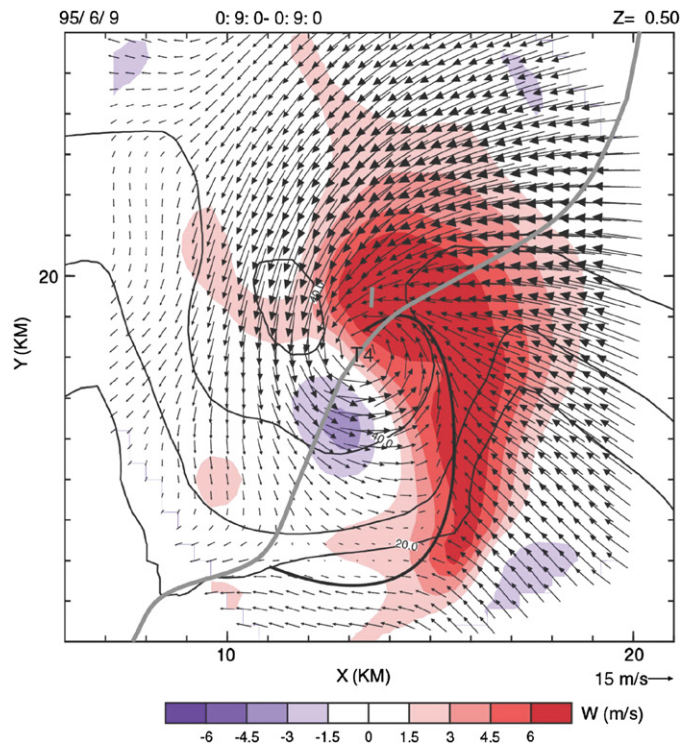


Figure 28. Storm-relative wind field in a tornadic supercell at 500 m above the ground, as determined from an analysis of airborne Doppler radar data, on 8 June 1995, over the northern Texas Panhandle, during VORTEX. Vertical velocity colour coded below; red (purple) area indicates rising (sinking) motion. Solid black contours indicate radar reflectivity (dBZ). Thick, grey line indicates the tornado tracks, the longest of which is for T4, whose location at the time of the analysis is noted. Courtesy of David Dowell; adapted from Dowell and Bluestein (2002).

adjacent to an updraft, that vertical vorticity created through tilting remains closer to the ground. In many cases, the tornado is indeed located along a gradient in vertical motion, in between the rear-flank downdraft (RFD) and the tip of the horseshoe-shaped updraft along the leading edge of the RFD (Dowell and Bluestein 2002) (figure 28). The role of baroclinically generated horizontal vorticity in the FFD region of a supercell has been called into question recently, however, owing to observations that temperature gradients at the surface near strong tornadoes seem to be much weaker than those in the absence of tornadoes (Shabbott and Markowski 2006).

It has also been postulated that horizontal vorticity associated with the vertical shear accompanying the thermal wind or other environmental features is tilted into vertical vorticity by the RFD downdraft and the cyclonic part of it can be advected into the storm's main updraft, which is located ahead and to the left of the RFD (Walko 1993).

Another source of vorticity is barotropic (vertical) vorticity associated with horizontal shear. Vortex 'sheets', bands of intense shear vorticity can be found along gust fronts or other sharp surface boundaries and these vortex sheets may be barotropically unstable, allowing for the growth of a series of vortices (Barcilon and Drazin 1972, Wakimoto and Wilson 1989, Carbone 1982, 1983, Lee and Wilhelmson 1997). Many nonsupercell tornadoes occur as periodically spaced vortices along a line. However, vortices strung out in a line along the rear-flank gust front in supercells have also been noted (Bluestein *et al* 2003a) (figure 29).

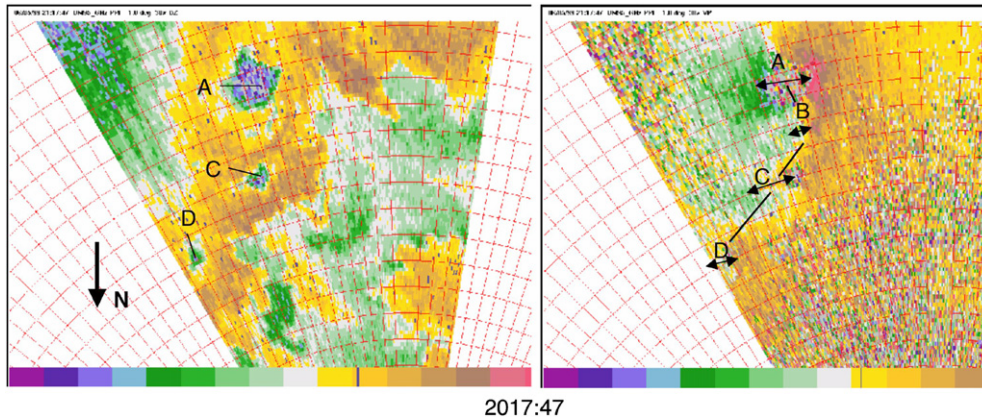


Figure 29. Horizontal cross section at low levels of radar reflectivity (left; intensity increases to the right) and Doppler velocity (right; colour coded below in m s^{-1} , with -60 at the left (purple) and 20 to the right (red, cutoff from view, just off scale)), from data collected by a W-band, mobile Doppler radar, on 5 June 1999, in north-central Nebraska. Cyclonic vortex signatures are located at A (a tornado), B, C and D. Arc-shaped line connects vortex signatures A–B–C–D. A, C and D are collocated with weak-echo holes. Range markers shown every 100 m. See Bluestein *et al* (2003a) for details on how the data were collected and processed. From Bluestein *et al* (2003a).

It is also possible that vertical vorticity is generated aloft in the convective storm by the tilting of environmental horizontal vorticity associated with thermal wind shear and then amplified by convergence in an updraft; it is then advected downwards or propagates downwards through the ‘dynamic pipe effect’ (DPE) (Leslie 1971, Smith and Leslie 1978). When a vortex forms at midlevels, air is drawn up into it by an upward-directed pressure-gradient force (associated with the increase in vorticity with height; see equation (4.9)). The resulting convergence increases vorticity below the original vortex, creating a mechanism for downward propagation of the vortex. It has been found from Doppler radar observations that many ‘tornadic vortex signatures’ (and hence tornadoes, it is assumed; Brown *et al* (1978)) begin at midlevels and then build downwards (Trapp *et al* 1999). Trapp and Davies-Jones (1997) showed that when buoyancy is greatest at midlevels, then there is the highest potential for the DPE; when buoyancy is greatest at low levels, vorticity increases throughout a vertical column simultaneously.

Davies-Jones (2006) has recently considered the possibility that the hook echo in supercells, which has been thought for decades to be formed as precipitation is transported in a curved trajectory by a low-level mesocyclone, actually plays an active role in tornadogenesis. There is some observational evidence that hook echoes can also form as precipitation falls (sometimes as a narrow rain curtain (Bluestein and Pazmany 2000)) and that advection is not the only mechanism responsible for the hook shape (e.g. Rasmussen *et al* 2006). Davies-Jones (2006) postulated that precipitation-induced drag just outside the centre of a strong updraft drives a downdraft that transports high-angular momentum downwards (Fujita 1975) and increases surface convergence, owing to surface friction. It is not the baroclinically generated azimuthal vorticity (due to the radial gradient in precipitation loading) that becomes the tornado, but rather the radially inward-directed frictionally generated vorticity that is tilted upwards and stretched.

It is thought that Earth’s vorticity does not contribute *directly* to tornadogenesis. Convergence of 10^{-2} s^{-1} would have to act on Earth’s vorticity ($\sim 10^{-4} \text{ s}^{-1}$) for about 15 min to produce a tornado, which would require a strong, very wide, and persistent updraft. Suppose

that a typical cloud base is ~ 5 km in diameter; in 15 min, air moving at 10 m s^{-1} would travel ~ 9 km, which is much farther than the radius of the updraft. Thus, air in that time period would have turned upwards into the updraft, advecting vorticity upwards and moving away from the region of low-level convergence. (However, in 6.5 min, convergence of 10^{-2} s^{-1} acting on Earth's vorticity could produce mesocyclone-intensity vorticity of $5 \times 10^{-3} \text{ s}^{-1}$, and air would only have moved horizontally ~ 4 km, which is \sim width of a mesocyclone.) In any event, numerical cloud models produce realistic-looking supercell structure and tornado-like vortices with no Earth's vorticity present in the model. However, in nature, the vertical wind shear necessary to produce a supercell is associated with Earth's rotation, so in a sense Earth's rotation (see (4.1)) is necessary for the production of supercell tornadoes in midlatitudes, even though it is not the source of vorticity itself. It is likely, though, that Earth's vorticity enhances whatever relative vorticity there already is and can in effect speed up tornadogenesis.

Localized, transient areas of convergence may act to spin up tornadoes. When the RFD descends to the ground, it spreads out and wraps around the low-level mesocyclone. As it hits the leading edge of the rear-flank gust front, it can produce localized strong convergence. This localized convergence may act to produce a strong vortex. Microbursts might therefore be able to trigger tornadoes (Bluestein *et al* 2003a). Rasmussen *et al* 2006, Byko *et al* (2006), Kennedy *et al* (2006) and Orf *et al* (2006) have considered 'descending reflectivity cores' (DRC) in supercells as being associated with wet microbursts capable of initiating tornadoes, though all the evidence has not yet been considered and work is still in progress.

The mechanisms hitherto considered involve the mean azimuthal velocities. In tornadoes that have eddies such as secondary vortices or vortex Rossby waves (these waves are analogous to Rossby waves in large-scale flow, except that the radial gradient of the centrifugal force plays the same role as the latitudinal gradient of Earth's vorticity (Montgomery and Kallenbach 1997)) or Ekman instabilities, it is possible that the eddies are tilted (with respect to the radial direction) so as to convert eddy angular momentum into mean angular momentum (Guadet *et al* 2006) (as happens for synoptic-scale flow in the baroclinic westerlies). Such a process has been called *negative viscosity* (Starr 1968) and could be responsible for affecting the intensity some tornadoes (Lilly 1969).

A process similar to that of negative viscosity might be the conglomeration of pre-existing, smaller-scale vortices into a larger one: Bluestein *et al* (2003a) found evidence of tornado formation when smaller vortices along a gust front seemed to interact to produce a larger-scale, tornadic vortex; similar behaviour has been noted in some numerical simulations (Noda and Niino 2005). Wakimoto and Liu (1998) have suggested that some tornadoes may be initiated when an occlusion/RFD downdraft forms in a mesocyclone (as a result of vorticity becoming less cyclonic with height and/or precipitation loading and/or evaporative cooling) and reaches the ground, leading to an annulus of barotropically unstable air in it, which then breaks down into multiple vortices, each which could become a tornado.

Just as mesocyclones sometimes form and decay in a cyclical fashion, so do tornadoes in a process referred to as *cyclic tornadogenesis* (Burgess *et al* 1982). Dowell and Bluestein (2002), using airborne Doppler radar data, further refined the conceptual model of cyclic tornadogenesis proposed by Burgess *et al* (1982) (figure 30). An incipient vortex forms along the rear-flank gust front and propagates along the horseshoe-shaped updraft associated with the flanking line towers, until it reaches the tip of the end of the horseshoe-shaped updraft, near the RFD. When it reaches this location of strong horizontal gradient in vertical motion, the tornado is mature. The tornado then propagates away from the updraft entirely, and it dissipates in the downdraft region. A new tornado may then form along the bulge in the rear-flank gust front, and the process of tornadogenesis is repeated. In some rare instances, a tornado may become locked into position so that it does not propagate away from the tip of the updraft region and

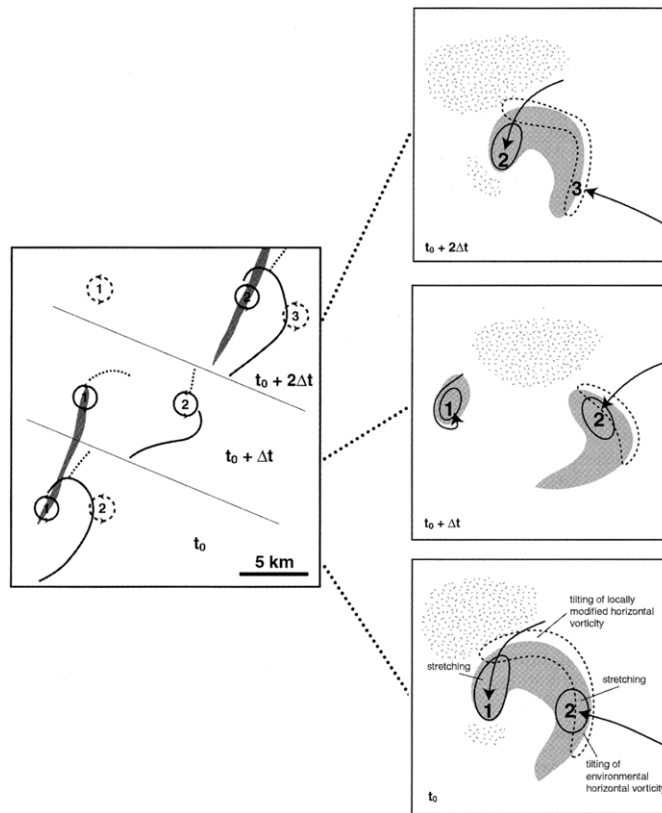


Figure 30. Conceptual model of cyclic tornadogenesis in horizontal cross sections at low levels. On the panel to the left: solid (dashed) line depicts the location of the rear-flank (forward-flank) wind shift; shaded regions depict tornado tracks; number of each tornado vortex, labelled in ascending order with respect to time. Insets at right for selected times t_0 , $t_0 + \Delta t$, and $t_0 + 2\Delta t$; shaded areas (speckled areas) denote updraft (downdraft) areas; solid (dashed) contours denote regions of the increase in cyclonic vorticity through stretching (tilting). From Dowell and Bluestein (2002).

a long-lived, very intense tornado may result. It is not known why in these rare instances the tornado remains locked into its mature phase, but observational evidence suggests that interaction with a gust front from a neighbouring convective storm may play a role.

Most tornadoes in supercells rotate cyclonically. There are a number of documented cases of anticyclonic tornadoes forming in cyclonically rotating, right-moving supercells (Brown and Knupp 1980, Burgess 1976, Fujita 1981, Bluestein *et al* 2007b). Anticyclonic tornadoes have not been documented, to the author's best knowledge, in any anticyclonically rotating, left-moving supercell. When anticyclonically rotating tornadoes are observed in cyclonically rotating supercells, they are found near or along the edge of the rear-flank gust front, $\sim 5\text{--}10$ km from a surface mesocyclone and/or cyclonic tornado; i.e. anticyclonic tornadoes in supercells are found paired with nearby cyclonic tornadoes or the remnants of them. Anticyclonic vortices of larger scale and weaker vorticity than that associated with tornadoes are sometimes observed in the region near where anticyclonic tornadoes have been found (e.g. Bluestein and Gaddy 2001). These anticyclonic vortices may be associated with the tilting of baroclinically generated horizontal vorticity along the edge of the rear-flank gust front in between the rear-flank downdraft and the main updraft or the tilting of environmental horizontal vorticity

(associated with vertical shear) along the edge of the rear-flank downdraft. Perhaps tornadoes can be formed when low-level convergence in the vicinity of such an anticyclonic vortex appears, in response to a rapidly growing updraft along the flanking line, above the rear-flank gust front. Numerical cloud models have not yet simulated anticyclonic tornadoes in supercells and their formation has not been well observed by Doppler radars. It is not known whether anticyclonic tornadoes are related dynamically to the cyclonic member of the pair of vortices or if they are independent of it.

7. Future research

In this author's opinion the most important, fundamental unanswered questions regarding the dynamics of severe weather systems are as follows.

- (a) What controls the intensity and depth of cold pools in precipitating convective clouds? It is recognized that the intensity and depth of cold pools play fundamental roles in many convective phenomena (e.g. tornadoes, microbursts). It is likely that understanding the microphysical processes responsible for precipitation formation and the feedback on the wind field is of paramount importance.
- (b) How do tornadoes form in convective storms and why do they form only on relatively rare occasions? In order to solve this conundrum, it is necessary to take a more holistic approach. In past studies, tornadogenesis has not been considered from the perspective of the entire airflow in the storm on many scales, owing to observational and simulation limitations.
- (c) How can the estimate of precipitation in convective storms be improved? To do so, it will be necessary, as in answering question (b), to improve our understanding of precipitation microphysics and its dependence on the airflow and thermodynamics of storms.
- (d) What controls the formation of convective storms? Often storms fail to form, even when the conditions for their formation seem to be met.

7.1. Numerical simulations

As the capacity and speed of computing systems are increasing, it is becoming possible to simulate the entire convective storm, not just small portions of it (e.g. just the tornado region). By simulating entire storms and convective storms explicitly, using very small grid spacing, it will be possible to study, using controls on the environment, processes such as tornadogenesis, precipitation efficiency and surface wind generation and to test specific hypotheses and isolate certain physical phenomena. It will also be possible to model microphysical processes more accurately, by using more detailed parametrizations of hydrometeor type (e.g. Straka *et al* 2000).

Data-assimilation techniques need to be perfected, in which observations are used to initialize a numerical model, which then is used to produce enhanced analyses that reveal features not resolvable by any observational system alone. Techniques such as ensemble Kalman filtering (Dowell *et al* 2004, French *et al* 2006), which are used to obtain better estimates of atmospheric variables, need to be further developed and applied.

7.2. Observations

Doppler radars are the primary devices used to map out the wind and precipitation fields in convective storms. Conventional radars systems take a minute or longer to scan just a portion

of a storm. The speed with which a storm can be scanned, so that rapidly evolving processes such as tornadogenesis can be monitored, must be increased. Tornadogenesis, for example, proceeds on time scales of tens of seconds. Phased-array (electronically scanning) and other rapidly scanning radar systems, which can scan entire storms every 10 s or so, need to be developed further and used. In addition, the spatial resolution must be adequate for resolving fine-scale features such as tornadoes and microbursts. Radars have been mounted on vans, trucks and aircraft and transported close to storms to achieve high spatial resolution and to overcome the over-the-horizon problem (coverage in the important boundary layer is limited, owing to the Earth's curvature). Networks of low-powered radars mounted on small towers are being developed as an alternative to the mobile systems and to supplement the existing, high-powered, but sparsely distributed operational radar network (McLaughlin *et al* 2005).

Remote identification of hydrometeor type and distribution need to be improved through the use of dual-polarization radar systems (e.g. Zrníc and Ryzhkov 1999) and *in situ* verification using penetrating aircraft equipped with cloud-physics monitoring systems.

While measurements of the wind field in convective clouds have been facilitated by the use of Doppler radar, the problem of mapping out the temperature and water vapour content in clouds has not been solved to such a high degree. Remote-sensing methods involving scanning lidars and Doppler lidars need to be perfected and remotely piloted vehicles (RPVs) need to be developed that can make measurements of temperature and water vapour in many areas of a storm nearly simultaneously.

Densely distributed surface networks of instrumented towers need to be developed further so that fine-scale measurements of the vertical variation of wind and thermodynamic variables can be made underneath convective storms.

In summary, it is seen that technology has played a major role in our evolving understanding of severe weather systems. It is likely that technology will continue to be the impetus for improving our understanding in the next decades. The room will always exist, however, for clever theoreticians who can clearly articulate the fundamental problems and solve them using novel techniques that do not necessarily require advanced technology.

Acknowledgments

This work was funded by National Science Foundation grants ATM – 0637148 and ATM – 0241037. Figures from publications in *Monthly Weather Review*, *Journal of the Atmospheric Sciences*, *Weather and Forecasting*, *Journal of Atmospheric and Oceanic Technology*, and *Bulletin of the American Meteorological Society* are reprinted courtesy of the American Meteorological Society. Much of the radar hardware and software for studies referenced was provided by the Microwave Remote Sensing Laboratory of the University of Massachusetts, Amherst, by the National Center for Atmospheric Research (NCAR) in Boulder, Colorado and by the Los Alamos National Laboratory (LANL) in Los Alamos, New Mexico. The author's graduate students participated in many of the field programs and in the analysis of the data collected for many of the analyzed datasets noted in the text. In particular, Robin Tanamachi, Mike French, Chris Weiss, David Dowell, Matt Kramar and Steve Gaddy are acknowledged. Collaboration and conversations with Morris Weisman (NCAR), Rich Rotunno (NCAR), Roger Wakimoto (NCAR), Steve Frasier (UMass.), Andy Pazmany (ProSensing), Bob McIntosh (UMass.), Wes Unruh (LANL), Brian Fiedler (OU) and personnel at the National Severe Storms Laboratory, Norman, Oklahoma are much appreciated.

References

- Adlerman E J and Droegemeier K K 2002 The sensitivity of numerically simulated cyclic mesocyclogenesis to variations in model physical and computational parameters *Mon. Weather Rev.* **130** 2671–91
- Adlerman E J and Droegemeier K K 2005 The Dependence of numerically simulated cyclic mesocyclogenesis upon environmental vertical wind shear *Mon. Weather Rev.* **133** 3595–623
- Adlerman E J, Droegemeier K K and Davies-Jones R 1999 A numerical simulation of cyclic mesocyclogenesis *J. Atmos. Sci.* **56** 2045–69
- Alexander C R and Wurman J 2005 The 30 May 1998 Spencer, South Dakota, storm: I. The structural evolution and environment of the tornadoes *Mon. Weather Rev.* **133** 72–96
- Alexander C R and Wurman J 2006 Mobile radar based climatology of tornado structure and dynamics *23rd Conf. on Severe Local Storms (St. Louis, MO, 6–10 November)* (Boston, MA: American Meteorological Society) (extended abstract not available)
- Atkins N T, Weisman M L and Wicker L J 1999 The influence of preexisting boundaries on supercell evolution *Mon. Weather Rev.* **127** 2910–27
- Barcilon A and Drazin P G 1972 Dust devil formation *Geophys. Fluid Dyn.* **4** 147–58
- Barnes S L 1968 On the source of thunderstorm rotation *Tech. Memo. Nat'l. Severe Storms Lab., ERLTM-NSSL* 38, 38pp
- Barnes S L 1970 Some aspects of a severe, right-moving thunderstorm deduced from mesonet network rawinsonde observations *J. Atmos. Sci.* **27** 634–48
- Bartels D L and Maddox R A 1991 Midlevel cyclonic vortices generated by mesoscale convective systems *Mon. Weather Rev.* **119** 104–18
- Beck J R, Schroeder J L and Wurman J M 2006 High-resolution dual-Doppler analyses of the 29 May 2001 Kress, Texas, cyclic supercell *Mon. Weather Rev.* **134** 3125–48
- Bedard A J 2005 Low-frequency atmospheric acoustic energy associated with vortices produced by thunderstorms *Mon. Weather Rev.* **133** 241–63
- Benjamin T B 1962 Theory of the vortex breakdown phenomenon *J. Fluid Mech.* **14** 593–629
- Biggerstaff M I and Houze R A Jr 1993 Kinematics and microphysics of the transition zone of the 10–11 June 1985 squall line *J. Atmos. Sci.* **50** 3091–110
- Bluestein H B 1985 The formation of a 'landspout' in a 'broken-line' squall line in Oklahoma *14th Conf. on Severe Local Storms (Indianapolis)* (Preprints) (Boston, MA: American Meteorological Society) pp 267–70
- Bluestein H B 1992 *Synoptic-Dynamic Meteorology in Midlatitudes, vol I: Principles of Kinematics and Dynamics* (Oxford: Oxford University Press) 431pp
- Bluestein H B 1993 *Synoptic-Dynamic Meteorology in Midlatitudes, vol II: Observations and Theory of Weather Systems* (Oxford: Oxford University Press) 594pp
- Bluestein H B 1994 High-based funnel clouds in the Southern Plains *Mon. Weather Rev.* **122** 2631–8
- Bluestein H B 1999 A history of storm-intercept field programs *Weather Forecast.* **14** 558–77
- Bluestein H B 2000 A tornadic supercell over elevated, complex terrain: The Divide, Colorado storm of 12 July 1996 *Mon. Weather Rev.* **128** 795–809
- Bluestein H B 2005 More observations of small funnel clouds and other tubular clouds *Mon. Weather Rev.* **133** 3714–20
- Bluestein H B and Parks C R 1983 A synoptic and photographic climatology of low-precipitation severe thunderstorms in the Southern Plains *Mon. Weather Rev.* **111** 2034–46
- Bluestein H B and Jain M 1985 Formation of mesoscale lines of precipitation: severe squall lines in Oklahoma during the spring *J. Atmos. Sci.* **42** 1711–32
- Bluestein H B and MacGorman D R 1998 Evolution of cloud-to-ground lightning characteristics in the Spearman, Texas tornadic supercells of 31 May 1990 *Mon. Weather Rev.* **126** 1451–67
- Bluestein H B and Weisman M L 2000 The interaction of numerically simulated supercells initiated along lines *Mon. Weather Rev.* **128** 3128–49
- Bluestein H B and Pazmany A L 2000 Observations of tornadoes and other convective phenomena with a mobile, 3 mm wavelength, Doppler radar: the spring 1999 field experiment *Bull. Am. Meteorol. Soc.* **81** 2939–51
- Bluestein H B and Gaddy S G 2001 Airborne pseudo-dual-Doppler analysis of a rear-inflow jet and deep convergence zone in a supercell *Mon. Weather Rev.* **129** 2270–89
- Bluestein H B and Banacos P C 2002 The vertical profile of wind and temperature in cyclones and anticyclones over the eastern two-thirds of the United States: a climatology *Mon. Weather Rev.* **130** 477–506
- Bluestein H B and Wakimoto R M 2003 Mobile radar observations of severe convective storms *Radar and Atmospheric Science: A Collection of Essays in Honor of David Atlas* ed R Wakimoto and R Srivastava (*Meteorological Monograph* vol 30) (Boston, MA: American Meteorological Society) pp 105–36

- Bluestein H B, McCaul E W Jr, Byrd G P and Woodall G 1988 Mobile sounding observations of a tornadic storm near the dryline: the Canadian, Texas storm of 7 May 1986 *Mon. Weather Rev.* **116** 1790–804
- Bluestein H B, Unruh W P, LaDue J, Stein H and Spehger D 1993 Dopplerradar wind spectra of supercell tornadoes *Mon. Weather Rev.* **121** 2200–21
- Bluestein H B, Weiss C C and Pazmany A L 2003a Mobile Doppler radar observations of a tornado in a supercell near Bassett, Nebraska, on 5 June 1999: I. Tornadogenesis *Mon. Weather Rev.* **131** 2954–67
- Bluestein H B, Lee W-C, Bell M, Weiss C C and Pazmany A L 2003b Mobile Doppler radar observations of a tornado in a supercell near Bassett, Nebraska, on 5 June 1999: II. Tornado-vortex structure *Mon. Weather Rev.* **131** 2968–84
- Bluestein H B, Weiss C C and Pazmany A L 2004a Doppler radar observations of dust devils in Texas *Mon. Weather Rev.* **132** 209–24
- Bluestein H B, Weiss C C and Pazmany A L 2004b The vertical structure of a tornado near Happy, Texas, on 5 May 2002: high-resolution, mobile, W-band Doppler radar observations *Mon. Weather Rev.* **132** 2325–37
- Bluestein H B, Weiss C C, French M M, Holthaus E M and Tanamachi R L 2007a The structure of tornadoes near Attica, Kansas, on 12 May 2004: high-resolution, mobile, Doppler radar observations *Mon. Weather Rev.* **135** 475–506
- Bluestein H B, French M M, Frasier S, Hardwick K, Junyent F and Pazmany A L 2007b Close-range observations of tornadoes in supercells made a dual-polarization, X-band, mobile Doppler radar *Mon. Weather Rev.* **135** 1522–43
- Brandes E A 1978 Mesocyclone evolution and tornadogenesis: Some observations *Mon. Weather Rev.* **106** 995–1011
- Brandes E A 1981 Finestructure of the Del City–Edmond tornadic mesocirculation *Mon. Weather Rev.* **109** 635–47
- Brandes E A 1984 Vertical vorticity generation and mesocyclone sustenance in tornadic thunderstorms: the observational evidence *Mon. Weather Rev.* **112** 2253–69
- Brandes E A 1990 Evolution and structure of the 6–7 May 1985 mesoscale convective system and associated vortex *Mon. Weather Rev.* **118** 109–27
- Braun S A and Houze R A Jr 1994 The transition zone and secondary maximum of radar reflectivity behind a midlatitude squall line: results retrieved from Doppler radar data *J. Atmos. Sci.* **51** 2733–55
- Brown J M and Knupp K R 1980 The Iowa cyclonic–anticyclonic tornado pair and its parent thunderstorm *Mon. Weather Rev.* **108** 1626–46
- Brown R A, Lemon L R and Burgess D W 1978 Tornado detection by pulsed Doppler radar *Mon. Weather Rev.* **106** 29–39
- Browning K A 1965 The evolution of tornadic storms *J. Atmos. Sci.* **22** 664–8
- Browning K A and Donaldson R J Jr 1963 Airflow and structure of a tornadic storm *J. Atmos. Sci.* **20** 533–45
- Bunkers M J, Klimowski B A, Zeitler J W, Thompson R L and Weisman M L 2000 Predicting supercell motion using a new hodograph technique *Weather Forecast.* **15** 61–79
- Burgess D W 1976 Anticyclonic tornado *Weatherwise* **29** 167
- Burgess D W, Wood V T and Brown R A 1982 Mesocyclone evolution statistics *12th Conf. on Severe Local Storms (San Antonio, TX)* (Preprints) (Boston, MA: American Meteorological Society) pp 422–4
- Byers H R and Braham R R Jr 1949 *The Thunderstorm* Superintendent of cuments, US Government Printing Office Washington DC
- Byko Z M, Markowski P and Richardson Y P 2006 Radar reflectivity ‘blobs’ observed by the Doppler on Wheels *23rd Conf. on Severe Local Storms (St Louis, MO, 6–10 November)* (extended abstracts) (Boston, MA: American Meteorological Society) CD - ROM, 15.7
- Carbone R E 1982 A severe frontal rainband: I. Stormwide hydrodynamic structure *J. Atmos. Sci.* **39** 258–79
- Carbone R E 1983 A severe frontal rainband: II. Tornado parent vortex circulation *J. Atmos. Sci.* **40** 2639–54
- Chisholm A J and Renick J H 1972 The kinematics of multicell and supercell Alberta hailstorms. Alberta hail studies, Research Council of Alberta Hail Studies *Rep.* 72–2, 24–31, 53pp
- Church C R and Snow J T 1993 Laboratory models of tornadoes *The Tornado: Its Structure, Dynamics, Prediction and Hazards* ed Church C R (Washington, DC: American Geophysical Union) pp 277–95
- Cohen C and McCaul E W Jr 2006 The sensitivity of simulated convective storms to variations in prescribed single-moment microphysics parameters that describe particle distributions, sizes and numbers *Mon. Weather Rev.* **134** 2547–65
- Colgate S 1982 Small rocket tornado probe *12th Conf. on Severe Local Storms (San Antonio, TX)* (Preprints) (Boston, MA: American Meteorological Society) pp 396–400
- Davies-Jones R P 1982 Observational and theoretical aspects of tornadogenesis *Intense Atmospheric Vortices* ed L Bengtsson and J Lighthill (Berlin: Springer) pp 175–89
- Davies-Jones R P 1984 Streamwise vorticity: the origin of updraft rotation in supercell storms *J. Atmos. Sci.* **41** 2991–3006
- Davies-Jones R P 1986 Tornado dynamics *Thunderstorm Morphology and Dynamics* ed E Kessler (Norman, OK: University of Oklahoma Press) pp 197–236

- Davies-Jones R P 2000 A Lagrangian model for baroclinic genesis of mesoscale Vortices: I. Theory *J. Atmos. Sci.* **57** 715–36
- Davies-Jones R P 2002 Linear and nonlinear propagation of supercell storms *J. Atmos. Sci.* **59** 3178–205
- Davies-Jones R P 2006 Tornadogenesis in supercell storms—What we know and what we don't know. Extended abstracts *23rd Conf. on Severe Local Storms (St. Louis, MO, 6–10 November)* (Boston, MA: American Meteorological Society) CD - ROM, 2.2
- Davies-Jones R P and Brooks H E 1993 Mesocyclogenesis from a theoretical perspective *The Tornado: Its Structure, Dynamics, Prediction and Hazards* ed Church C R (Washington, DC: American Geophysical Union) pp 105–114
- Davies-Jones R P, Burgess D and Foster M 1990 Test of helicity as a tornado forecast Parameter *16th Conf. on Severe Local Storms (Kananaskis Park, AB, Canada) (Preprints)* (Boston, MA: American Meteorological Society) pp 588–92
- Davies-Jones R P, Trapp R J and Bluestein H B 2001 Tornadoes *Severe Convective Storms (Meteorological Monographs vol 28)* ed C Doswell III (Boston, MA: American Meteorological Society) pp 167–221
- Davis C A and Weisman M L 1994 Balanced dynamics of mesoscale vortices produced in simulated convective systems *J. Atmos. Sci.* **51** 2005–30
- Donaldson R J Jr 1970 Vortex recognition by a Doppler radar *J. Appl. Meteorol.* **9** 661–70
- Doswell C A 2001 Severe convective storms—an overview *Severe Convective Storms (Meteorological Monographs, vol 28)* ed C Doswell III (Boston, MA: American Meteorological Society) pp 1–26
- Doswell C A, Moller A R and Przybylinski R, 1990 A unified set of conceptual models for variations on the supercell theme *16th Conf. on Severe Local Storms (Indianapolis) (Preprints)* (Boston, MA: American Meteorological Society) pp 398–401
- Doviak R J and Zrnic D S 1993 *Doppler Radar and Weather Observations*. (New York: Academic) 562pp
- Dowell D C and Bluestein H B, 2002 The 8 June 1995 McLean, Texas, storm: II. Cyclic tornado formation, maintenance and dissipation *Mon. Weather Rev.* **130** 2649–70
- Dowell D C, Zhang F, Wicker L J, Snyder C and Crook N A 2004 Wind and temperature retrievals in the 17 May 1981 Arcadia, Oklahoma, supercell: Ensemble Kalman filter experiments *Mon. Weather Rev.* **132** 1982–2005
- Dowell D C, Alexander C R, Wurman J M and Wicker L J 2005 Reflectivity patterns and wind-measurement errors in high-resolution radar observations of tornadoes *Mon. Weather Rev.* **133** 1501–24
- Droegemeier K R and Wilhelmson R B 1987 Numerical simulation of thunderstorm outflow dynamics: I. Outflow sensitivity experiments and turbulence dynamics *J. Atmos. Sci.* **44** 1180–210
- Emanuel K A 1994 *Atmospheric Convection* (Oxford: Oxford University Press) 580pp
- Faller A J 1963 An experimental study of the instability of the laminar Ekman layer *J. Fluid Mech.* **15** 560–76
- Fiedler B H 1994 The thermodynamic speed limit and its violation in axisymmetric numerical simulations of tornado-like vortices *Atmos.-Ocean* **32** 335–59
- Fiedler B H and Rotunno R 1986 A theory for the maximum windspeeds in tornado-like vortices *J. Atmos. Sci.* **43** 2328–40
- Forbes G S and Wakimoto R M 1983 A concentrated outbreak of tornadoes, downbursts and microbursts and implications regarding vortex classification *Mon. Weather Rev.* **111** 220–35
- Fovell R G and Dailey P S 1995 The temporal behavior of numerically simulated multicell-type storms: I. Modes of behavior *J. Atmos. Sci.* **52** 2073–95
- Fovell R G and Tan P-H 1998 The temporal behavior of numerically simulated multicell-type storms: II. The convective cell life cycle and cell regeneration *Mon. Weather Rev.* **126** 551–77
- French M M, Bluestein H B, Dowell D C, Wicker L J, Kramar M R and Pazmany A L 2006 The 15 May 2003 Shamrock, Texas, supercell: a dual-Doppler analysis and EnKF data-assimilation experiment *23rd Conf. on Severe Local Storms (St. Louis, MO, 6–10 November)* (Boston, MA: American Meteorological Society) (extended abstract not available)
- Fritsch J M, Kane R J and Chelius C R 1986 The contribution of mesoscale convective weather systems to the warm-season precipitation in the United States *J. Clim. Appl. Meteorol.* **25** 1333–45
- Fritsch J M, Murphy J D and Kain J S 1994 Warm core vortex amplification over land *J. Atmos. Sci.* **51** 1780–807
- Fujita T T 1965 Formation and steering mechanism of tornado cyclones associated hook echoes *Mon. Weather Rev.* **93** 67–78
- Fujita T T 1974 Jumbo tornado outbreak of 3 April 1974 *Weatherwise* **27** 116–26
- Fujita T T 1975 New evidence from April 3–4, 1974 tornadoes *Conf. on Severe Local Storms (Norman, OK) (Preprints)* (Boston, MA: American Meteorological Society) pp 248–55
- Fujita T T 1978 Manual of downburst identification for Project Nimrod *Satellite and Mesometeorology Research Paper No 156* Department of Geophysical Sciences, University of Chicago 104pp
- Fujita T T 1981 Tornadoes and downbursts in the context of generalized planetary scales *J. Atmos. Sci.* **38** 1511–34
- Fujita T T 1989 The Teton - Yellowstone tornado of 21 July 1987 *Mon. Weather Rev.* **117** 1913–40

- Fujita T T and Grandoso H 1968 Split of a thunderstorm into anticyclonic and cyclonic storms and their motion as determined from numerical model experiments *J. Atmos. Sci.* **25** 416–39
- Fujita T T, Forbes G S and Umehofer T A 1976 Close-up view of 20 March 1976 tornadoes: sinking cloud tops to suction vortices *Weatherwise* **29** 116–31
- Fujita T T, Forbes G S and Umehofer T A, 1976 Close-up view of 20 March 1976 tornadoes: sinking cloud tops to suction vortices *Weatherwise* **29** 145
- Gaudet B J, Cotton W R and Montgomery M T 2006 Low-level mesocyclonic concentration by nonaxisymmetric transport: II. Vorticity dynamics *J. Atmos. Sci.* **63** 1134–50
- Gilmore M S and Wicker L J 1998 The influence of midtropospheric dryness on supercell morphology and evolution *Mon. Weather Rev.* **126** 943–58
- Gilmore M S, Straka J M and Rasmussen E N 2004 Precipitation and evolution sensitivity in simulated deep convective storms: comparisons between liquid-only and simple ice and liquid phase microphysics *Mon. Weather Rev.* **132** 1897–916
- Heymsfield G M 1978 Kinematic and dynamic aspects of the Harrah tornadic storm analyzed from dual-Doppler radar data *Mon. Weather Rev.* **106** 233–54
- Houze R A Jr 1989 Observed structure of mesoscale convective systems and implications for large-scale heating *Q. J. R. Meteorol. Soc.* **115** 424–61
- Houze R A Jr 1993 *Cloud Dynamics* (New York: Academic) 573pp
- Houze R A Jr, Biggerstaff M I, Rutledge S A and Smull B P 1989 Interpretation of Doppler weather radar displays of midlatitude mesoscale convective systems *Bull. Am. Meteor. Soc.* **70** 608–19
- Houze R A Jr, Smull B F and Dodge P 1990 Mesoscale organization of springtime rainstorms in Oklahoma *Mon. Weather Rev.* **118** 613–54
- Howard L N and Gupta A S 1962 On the hydrodynamic and hydromagnetic stability of swirling flows *J. Fluid Mech.* **14** 463–76
- Jorgensen D and Weckwerth T 2003 Forcing and organization of convective systems *Radar and Atmospheric Science: A Collection of Essays in Honor of David Atlas* ed R Wakimoto and R Srivastava (*Meteorological Monograph* vol 30) (Boston, MA: American Meteorological Society) pp 75–103
- Kennedy A D, Straka J M and Rasmussen E N 2006 The existence of descending reflectivity cores in rear-flank appendages of supercells *23rd Conf. on Severe Local Storms (St. Louis, MO, 6–10 November)* (extended abstracts) (Boston, MA: American Meteorological Society) P10.4 CD - ROM
- Kennedy P C, Wescott N E and Scott R W 1993 Single-Doppler radar observations of a mini-supercell tornadic thunderstorm *Mon. Weather Rev.* **121** 1860–70
- Klemp J B 1987 Dynamics of tornadic thunderstorms *Annu. Rev. Fluid Mech.* **19** 369–402
- Klemp J B and Wilhelmson R B 1978 The simulation of three-dimensional convective storm dynamics *J. Atmos. Sci.* **35** 1070–96
- Klemp J B and Rotunno R 1983 A study of the tornadic region within a supercell thunderstorm *J. Atmos. Sci.* **40** 359–77
- Knight C A and Knight N C 2001 Hailstorms *Severe Convective Storms (Meteorological Monograph* vol 28) ed C Doswell III (Boston, MA: American Meteorological Society) pp 223–54
- Knupp K, Stalker J and McCaul E W Jr 1998 An observational and numerical study of a mini-supercell storm *Atmos. Res.* **49** 35–63
- Lee B D and Wilhelmson R B 1997 The numerical simulation of nonsupercell tornadogenesis: II. Evolution of a family of tornadoes along a weak outflow boundary *J. Atmos. Sci.* **54** 2387–415
- Lee J J, Samaras T M and Young C R 2004 Pressure measurements at the ground in an F-4 tornado *22nd Conf. on Severe Local Storms (Hyannis, MA, 4–8 October)* (extended abstracts) (Boston, MA: American Meteorological Society) p 15.3 CD - ROM
- Lee W-C and Wurman J 2005 Diagnosed three-dimensional axisymmetric structure of the Mulhall tornado on 3 May 1999 *J. Atmos. Sci.* **62** 2373–93
- Lemon L R and Doswell C A III 1979 Severe thunderstorm evolution and mesocyclone structure as related to tornadogenesis *Mon. Weather Rev.* **107** 1184–97
- Lemon L R and Parker S 1996 The Lahoma storm deep convergence zone: Its characteristics and role in storm dynamics and severity *18th Conf. on Severe Local Storms (San Francisco, CA) (Preprints)* (Boston, MA: American Meteorological Society) pp 70–5
- Leslie L M 1971 The development of concentrated vortices: a numerical study *J. Fluid Mech.* **48** 1–21
- Lewellen W S 1976 Theoretical models of the tornado vortex *Proc. Symp. on Tornadoes: Assessment of Knowledge and Implications for Man (Lubbock, TX, Texas Tech. University)* pp 107–43
- Lewellen D C and Lewellen W S 2006 On the limits to near-surface intensification of tornadic vortices *23rd Conf. on Severe Local Storms (St. Louis, MO, 6–10 November)* (extended abstracts) (Boston, MA: American Meteorological Society) p 13.5 CD - ROM

- Lewellen W S, Lewellen D C and Sykes R I 1997 Large-eddy simulation of a tornado's interaction with the surface *J. Atmos. Sci.* **54** 581–605
- Lewellen D C, Lewellen W S and Xia J 2000 The influence of a local swirl ratio on tornado intensification near the surface *J. Atmos. Sci.* **57** 527–44
- Lilly D K 1969 Tornado dynamics *NCAR Manuscript* 69–117 (Boulder, CO: National Center for Atmospheric Research)
- Lilly D K 1986 The structure, energetics and propagation of rotating convective storms: II. Helicity and storm stabilization *J. Atmos. Sci.* **43** 126–40
- Maddox R A 1980 Mesoscale convective complexes *Bull. Am. Meteorol. Soc.* **61** 1374–87
- Magsig M A and Snow J T 1998 Long-distance debris transport by tornadic thunderstorms: I. The 7 May 1995 supercell thunderstorm *Mon. Weather Rev.* **126** 1430–49
- Markowski P M and Harrington J Y 2005 A simulation of supercell thunderstorm with emulated radiative cooling beneath the anvil *J. Atmos. Sci.* **62** 2607–17
- Markowski P M, Rasmussen E N, Straka J M and Dowell D C 1998 Observations of low-level baroclinity generated by anvil shadows *Mon. Weather Rev.* **126** 2942–58
- Markowski P M, Straka J M and Rasmussen E N 2003 Tornado genesis resulting from the transport of circulation by a downdraft: idealized numerical simulations *J. Atmos. Sci.* **60** 795–823
- Marwitz J D 1972a The structure and motion of severe hailstorms: I. Supercell storms *J. Appl. Meteor.* **11** 166–79
- Marwitz J D 1972b The structure and motion of severe hailstorms: II. Multi-cell storms *J. Appl. Meteor.* **11** 180–8
- Marwitz J D 1972c The structure and motion of severe hailstorms: III. Severely sheared storms *J. Appl. Meteor.* **11** 189–201
- Maxworthy T 1973 Vorticity source for large scale dust devils and other comments on naturally occurring vortices *J. Atmos. Sci.* **30** 1717–20
- McCarthy D, Schaefer J and Edwards R 2006 What are we doing with (or to) the F-scale? *23rd Conf. on Severe Local Storms (St. Louis, MO, 6–10 November)* (extended abstracts) (Boston, MA: American Meteorological Society) p 5.6 CD - ROM
- McCaul E W Jr 1991 Buoyancy and shear characteristics of hurricane tornado environments *Mon. Weather Rev.* **119** 1954–78
- McCaul E W Jr 1993 Observations and simulations of hurricane-spawned tornadic storms *The Tornado: Its Structure, Dynamics, Prediction and Hazards* ed C R Church (Washington, DC: American Geophysical Union) pp 119–42
- McCaul E W Jr and Weisman M L 1996 Simulations of shallow supercell storms in landfalling hurricane environments *Mon. Weather Rev.* **124** 408–29
- McCaul E W Jr and Weisman M L 2001 The sensitivity of simulated supercell structure and intensity to variations in the shapes of environmental buoyancy and shear profiles *Mon. Weather Rev.* **129** 664–87
- McCaul E W Jr and Cohen C 2002 Impact on simulated storm structure and intensity of variations in the mixed layer and moist layer depths *Mon. Weather Rev.* **130** 1722–48
- McDonald J R and Mehta K 2004 *A Recommendation for an Enhanced Fujita Scale (EF-Scale)* Wind Engineering Center, Texas Tech University 109pp
- McLaughlin D, Chandrasekar V, Droememeier K, Frasier S, Kurose J, Junyent F, Philips B, Cruz-Pol S and Colom J 2005 Distributed collaborative adaptive sensing (DCAS) for improved detection, understanding and predicting of atmospheric hazards *9th Symp. on Integrated Observing and Assimilation Systems for the Atmosphere, Oceans and Land Surface (San Diego, CA)* (extended abstracts) (Boston, MA: American Meteorological Society) P11.3 CD-ROM
- Menard R D and Fritsch J M 1989 A mesoscale convective complex-generated inertially stable warm core vortex *Mon. Weather Rev.* **117** 1237–60
- Moller A R, Doswell C A III and Przybylinski R 1990 High-precipitation supercells: A conceptual model and documentation *16th Conf. on Severe Local Storms (Kananaskis Park, AB, Canada) (Preprints)* (Boston, MA: American Meteorological Society) pp 52–7
- Montervedi J P and Quadros J 1994 Convective and rotational parameters associated with three tornado episodes in northern and central California *Weather Forecast.* **9** 285–300
- Montervedi J P, Edwards R, Stumpf G A and Gudgel D 2006 An analysis of the 7 July 2004 Rockwell Pass, CA tornado: highest elevation tornado documented in the US *23rd Conf. on Severe Local Storms (St. Louis, MO, 6–10 November)* (extended abstracts) (Boston, MA: American Meteorological Society) P12.2 CD - ROM
- Montgomery M T and Kallenbach R J 1997 A theory for vortex Rossby-waves and its application to spiral bands and intensity changes in hurricanes *Q. J. R. Meteorol. Soc.* **123** 435–65
- Musil D J, Heymsfield A J and Smith P L 1986 Microphysical characteristics of a well-developed weak echo region in a high plains supercell thunderstorm *J. Clim. Appl. Meteorol.* **25** 1037–51

- Nelson S P and Young S K 1979 Characteristics of Oklahoma hailfalls and hailstones *J. Appl. Meteorol.* **18** 339–47
- Noda A T and Niino H 2005 Genesis and structure of a major tornado in a numerically- simulated supercell storm: importance of vertical vorticity in a gust front *SOLA* **1** 5–8
- Ogura Y and Phillips N A 1962 Scale analysis of deep and shallow convection in the atmosphere *J. Atmos. Sci.* **19** 173–9
- Orf L, Gilmore M S, Wilhelmson R B, Straka J M and Rasmussen E N 2006 The role of hook echo microbursts in simulated tornadic supercells I. Association with counter-rotating vortices and tornadogenesis *23rd Conf. on Severe Local Storms (St. Louis, MO, 6–10 November)* (Boston, MA: American Meteorological Society) (extended abstract not available)
- Pauley R L and Snow J T 1988 On the kinematics and dynamics of the 18 June 1986 Minneapolis tornado *Mon. Weather Rev.* **116** 2731–6
- Petterssen S 1956 *Weather Analysis and Forecasting. Vol 1, Motion and Motion Systems* 2nd edn (New York: McGraw-Hill) 428pp
- Przybylinski R W 1995 The bow echo: observations, numerical simulations and severe weather detection methods *Weather Forecast.* **10** 203–18
- Rasmussen E N and Straka J M 1998 Variations in supercell morphology: I. Observations of the role of upper-level storm-relative flow *Mon. Weather Rev.* **126** 2406–21
- Rasmussen E N, Straka J M, Gilmore M S and Davies-Jones R 2006 A preliminary survey of rear-flank descending reflectivity cores in supercell storms *Weather Forecast.* **21** 923–38
- Ray P S, Johnson B C, Johnson K W, Bradberry J S, Stephens J J, Wagner K K, Wilhelmson R B and Klemp J B 1981 The morphology of several tornadic storms on 20 May 1977 *J. Atmos. Sci.* **38** 1643–63
- Richardson Y, Droegemeier K K and Davies R P-Jones 2000 The influence of horizontal variations in vertical shear and low-level moisture on numerically simulated convective storms *20th Conf. on Severe Local Storms (Orlando, FL) (Preprints)* (Boston, MA: American Meteorological Society) pp 599–602
- Rotunno R 1977 Numerical simulation of a laboratory vortex *J. Atmos. Sci.* **34** 1942–56
- Rotunno R 1978 A note on the stability of a cylindrical vortex sheet *J. Fluid Mech.* **87** 761–71
- Rotunno R 1979 A study in tornado-like vortex dynamics *J. Atmos. Sci.* **36** 140–55
- Rotunno R 1981 On the evolution of thunderstorm rotation *Mon. Weather Rev.* **109** 577–86
- Rotunno R 1986 Tornadoes and tornadogenesis *Mesoscale Meteorology and Forecasting* ed P Ray (Boston, MA: American Meteorological Society) pp 414–36
- Rotunno R and Klemp J B 1985 On the rotation and propagation of simulated supercell thunderstorms *J. Atmos. Sci.* **42** 271–92
- Rotunno R, Klemp J B and Weisman M L 1988 A theory for strong, long-lived squall lines *J. Atmos. Sci.* **45** 463–85
- Rutledge S A and Houze R A Jr 1987 Diagnostic modeling study of the trailing stratiform region of a midlatitude squall line *J. Atmos. Sci.* **44** 2640–56
- Ryzhkov A V, Schuur T J, Burgess D W and Zrnic D S 2005 Polarimetric tornado detection *J. Appl. Meteorol.* **44** 557–70
- Samaras T M 2004 A historical perspective of *in situ* observations within tornado cores *22rd Conf. on Severe Local Storms (Hyannis, MA, 4–8 October)* (extended abstracts) (Boston, MA: American Meteorological Society) P11.4 CD-ROM
- Schlesinger R E 1975 A three-dimensional numerical model of an isolated deep convective cloud: preliminary results *J. Atmos. Sci.* **32** 934–57
- Shabbott C J and Markowski P M 2006 Surface *in situ* observations within the outflow of forward-flank downdrafts of supercell thunderstorms *Mon. Weather Rev.* **134** 1422–41
- Skamarock W C and Klemp J B 1992 The stability of time-split numerical methods for the hydrostatic and the nonhydrostatic elastic equations *Mon. Weather Rev.* **120** 2109–27
- Smith R K and Leslie L M 1978 Tornadogenesis *Q. J. R. Meteorol. Soc.* **104** 189–99
- Smull B F and Houze R A Jr 1985 A midlatitude squall line with a trailing region of stratiform rain: radar and satellite observations *Mon. Weather Rev.* **113** 117–33
- Smull B F and Houze R A Jr 1987a Dual-Doppler radar analysis of a midlatitude squall line with a trailing region of stratiform rain *J. Atmos. Sci.* **44** 2128–48
- Smull B F and Houze R A Jr 1987b Rear inflow in squall lines with a trailing stratiform precipitation *Mon. Weather Rev.* **115** 2869–89
- Smull B F and Augustine J A 1993 Multiscale analysis of a mature mesoscale convective system *Mon. Weather Rev.* **121** 103–32
- Snow J T 1982 A review of recent advances in tornado vortex dynamics *Rev. Geophys. Space Phys.* **20** 953–64
- Snow J T 1984 On the formation of particle sheaths in columnar vortices *J. Atmos. Sci.* **41** 2477–91

- Snow J T, Wyatt A L, McCarthy A K and Bishop E K 1995 Fallout of debris from tornadic thunderstorms: an historical perspective and two examples from VORTEX *Bull. Am. Meteorol. Soc.* **76** 1777–90
- Starr V P 1968 *Physics of Negative Viscosity Phenomena* (New York: McGraw-Hill) 256pp
- Straka J M, Zrnic D S and Ryzhkov A V 2000 Bulk hydrometeor classification and quantification using polarimetric radar data: synthesis of relations *J. Appl. Meteorol.* **39** 1341–72
- Stirling J and Wakimoto R M 1989 Mesoscale vortices in the stratiform region of a decaying midlatitude squall line *Mon. Weather Rev.* **117** 452–8
- Stumpf G J, Witt A, Mitchell E D, Spencer P L, Johnson J T, Eilts M D, Thomas K W and Burgess D W 1998 The National Severe Storms Laboratory mesocyclone detection algorithm for the WSR-88D *Weather Forecast.* **13** 304–26
- Tanamachi R L, Bluestein H B, Moore S S and Madding R P 2006 Infrared thermal imagery of cloud base in tornadic supercells *J. Atmos. Ocean. Technol.* **23** 1445–61
- Tanamachi R L, Bluestein H B, Lee C-W, Bell M and Pazmany A 2007 Ground-based velocity display (GBVTD) analysis of W-band Doppler radar data in a tornado near Stockton, Kansas on 15 May 1999 *Mon. Weather Rev.* **135** 783–800
- Trapp R J and Fiedler B H 1995 Tornado-like vortex genesis in a simplified numerical model *J. Atmos. Sci.* **52** 3757–78
- Trapp R J and Davies-Jones R 1997 Tornadogenesis with and without a dynamic pipe effect *J. Atmos. Sci.* **54** 113–33
- Trapp R J, Mitchell E D, Tipton G A, Effertz D A, Watson A I, Andra D L and Magsig M A 1999 Descending and nondescending tornadic vortex signatures detected by WSR-88D's *Weather Forecast.* **14** 625–39
- Trapp R J, Tessendorf S A, Godfrey E S and Brooks H E 2005 Tornadoes from squall lines and bow echoes I. Climatological distribution *Weather Forecast.* **20** 23–34
- Wakimoto R M 2001 Convectively driven high wind events *Severe Convective Storms (Meteorological Monograph vol 28)* ed C Doswell III (Boston, MA: American Meteorological Society) pp 255–98
- Wakimoto R M and Wilson J W 1989 Non-supercell tornadoes *Mon. Weather Rev.* **117** 1113–40
- Wakimoto R M and Martner B E 1992 Observations of a Colorado tornado: II. Combined photogrammetric and Doppler radar analysis *Mon. Weather Rev.* **120** 522–43
- Wakimoto R M and Liu C 1998 The Garden City, Kansas, storm during VORTEX 95: II. The wall cloud and tornado *Mon. Weather Rev.* **126** 393–408
- Wakimoto R M, Lee W-C, Bluestein H B, Liu C-H and Hildebrand P H 1996 ELDORA observations during VORTEX 95 *Bull. Am. Meteorol. Soc.* **77** 1465–81
- Walko R L 1988 Plausibility of substantial dry adiabatic subsidence in a tornado core *J. Atmos. Sci.* **45** 2251–67
- Walko R L 1993 Tornado spin-up beneath a convective cell: required basic structure of the near-field boundary layer winds *The Tornado: Its Structure, Dynamics, Prediction and Hazards* ed C R Church (Washington, DC: American Geophysical Union) pp 89–95
- Weisman M L 1992 The role of convectively generated rear-inflow jets in the evolution of long-lived mesoconvective systems *J. Atmos. Sci.* **49** 1826–47
- Weisman M L 1993 The genesis of severe, long-lived bow echoes *J. Atmos. Sci.* **50** 645–70
- Weisman M L and Klemp J B 1982 The dependence of numerically simulated convective storms on vertical wind shear and buoyancy *Mon. Weather Rev.* **110** 504–20
- Weisman M L and Klemp J B 1984 The structure and classification of numerically simulated convective storms in directionally varying wind shears *Mon. Weather Rev.* **112** 2479–98
- Weisman M L and Rotunno R 2000 The use of vertical wind shear versus helicity in interpreting supercell dynamics *J. Atmos. Sci.* **57** 1452–72
- Weisman M L and Davis C A 1998 Mechanisms for the generation of mesoscale vortices within quasi-linear convective systems *J. Atmos. Sci.* **55** 2603–22
- Wicker L J 1996 The role of near surface wind shear on low-level mesocyclone generation and tornadoes *18th Conf. on Severe Local Storms (San Francisco, CA) (Preprints)* (Boston, MA: American Meteorological Society) pp 115–19
- Wicker L J and Wilhelmson 1995 Simulation and analysis of tornado development and decay within a three-dimensional supercell thunderstorm *J. Atmos. Sci.* **52** 2675–703
- Wilhelmson R B and Klemp J B 1978 A numerical study of storm splitting that leads to long-lived storms *J. Atmos. Sci.* **35** 1974–86
- Wilhelmson R B and Wicker L J 2001 Numerical modeling of severe local storms *Severe Convective Storms (Meteorological Monograph vol 28)* ed C Doswell III (Boston, MA: American Meteorological Society) pp 123–66
- Williams E A 2001 The electrification of severe storms *Severe Convective Storms (Meteorological Monograph vol 28)* ed C Doswell III (Boston, MA: American Meteorological Society) pp 527–61
- Wurman J 2002 The multiple vortex structure of a tornado *Weather Forecast.* **17** 473–505

- Wurman J and Gill S 2000 Finescale radar observations of the Dimmit, Texas (2 June 1995) tornado *Mon. Weather Rev.* **128** 2135–64
- Wurman J and Alexander C R 2005 The 30 May 1998 Spencer, South Dakota, storm: II. Comparison of observed damage and radar-derived winds in the tornadoes *Mon. Weather Rev.* **133** 97–119
- Wurman J, Straka J M and Rasmussen E N 1996 Fine-scale Doppler radar observations of tornadoes *Science* **272** 1774–7
- Xue M, Xu Q and Droegemeier K K 1997 A theoretical and numerical study of density currents in nonconstant shear flows *J. Atmos. Sci.* **54** 1998–2019
- Zipser E J 1982 Use of a conceptual model of the life-cycle of mesoscale systems to improve very-short range forecasts *Nowcasting* ed K A Browning (New York: Academic) pp 191–204
- Zrnic D S and Ryzhkov A V 1999 Polarimetry for weather surveillance radars *Bull. Am. Meteorol. Soc.* **80** 389–406